Design and Synthesis of Metallopeptides: Incorporation of Unnatural α-Amino Acids and Construction of a Structural Template

Thesis by

Richard Ping Cheng

In Partial Fulfillment of the Requirements

for the Degree of

Doctor of Philosophy

California Institute of Technology

Pasadena, California

1998

(Submitted January 7, 1998)

© 1998

Richard Ping Cheng

All Rights Reserved

For my family

my wife Chia-Wen

my parents

and my sister Ann

Acknowledgments

I would like to thank my advisor, Barbara Imperiali, for providing such an exciting research environment and for her extreme enthusiasm for science. I would also like to thank my co-advisor, Harry Gray, for his enormous support throughout my graduate career at Caltech. Professors Robert Grubbs, William Goddard III, and John Bercaw have all provided advice at certain times and have been very supportive.

I must not forget to mention numerous members of the Imperiali group that have made the experience at Caltech a memorable one. I would want to thank Dr. Stewart Fisher for introducing me to the ins and outs of the group, and Dr. Mary Struthers for collaborating in the later stages of a very successful project. I would like to thank Dr. Ranabir Sinha Roy for many helpful discussions. I should not leave out Dr. Jeff Spencer for his input on synthesizing unnatural amino acids and solution phase peptide chemistry. I will always remember Grant Walkup for his long time companionship in the lab. He and Vincent Tai have been very good friends for discussing scientific and non-scientific subjects. The completion of this thesis would not be possible without the help from Vincent Tai, Sarah O'Connor, and Michael Shogren-Knaak, and Dr. Dierdre Pearce. There is also Dr. Keith Rickert, Dr. Tamara Hendrickson, Dr. Rahul Pathak, Dr. Lisa Wang, Robert Davis, Dr. William Shrader, Dr. Chris Davis, Jennifer Ottesen, Kevin McDonnell, Maria Ufret, and Dr. Paula Eason, who have spiced up the lab at various periods to create a wonderful atmosphere. I am also grateful to have a second home at the Gray group with many members that have enlightened my experience at Caltech. I have also interacted with many other people on campus that have made this experience unforgettable.

Beyond science, my family has been extremely supportive throughout these years. Especially, I would like to thank my wife for taking care of my everyday life, and she deserves half of this thesis. My parents and my sister have provided mental support through long phone conversations. I must thank Dr. Po-Hsin Liu and Young May for tremendous support. Their inexhaustible hospitality served to refresh my mind about my science as well as my overall career. Let me also mention a bunch of friends at the Caltech Chinese Culture Club for providing opportunities to chat about Taiwan and related subjects, as well as the weekend tennis meets. In particular, I would like to thank Dr. Chao-Ping Hsu, Pei-Lin Chen, Dr. See May Phoong, and Dr. Jung-Fu Cheng for being supportive as very good friends, and for providing opportunities for out-of-the-lab entertainment. It has been a pleasure knowing you guys. I must thank Glenn Turner, who has shared the rent for all of my stay at Caltech. His warm personality and hard-working attitude shall not be forgotten, and I will treasure this friendship. I would also like to thank Sally Asmundson at the career development center for her support and advice during the last year.

Finally, I would like to thank the NIH Bio-organic/Bio-inorganic training grant for providing financial support.

Abstract

For the design of metallopeptides, an approach involving unnatural α-amino acids has been adopted for designing metallopeptides. Unnatural α-amino acids bearing 1,10-phenanthroline and methyl-1,10-phenanthroline side chain functionalities were synthesized. The metal-binding properties of hexapeptides incorporating these chelating residues and the 2,2'-bipyridyl-containing residues were investigated. The modulation of metal binding affinity, preference, and stoichiometry for the designed peptides was achieved by varying three different features: selection of unnatural bidentate residue, incorporation of auxiliary metal-binding amino acid and control of structural preorganization of the peptide architecture. These chelating residues and the guidelines for their utilization can be exploited in future metalloprotein design.

Towards the design of a functional metallopeptide, the phenanthrolyl-containing residue was incorporated into a series of peptide motifs which have been designed to adopt a ββα super-secondary structure patterned after individual zinc finger domains. Uncoupling the tertiary structure of the polypeptide from metal binding would allow increased versatility in the design of the metal-binding site. Following this guideline, an iterative design process was performed, resulting in a metal independent 23 residues motif, **BBA1**.

Using **BBA1** as a scaffold, attempts to construct a functional metallopeptide involved nine peptides utilizing combinations of residues with phenanthroline, imidazole, amine, carboxylate or pyridine side chains to form the metal-binding site. Studies on these peptides revealed basic guidelines for designing metal-binding sites in ββα motifs. Since the iterative

design process is impeded by studying peptides individually, a rational approach involving combinatorial techniques would allow evaluation of multiple peptides simultaneously.

The linear synthesis of peptides that adopt the ββα fold had been proven difficult, therefore a synthetic route involving solid phase native ligation was developed. The synthesis of peptide benzyl thioesters *via* a protected peptide intermediate was developed for Fmoc-based chemistry. Solid phase native ligation of this benzyl thioester and resin bound peptide has been demonstrated. This will enable the generation of combinatorial libraries of ββα peptides for achieving hydrolase activity. Furthermore, larger peptides containing unnatural amino acids may be synthesized using solid phase native ligation.

Table of Contents

Abstract vi

List of Figures xii

List of Schemes xv

List of Tables xvi

List of Abbreviations xviii

Chapter 1: Introduction
References 8

Chapter 2: Tuning the Metal Binding Affinity of Metallopeptides: Incorporation of Unnatural Bidentate α-Amino Acids and Exploitation of Peptide Structure
Introduction 14
Results and Discussion 18
Synthesis of Fmoc-Fen-OH and Fmoc-Neo-OH 18
Dissociation Constants of the Peptide-M^{II} Complexes 21
Bpa-Containing Peptides 21
Fen- and Neo-Containing Peptides 26
Summary 33
Conclusion 34
Acknowledgments 35
Experimental Section 35
References 47

Chapter 3: Evolution of a ββα Motif Based on the Zinc Finger Domains
Introduction 51
Results and Discussion 58
Peptide Synthesis 61
Peptide **ZF01** 63
Design of Peptide **ZF01** 63

Circular Dichroism Studies on Peptide **ZF01**.....64
Peptide **ZF02**.....66
Design of Peptide **ZF02**.....66
Circular Dichroism Studies on Peptide **ZF02**.....66
Peptide ZF03.....68
Design of Peptide **ZF03**.....68
Circular Dichroism Studies on Peptide **ZF03**.....69
NMR Analysis on Peptide **ZF03**.....71
Examining the *cis-trans* Isomerization of DPro in Type II' Turns with the **Fens** Peptides.....71
Peptides **ZF04** and **ZF05**.....73
Circular Dichroism Studies on Peptide **ZF05**.....73
NMR Analysis on Peptide **ZF05**.....75
Peptide **ZF06**.....78
Circular Dichroism Studies on Peptide **ZF06**.....78
Peptide **ZF07**.....80
The Zn^{II}-Binding Properties of the Metallopeptides.....81
Conclusions.....84
Acknowledgments.....85
Experimental Section.....85
References.....88

Chapter 4: Design of Zinc Metallopeptides Based on a ββα Motif
Introduction.....94
Results and Discussion.....98
CA-I Peptides.....101
Design of the **CA-I** Peptides.....101
Circular Dichroism Studies on **CA-I** Peptides.....103
Ac-Gly-ONp Hydrolysis with M^{II} Complexes of the **CA-I** Peptides.....109
CA-II Peptides.....112
The Design of the **CA-II** Peptides.....112
Circular Dichroism Studies on the **CA-II** Peptides.....114
Ac-Gly-ONp Hydrolysis with Zn^{II} Complexes of the **CA-II** Peptides.....118

Gly-ONp Hydrolysis with Zn^{II} Complexes of Designed ββα Metallopeptides 119
Initial Gly-ONp Hydrolysis Rates for Peptide-Zn^{II} Complexes 119
Gly-ONp Hydrolysis Under Pseudo-First Order Conditions 120
CA-III Peptides 124
The Design of the **CA-III** Peptides 124
Circular Dichroism Studies on the **CA-III** Peptides 126
Zn^{II} Titration on Peptide **CA08** Monitored by NMR Spectroscopy 128
Conclusions 129
Acknowledgments 130
Experimental Section 130
References 137

Chapter 5: Solid Phase Native Ligation for the Assembly of ββα Peptides
Introduction 140
Results and Discussion 146
Design of the Sequences for the *N*-Peptide and the *C*-Peptide 146
Synthesis of the *N*-Peptide Benzyl Thioester 148
Synthesis of the *N*-Peptide Thioester Utilizing the HMBA Linker 148
Synthesis of the *N*-Peptide Thioester Utilizing the Thiol Methoxytrityl Linker 150
Synthesis of the *N*-Peptide Thioester Utilizing the Hydroxytrityl Linker 151
Solid Phase Native Ligation 153
Ligation of **CPep**-PAL-PEG-PS and Protected **NPep**-SBn 158
Ligation of **CPep**-Met-TG and Protected **NPep**-SBn 158
Ligation of **CPep**-HMBA-TG and **NPep**-SBn 159
Ligation of **CPep**-HMBA-PEGA and **NPep**-SBn 160
Conclusion 162

Acknowledgments.....162
Experimental Section.....163
References.....167

List of Figures

Chapter 1

Figure 1-1 Schematic diagram of the distribution of hydrophobic and hydrophilic functional groups for a typical metalloprotein.....3

Figure 1-2 Three unnatural metal-binding α-amino acids reported in the literature.....6

Figure 1-3 Three unnatural α-amino acids featuring the 2,2′-bipyridine functionality that have been synthesized in the group.....7

Chapter 2

Figure 2-1 Various unnatural α-amino acids featuring the 2,2′-bipyridine, 1,10-phenanthroline and methyl-1,10-phenanthroline functionalities.....15

Figure 2-2 Schematic diagram of the β-hairpin motif designed to bring two 6Bpa residues into close proximity.....17

Figure 2-3 A typical metal cation titration of a Bpa-containing peptide monitored by absorption spectroscopy.....22

Figure 2-4 Schematic diagram of the metal binding event for the hexapeptides 6Bpa6Bpa and $6Bpa6Bpa_W$.....25

Figure 2-5 A typical metal cation titration of a Fen-containing peptide monitored by absorption spectroscopy.....27

Figure 2-6 A typical metal cation titration of a Neo-containing peptide monitored by absorption spectroscopy.....28

Figure 2-7 A Co^{II} titration of a Neo-containing peptide monitored by circular dichroism spectroscopy.....29

Figure 2-8 The final analysis of a typical metal cation titration to obtain the apparent dissociation constant based on the Scott equation.....30

Chapter 3

Figure 3-1 Schematic diagram of the nest-like construct and the cage-like structure.....52

Figure 3-2 The structure of the Zn^{II}-binding site of carbonic anhydrase.....53

Figure 3-3 The mechanism for CO_2 hydration catalyzed by carbonic anhydrase.....54

Figure 3-4 The structure of a natural zinc finger peptide bound to Zn^{II}.....56

Figure 3-5 CD spectra of typical zinc fingers.....56

Figure 3-6 Sequences of the peptides in the iterative design process that are intended to adopt a ββα super-secondary structure.....59

Figure 3-7 RP-HPLC traces for the peptide synthesis products involving free acid chemistry and activated pentafluorophenyl ester chemistry.....62

Figure 3-8 CD spectra of peptide **ZF01**.....65

Figure 3-9 CD spectra of peptide **ZF02**.....67
Figure 3-10 Results from molecular modeling to illustrate the effects of type II turn and type II′ turn on β-sheet formation.....69
Figure 3-11 CD spectra of peptide **ZF03**.....70
Figure 3-12 Expected NOE interactions in the heterochiral type II' reverse turn.....73
Figure 3-13 CD spectra of peptide **ZF05**. 74
Figure 3-14 NOE crosspeaks indicative of structure for peptides **ZF05** and **ZF04**. 77
Figure 3-15 CD spectra of peptide **ZF06** (**BBA1**). 79
Figure 3-16 The structure of peptide **ZF06** (**BBA1**) solved by NOE-restrained simulated annealing.....80

Chapter 4

Figure 4-1 The structure of peptide **BBA1** which folds into a well defined structure in the absence of crosslinks. 94
Figure 4-2 The structure of the Zn^{II}-binding site of carbonic anhydrase and carboxypeptidase.....95
Figure 4-3 The mechanism for CO_2 hydration catalyzed by carbonic anhydrase.....96
Figure 4-4 A model for carbonic anhydrase, Zn^{II}[12]ane$N_3(OH_2)$.....97
Figure 4-5 Sequences of the metallopeptides patterned after the ββα structural scaffold, peptide **BBA1**. 99
Figure 4-6 Proposed structure of the Zn^{II} complex of a ββα motif with metal-binding histidines at positions 3, 6, and 21.....102
Figure 4-7 Proposed structure of the Zn^{II} complex of a ββα motif with metal-binding histidines at positions 3, 6, and 17 and a potential proton abstractor homoserine at position 21. 102
Figure 4-8 A typical Zn^{II} titration of a **CA-I** peptide monitored by CD. 105
Figure 4-9 CD spectra of peptide **CA01**.....107
Figure 4-10 CD spectra of peptide **CA02**.....107
Figure 4-11 The CD spectra of peptide **CA03**. 108
Figure 4-12 Proposed structure of the Zn^{II} complex of a ββα motif with metal-binding histidines at positions 6, 17, and 21.....113
Figure 4-13 Various amino acids with side chains that may serve as ligating residues by ligating through a nitrogen atom. 113
Figure 4-14 CD spectra of peptide **CA04**.....116
Figure 4-15 CD spectra of peptide **CA05**. 117
Figure 4-16 CD spectra of peptide **CA06**.....117
Figure 4-17 The *p*-nitrophenyl esters of glycine derivatives used as substrates for hydrolysis assays. 119
Figure 4-18 A typical Gly-ONp hydrolysis monitored by absorption (UV-vis) spectroscopy with initial analysis. 121
Figure 4-19 The least square fits for the data of a typical Gly-ONp hydrolysis.....122

Figure 4-20 Three positional isomers for (*S*)-2-amino-3-pyridylpropionic acid. 125
Figure 4-21 Proposed structure of the Zn^{II} complex of a ββα motif with metal-binding 3Pyr at positions 6, 18, and 21. 126
Figure 4-22 CD spectra of peptide **CA07** 127
Figure 4-23 CD spectra of peptide **CA08** 128

Chapter 5

Figure 5-1 The structure of peptide **BBA1** which folds into a well defined structure in the absence of crosslinks 141
Figure 5-2 Proposed structure of the Zn^{II} complex of a ββα motif with metal-binding histidines at positions 6, 17, and 21, and glutamate at position 18 to serve as a proton abstractor 147
Figure 5-3 Various linkers utilized to facilitate characterization of the resin bound product of solid phase ligations 156
Figure 5-4 The disappearance of **NPep**-SBn monitored by RP-HPLC for the ligation of **CPep**-HMBA-PEGA and **NPep**-SBn. 160

List of Schemes

Chapter 2
Scheme 2-1 Synthesis of Fmoc-Protected Fen and Neo Amino Acids.....20

Chapter 3
Scheme 3-1 Schematic Diagram of the Iterative Design Process to Generate a Zinc Metallopeptide with Hydrolase Activity 57

Chapter 4
Scheme 4-1 Hydrolysis of the *p*-Nitrophenyl Ester of *N*-Acetylglycine.....110
Scheme 4-2 Protonation States for Imidazole and Pyridine.....124

Chapter 5
Scheme 5-1 Different Strategies for Joining Two Peptide Segments 143
Scheme 5-2 Mechanism for Native Ligation.....145
Scheme 5-3 Synthesis of the *N*-Peptide Benzyl Thioester Involving Boc-Based Chemistry.....145
Scheme 5-4 Outline of Solid Phase Native Ligation.....146
Scheme 5-5 Iodoacetamide Capping of Cysteine.....148
Scheme 5-6 Retrosynthetic Scheme for Synthesizing the *N*-Peptide Benzyl Thioester Using the HMBA Linker.....149
Scheme 5-7 Attempts to Synthesize Ac-Phe-Ser-SBn Using the HMBA Linker 149
Scheme 5-8 Retrosynthetic Scheme for Synthesizing the *N*-Peptide Benzyl Thioester Using the Thiol Methoxytrityl Linker 150
Scheme 5-9 Retrosynthetic Scheme for Synthesizing the *N*-Peptide Benzyl Thioester Using the Hydroxytrityl Linker 151
Scheme 5-10 Synthesis of *N*-Acetyl-L-Phenylalanine Benzyl Thioester.....152
Scheme 5-11 Synthesis of **NPep**-SBn.....153

List of Tables

Chapter 2

Table 2-1 Apparent Dissociation Constants (μM) for Bpa-Containing Peptide-M^{II} Complexes....23
Table 2-2 Apparent Dissociation Constants (μM) of Fen- and Neo-Containing Peptide-M^{II} Complexes....31
Table 2-3 The Calculated and Observed High Resolution Mass Values for the Synthesized Hexapeptides....45

Chapter 3

Table 3-1 Characteristics of Structural and Catalytic Zn^{II} Sites....52
Table 3-2 Conformational Analysis on the **Fens** Peptides....72
Table 3-3 Sequence Specific Assignments for Peptide **ZF05**....76
Table 3-4 Apparent Dissociation Constants (μM) for the Peptide-Zn^{II} Complexes....82
Table 3-5 The Calculated and Observed Mass Values for the Synthetic Peptides....87

Chapter 4

Table 4-1 Apparent Dissociation Constants for the Zn^{II} Complexes of the **CA-I** Peptides....104
Table 4-2 Dissociation Constants for Zn^{II} Complexes of Glycine Derivatives....109
Table 4-3 Initial Ac-Gly-ONp Hydrolysis Rates for Zn^{II} Complexes of the **CA-I** Peptides....110
Table 4-4 Relative Initial Ac-Gly-ONp Hydrolysis Rates for the M^{II} Complexes of the **CA-I** Peptides....111
Table 4-5 Apparent Dissociation Constants for the Zn^{II} Complexes of the **CA-I** and **CA-II** Peptides....115
Table 4-6 Initial Ac-Gly-ONp Hydrolysis Rates for the Zn^{II} Complexes of the **CA-II** Peptides....118
Table 4-7 Initial Gly-ONp Hydrolysis Rates for Zn^{II} Complexes of Designed ββα Metallopeptides....120
Table 4-8 Pseudo-First Order Rate Constants for Gly-ONp Hydrolysis for Zn^{II} Complexes of Designed ββα Metallopeptides....123
Table 4-9 Mass Spectroscopy and HPLC Data on the **CA** Peptides....133

Chapter 5

Table 5-1 Characteristics of Various Solid Supports for Solid Phase Peptide Synthesis 155
Table 5-2 Solid Phase Ligations for Synthesizing ββα Peptides 157
Table 5-3 Amino Acid Analysis Results of **NPep-CPep**-HMBA-PEGA 161
Table 5-4 Mass Analysis on Various Resin Bound Peptides After Cleavage 166

List of Abbreviation

Standard three-letter codes are used for the naturally occurring amino acids.

1D	One dimensional
2D	Two dimensional
2Pyr	(*S*)-2-Amino-3-(pyrid-2-yl)propionic acid
3Pyr	(*S*)-2-Amino-3-(pyrid-3-yl)propionic acid
4Bpy	(*S*)-2-Amino-3-(2,2′-bipyrid-4-yl)propionic acid
4Pyr	(*S*)-2-Amino-3-(pyrid-4-yl)propionic acid
5Bpy	(*S*)-2-Amino-3-(2,2′-bipyrid-5-yl)propionic acid
6Bpy	(*S*)-2-Amino-3-(2,2′-bipyrid-6-yl)propionic acid
Ac	Acetyl
AU	Absorption unit
Bn	Benzyl
Boc	*tert*-Butyloxycarbonyl
BOP	Benzotriazole-1-yloxy-tris(dimethylamino)-phosphoniumhexafluoro-phosphate
calcd	Calculated
CD	Circular dichroism
CHES	2-(Cyclohexylamino)-ethanesulfonic acid
CLEAR	Cross-linked ethoxylate acrylate resin
CZE	Capillary zone electrophoresis
Dab	(*S*)-2,4-Diaminobutyric acid
Dap	(*S*)-2,3-Diaminoprionic acid
DBU	1,7-Diazabicyclo[5,4,0]-undec-7-ene
DIEA	Diisopropylethylamine
DIPCDI	Diisopropylcarbodiimide
DMAP	4-*N*,*N*-Dimethylaminopyridine
DMF	Dimethylformamide
DMSO	Dimethylsulfoxide
DNS	Dansylsulfonamide
EDTA	Ethylenediaminetetraacetic acid
Et	Ethyl
ee	Enantiomeric excess
EPPS	*N*-2-Hydroxyethylpiperazine-*N*′-3-propanesulfonic acid
ES-MS	Electrospray mass spectrometry
FAB	Fast atom bombardment mass spectrometry
Fen	(*S*)-2-Amino-3-(1,10-phenanthrol-2-yl)propionic acid
Fmoc	9-Fluorenylmethyloxycarbonyl
Fmoc-OSu	9-Fluorenylmethyloxycarbonylsuccinimidyl carbonate
HEPES	*N*-(2-Hydroxyethyl)piperazine-*N*′-(2-ethane-sulfonic acid
HATU	*O*-(7-Azabenzotriazol-1-yl)-1,1,3,3-tetramethyluronium hexafluorophosphate

HMBA	4-Hydroxymethylbenzoic acid
HOAt	1-Hydroxy-7-azabenzotriazole
HOBt	1-Hydroxybenzotriazole
HPLC	High performance liquid chromatography
HRMS	High resolution mass spectrometry
Hse	Homoserine
K_D	Dissociation constant
MALDI-MS	Matrix assisted laser desorption ionization mass spectrometry
max	Maximum
min	Minute
Me	Methyl
Mmt	Monomethoxytrityl
MOPS	3-*N*-Morpholino-propanesulfonic acid
MS	Mass spectrometry
Neo	(*S*)-2-Amino-3-(9-methyl-1,10-phenanthrol-2-yl)propionic acid
nm	Nanometer
NMP	*N*-Methylpyrolidinone
NMR	Nuclear magnetic resonance
NOE	Nuclear Overhauser spectroscopy
obsd	Observed
ONp	*para*-Nitrophenyl
OPfp	Pentafluorophenyl
Orn	Ornithine
PAL	5-(4'-Aminomethyl-3',5'-dimethoxyphenoxy)valeric acid
PD-MS	Plasma desorption mass spectrometry
PEG-PS	Polyethyleneglycol-grafted polystyrene
PEGA	Polyethyleneglycol-poly-(*N*,*N*-dimethylacrylamide) copolymer
ppb	Parts per billion
ROESY	Rotating frame Overhauser spectroscopy
RP	Reverse phase
sec	Seconds
SPPS	Solid phase peptide synthesis
^{t}Bu	*tert*-Butyl
TAPS	*N*-Tris(hydroxymethyl)methylaminopropanesulfonic acid
TEA	Triethylamine
TFA	Trifluoroacetic acid
TG	TentaGel,polystyrene–poly(ethyleneglycol)–tentacle copolymer
THF	Tetrahydrofuran
TIS	Triisopropylsilane
TLC	Thin layer chromatography
TOCSY	Total Correlation Spectroscopy
TRIS	2-Amino-2-(hydroxymethyl)-1,3-propanediol
Trt	Trityl
UV	Ultra violet
vis	Visible
VT	Variable Temperature

Chapter 1

Introduction

Metalloproteins exhibit enviable reactivities by catalyzing some of the most important reactions in nature such as photosynthesis, oxidative phosphorylation, and nitrogen fixation.[1-3] In addition, metalloproteins perform a wide variety of functions such as electron transfer, dioxygen transport and activation, hydrolysis, group transfer, and rearrangements. Furthermore, metal cations are responsible for the transfer of information in biological processes such as the flow of sodium and potassium in voltage-gated channels, and calcium waves in intracellular signal transduction. This provides a wealth of opportunity to explore the basic principles of structure and reactivity as well as the creation of new metalloproteins and metallopeptides.

Almost any given metal cation can potentially perform several different reactions depending on the surrounding environment. For example, the iron in the heme can act as a dioxygen carrier in hemoglobin, an electron shuttler in cytochrome *c*, or a dioxygen activator in cytochrome P450. In each case, the metal center is identical, but the difference in the surrounding protein matrix is responsible for the diverse reactivity. In general, the metal cation is ligated by a shell of hydrophilic atomic groups (oxygen, nitrogen, or sulfur atoms) called the primary ligand sphere, and this hydrophilic shell is embedded within a larger shell of hydrophobic groups designated the secondary ligand sphere (Figure 1-1).[4] The behavior of the metal center is a result of subtle interplay between the inherent properties of the metal cation, the primary hydrophilic ligand sphere, and the secondary hydrophobic ligand sphere. In some cases, the coordination chemistry of the metal cation dominates such as the zinc finger domains.[5] In other cases, the protein matrix dominates exemplified by the zinc hydrolase carbonic anhydrase.[6] This subtle interplay presents great challenge for the

metalloprotein and metallopeptide design. To date, most design efforts have focused on the metal-binding site, which does not involve the secondary ligand sphere.

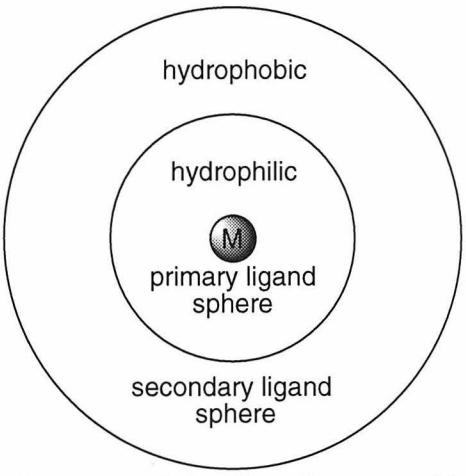

Figure 1-1 Schematic diagram of the distribution of hydrophobic and hydrophilic functional groups for a typical metalloprotein.

Several different strategies have been adopted for metalloprotein design. One common strategy involves the re-engineering of existing natural metal-binding sites.[7-10] Berg and coworkers have removed one of the ligating histidines from a zinc finger domain which affected the geometry of the metal center.[11] Valentine and coworkers have re-engineered the type II copper site in zinc-copper superoxide dismutase into a blue copper site.[12, 13] Several variations of azurin have been investigated by Gray and coworkers to include an aspartic acid in the native Cu^{II}-binding site.[14-18] Similarly, many variation of the metal binding site for carbonic anhydrase have been investigated by Christianson and coworkers.[19] Furthermore, Gray and coworkers have engineered the metal-binding site of cytochrome *c* to bind exogenous ligands such as dioxygen and cyanide.[20-23] Since there is a great need to sense metal cations *in situ* and in real time, efforts in metallopeptide design have expanded to this area.[24] Zinc sensors have been designed in the

Imperiali group patterned after zinc finger domains.[25, 26] Similarly, Berg and coworkers have exploited the same peptide framework to sense Zn^{II} by a different operating mechanism.[27] Furthermore, peptides based on the sequence Gly-Gly-His from serum albumin have been developed in the Imperiali group to sense Cu^{II} selectively.[28]

A second approach for metalloprotein design concentrates on the introduction of novel metal-binding sites into natural protein frameworks.[10, 29] Arnold and coworkers introduced a His-Xaa_3-His Cu^{II}-binding site onto the surface of cytochrome *c* and somatotropin.[30, 31] In several cases, the carbonic anhydrase Zn^{II}-binding site has been incorporated into the sequence-variable complementary determining regions of the light chain on an antibody.[32-36] Similarly, the heavy chain variable domain of an immunoglobulin has been exploited for metal binding by Sollazzo and coworkers.[37] Caradonna and coworkers have incorporated the iron center of superoxide dismutase into thioredoxin.[38] Furthermore, a tetrahedral His_3Cys Zn^{II}-binding site has been introduced into the B1 domain of *Streptococcal* protein G by Regan and coworkers.[39]

In many cases, metal-binding sites have been incorporated to increase protein stability upon binding metal cations. Several groups have shown that the introduction of a Ca^{II}-binding site into human lysozyme enhances thermal stability. [40-42] The Ca^{II} binding loop of thermolysin was grafted into the *Bacillus subtilis* neutral protease to improve the thermostability of the protease.[43] Similarly, a Ca^{II} binding loop from thermitase was introduced into subtilisin BPN' to increase the resistivity to thermal-induced autoproteolysis.[44] Gray and coworkers have demonstrated that a metal-binding site comprising two histidines bound to a $Ru^{II}(bipyridine)_2$ moiety increased the stability of cytochrome *c* considerably.[45] The Zn^{II}-binding site of

carbonic anhydrase was introduced into the β-barrel retinol-binding protein which resulted in enhance stability towards chemical denaturation.[46]

In addition to affecting the stability of the host protein, engineered metal-binding sites have been exploited to control enzyme activity. Reversible inhibition by Cu^{II} has been demonstrated for trypsin through incorporation of a histidine near the active site.[47, 48] Furthermore, the specificity of trypsin was altered at the S_2' site to favor histidines at this position upon binding of Zn^{II} or Ni^{II}.[49] Interestingly, an additional metal-dependent allosteric switch was successfully engineered into glycogen phosphorylase.[50]

The approach was adopted for designing sensor molecules as well. A rationally designed Zn^{II}-binding antibody constructed by grafting the Zn^{II}-binding site from carbonic anhydrase to a homologous region of the heavy chain was capable of transducing the selective Zn^{II} binding event into a fluorescence signal through the quenching of a nearby tryptophan.[51]

The incorporation of cofactors into proteins to bind metal cations presents another approach. The incorporation of the heme group into four helix bundles has been demonstrated by DeGrado and coworkers.[52, 53] More recently, the $[Fe_4S_4]$ cluster has been introduced into thioredoxin by Caradonna and coworkers.[54]

Template-assisted synthetic protein (TASP) is a different design concept introduced by Mutter and coworkers for the assembly of diverse protein structures.[55] Synthetic templates involving metal cations have been employed to direct the folding of polypeptide chains. Several groups have employed this strategy in the construction of three helix bundles, in which a template involving the metal directs the bundle formation.[56-58]

Another strategy for the design of metallopeptides and metalloproteins involves *de novo* design. DeGrado and coworkers have introduced Zn^{II}-binding sites into four-helix bundles.[59, 60] Similarly, Regan and coworkers have designed a His_2Cys_2 Zn^{II} site into a bundle motif. [61]

The utilization of non-encoded metal-binding α-amino acids for designing metallopeptides is compatible with *de novo* design. This combined approach allows one to design, synthesize and incorporate "in-house" "home-made" amino acids into small peptidyl constructs. Several research groups have focused on the synthesis of unnatural metal-binding residues (Figure 1-2). Ruan *et al.* have synthesized several α-amino acids that bear an aminodiacetic acid functionality with varying side chain length.[62] Rana and coworkers have focused on an amino acid containing an EDTA (ethylenediaminetetraacetic acid) moiety.[63] Gilbertson *et al.* have synthesized a diphenylphosphine-containing amino acid and incorporated the residue into a helical peptide.[64]

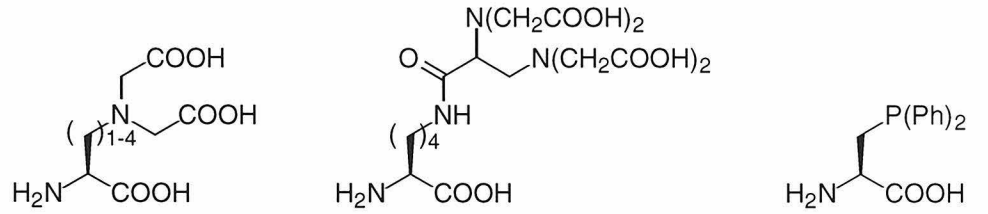

Ruan *et al.* 1990 Rana *et al.* 1992 Gilbertson *et al.* 1994

Figure 1-2 Three unnatural metal-binding α-amino acids reported in the literature.

For the construction of metallopeptides, the Imperiali group utilizes unnatural chelating residues in designed peptide motifs. An advantage for the incorporation of such residues in small peptidyl constructs is that enhanced metal binding affinities may be achieved readily. Whereas nature exploits the protein architecture to carefully position the metal-binding side chain functionalities within metalloprotein systems, unnatural metal-

chelating amino acids simplify the task by simultaneously orienting more than one ligating atom.

Unnatural chelating amino acids bearing 2,2'-bipyridyl functionalities were synthesized and investigated in the group earlier (Figure 1-3).[65-67] Chapter 2 describes the syntheses of α-amino acids bearing the phenanthrolyl functionality to further expand the amino acid repertoire. Investigations on the metal binding properties for the peptides bearing bipyridyl- and phenanthrolyl-containing amino acids are presented as well. An iterative design process for constructing a metal independent, monomeric, 23-residue ββα motif is described in Chapter 3. This motif served as a structural template for designs intended to implement zinc dependent hydrolase activity which are discussed in Chapter 4. The development of solid phase native ligation for the assembly of peptides bound to the solid support is reported in Chapter 5. These protocols for solid phase native ligation should prove useful in the future for the synthesis of combinatorial libraries of the 23-residue ββα motifs and larger peptides to enable the generation of metallopeptides with hydrolase activity.

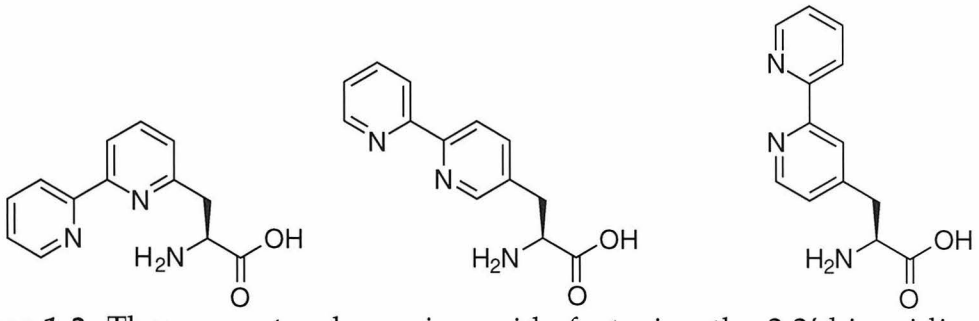

Figure 1-3 Three unnatural α-amino acids featuring the 2,2′-bipyridine functionality that have been synthesized in the group.

References

1. Bertini, I.; Gray, H. B.; Lippard, S. J.; Valentine, J. S. *Bioinorganic Chemistry*; University Science Books: Sausalito, 1994 .
2. da Silva, J. J. R. F.; Williams, R. J. P. *The Biological Chemistry of Elements*; Oxford University Press, Inc.: New York, 1991 .
3. Lippard, S. J.; Berg, J. M. *Principles of Bioinorganic Chemistry*; University Science Books: Mill Valley, 1994 .
4. Yamashita, M. M.; Wesson, L.; Eisenman, G.; Eisenberg, D. *Proc. Natl. Acad. Sci. U.S.A.* **1990**, *87*, 5648-5652.
5. Berg, J. M. *Acc. Chem. Res.* **1995**, *28*, 14-19.
6. Vallee, B. L.; Auld, D. S. *Acc. Chem. Res.* **1993**, *26*, 543-551.
7. Tainer, J. A.; Roberts, V. A.; Getzoff, E. D. *Curr. Opin. Biotechnol.* **1991**, *2*, 582-591.
8. Tainer, J. A.; Roberts, V. A.; Getzoff, E. D. *Curr. Opin. Biotechnol.* **1992**, *3*, 582-591.
9. Regan, L. *Annu. Rev. Biophys. Biomol. Struct.* **1993**, *22*, 257-281.
10. Regan, L. *Trends Biochem. Sciences* **1995**, *20*, 280-285.
11. Merkle, D. L.; Schmidt, M. H.; Berg, J. M. *J. Am. Chem. Soc.* **1991**, *113*, 5450-5451.
12. Lu, Y.; Gralla, E. B.; Roe, J. A.; Valentine, J. S. *J. Am. Chem. Soc.* **1992**, *114*, 3560-3562.
13. Lu, Y.; Vacroix, L. B.; Lowery, M. D.; Solomon, E. I.; Bender, C. J.; Peisach, J.; Roe, J. A.; Fralla, E. B.; Valentine, J. S. *J. Am. Chem. Soc.* **1993**, *115*, 5907-5918.
14. Vila, A. J.; Ramirez, B. E.; Dibilio, A. J.; Mizoguchi, T. J.; Richards, J. H.; Gray, H. B. *Inorg. Chem.* **1997**, *36*, 4567-4570.

15. Faham, S.; Mizoguchi, T. J.; Adman, E. T.; Gray, H. B.; Richards, J. H.; Rees, D. C. *J. Biol. Inorg. Chem.* **1997**, *2*, 464-469.

16. Piccioli, M.; Luchinat, C.; Mizoguchi, T. J.; Ramirez, B. E.; Gray, H. B.; Richards, J. H. *Inorg. Chem.* **1995**, *34*, 737-742.

17. Germanas, J. P.; Dibilio, A. J.; Gray, H. B.; Richards, J. H. *Biochemistry* **1993**, *32*, 7698-7702.

18. Mizoguchi, T. J.; Dibilio, A. J.; Gray, H. B.; Richards, J. H. *J. Am. Chem. Soc.* **1992**, *114*, 10076-10078.

19. Christianson, D. W.; Fierke, C. A. *Acc. Chem. Res.* **1996**, *29*, 331-339.

20. Bren, K. L.; Gray, H. B.; Banci, L.; Bertini, I.; Turano, P. *J. Am. Chem. Soc.* **1995**, *117*, 8067-8073.

21. Banci, L.; Bertini, I.; Bren, K. L.; Gray, H. B.; Turano, P. *Chem. Biol.* **1995**, *2*, 377-383.

22. Smulevich, G.; Bjerrum, M. J.; Gray, H. B.; Spiro, T. G. *Inorg. Chem.* **1994**, *33*, 4629-4634.

23. Lu, Y.; Casimiro, D. R.; Bren, K. L.; Richards, J. H.; Gray, H. B. *Proc. Natl. Acad. Sci. U.S.A.* **1993**, *90*, 11456-11459.

24. Czarnik, A. W. *Chem. Biol.* **1995**, *2*, 423-428.

25. Walkup, G. K.; Imperiali, B. *J. Am. Chem. Soc.* **1996**, *118*, 3053-3054.

26. Walkup, G. K.; Imperiali, B. *J. Am. Chem. Soc.* **1997**, *119*, 3443-3450.

27. Godwin, H. A.; Berg, J. M. *J. Am. Chem. Soc.* **1996**, *118*, 6514-6515.

28. Torrado, A.; Walkup, G. K.; Imperiali, B. *J. Am. Chem. Soc.* **1998**, in press.

29. Hellinga, H. W. *Curr. Opin. Biotech.* **1996**, *7*, 437-441.

30. Todd, R. J.; Van Dam, M. E.; Casimiro, D.; Haymore, B. L.; Arnold, F. H. *Proteins* **1991**, *10*, 156-161.

31. Suh, S.-S.; Haymore, B. L.; Arnold, F. H. *Protein Eng.* **1991**, *4*, 301-305.

32. Crowder, M. W.; Stewart, J. D.; Roberts, V. A.; Bender, C. J.; Tevelrakh, E.; Peisach, J.; Getzoff, E. D.; Gaffney, B. J.; Benkovic, S. J. *J. Am. Chem. Soc.* **1995**, *117*, 5627-5634.

33. Roberts, V. A.; Getsoff, E. D. *FASEB J.* **1995**, *9*, 94-100.

34. Wade, W. S.; Koh, J. S.; Han, N.; Hoekstra, D. M.; Lerner, R. A. *J. Am. Chem. Soc.* **1993**, *115*, 4449-4456.

35. Iverson, B. L.; Iverson, S. A.; Roberts, V. A.; Getzoff, E. D.; Tainer, J. A.; Benkovic, S. J.; Lerner, R. A. *Science* **1990**, *249*, 659-662.

36. Roberts, V. A.; Iverson, B. L.; Iverson, S. A.; Benkovic, S. J.; Lerner, R. A.; Getzoff, E. D.; Tainer, J. A. *Proc. Natl. Acad. Sci. U.S.A.* **1990**, *87*, 6654-6658.

37. Pessi, A.; Bianchi, E.; Crameri, A.; Venturini, S.; Tramontano, A.; Sollazzo, M. *Nature* **1993**, *362*, 367-369.

38. Pinto, A. L.; Hellinga, H. W.; Caradonna, J. P. *Proc. Natl. Acad. Sci. U.S.A.* **1997**, *94*, 5562-5567.

39. Klemba, M.; Gardner, K. H.; Marino, S.; Clarke, N. D.; Regan, L. *Nat. Struct. Biol.* **1995**, *2*, 368-373.

40. Kuroki, R.; Taniyama, Y.; Seko, C.; Nakamura, H.; Kikuchi, M.; Ikehara, M. *Proc. Natl. Acad. Sci. U.S.A.* **1989**, *86*, 6903-6907.

41. Inaka, K.; Kuroki, R.; Kikuchi, M.; Matsushima, M. *J. Biol. Chem.* **1991**, *31*, 20666-20671.

42. Haezebrouk, P.; De Baetselier, A.; Joniau, M.; Van Dael, H.; Rosenberg, S.; Hanssens, I. *Protein Eng.* **1993**, *6*, 643-649.

43. Toma, S.; Campagnoli, S.; Margarit, I.; Gianna, R.; Grandi, G.; Bolognesi, M.; De Filippis, V.; Fontana, A. *Biochemistry* **1991**, *30*, 97-106.

44. Braxton, S.; Wells, J. A. *Biochemistry* **1992**, *31*, 7796-7801.

45. Muheim, A.; Todd, R. J.; Casimiro, D. R.; Gray, H. B.; Arnold, F. H. *J. Am. Chem. Soc.* **1993**, *115*, 5312-5313.

46. Muller, H. N.; Skerra, A. *Biochemistry* **1994**, *33*, 14126-14135.

47. Higaki, J. N.; Haymore, B. L.; Chen, S.; Fletterick, R. J.; Craik, C. S. *Biochemistry* **1990**, *29*, 8582-8586.

48. McGrath, M. E.; Haymore, B. L.; Summers, N. L.; Craik, C. S.; Fletterick, R. J. *Biochemistry* **1993**, *32*, 1914-1919.

49. Willett, W. S.; Gillmor, S. A.; Perona, J. J.; Fletterick, R. J.; Craik, C. S. *Biochemistry* **1995**, *34*, 2172-2180.

50. Browner, M. F.; Hackos, D.; Fletterick, R. J. *Nat. Struct. Biol.* **1994**, *1*, 327-333.

51. Stewart, J. D.; Roberts, V. A.; Crowder, M. W.; Getzoff, E. D.; Benkovic, S. J. *J. Am. Chem. Soc.* **1994**, *116*, 415-416.

52. Toma, C. T.; Lear, J. D.; Nelson, M. J.; Dutton, P. L.; Robertson, D. E.; DeGrado, W. F. *J. Am. Chem. Soc.* **1994**, *116*, 856-865.

53. Robertson, D. E.; Faird, R. S.; Moser, C. C.; Urbauer, J. L.; Mulholland, S. E.; Pidikiti, J. D.; Lear, J. D.; Wand, A. J.; DeGrado, W. F. *Nature* **1994**, *368*, 425-431.

54. Coldren, C. D.; Hellinga, H. W.; Caradonna, J. P. *Proc. Natl. Acad. Sci. U.S.A.* **1997**, *94*, 6635-6640.

55. Mutter, M. *Angew. Chem. Int. Ed. Engl.* **1985**, *24*, 639-653.

56. Ghadiri, M. R.; Case, M. A. *Angew. Chem. Int. Ed. Engl.* **1991**, *32*, 1594-1597.

57. Ghadiri, M. R.; Fernholtz, A. K. *J. Am. Chem. Soc.* **1990**, *112*, 9633-9635.

58. Lieberman, M.; Sasaki, T. *J. Am. Chem. Soc.* **1991**, *113*, 1470-1471.

59. Handel, T. M.; Williams, S. A.; DeGrado, W. F. *Science* **1993**, *261*, 879-885.

60. Handel, T.; DeGrado, W. F. *J. Am. Chem. Soc.* **1990**, *112*, 6710-6712.

61. Regan, L.; Clarke, N. D. *Biochemistry* **1990**, *29*, 10878-10883.

62. Ruan, F.; Chen, Y.; Hopkins, P. B. *J. Am. Chem. Soc.* **1990**, *112*, 9403-9404.

63. Rana, T. M.; Ban, M.; Hearst, J. E. *Tetrahedron Lett.* **1992**, *33*, 4521-4524.

64. Gilbertson, S. R.; Chen, G.; McLoughlin, M. *J. Am. Chem. Soc.* **1994**, *116*, 4481-4482.

65. Imperiali, B.; Prins, T. J.; Fisher, S. L. *J. Org. Chem.* **1993**, *58*, 1613-1616.

66. Imperiali, B.; Fisher, S. L. *J. Org. Chem.* **1992**, *57*, 757-759.

67. Imperiali, B.; Fisher, S. L. *J. Am. Chem. Soc.* **1991**, *113*, 8527-8528.

Chapter 2

Tuning the Metal Binding Affinity of Metallopeptides: Incorporation of Unnatural Bidentate α-Amino Acids and Exploitation of Peptide Structure

Reprinted in part with permission from Cheng, R. P.; Fisher, S. L.; Imperiali, B. *J. Am. Chem. Soc.* **1996**, *118*, 11349-11356. Copyright 1996 American Chemical Society.

Introduction

Recent efforts in the *de novo* design of metalloproteins have focused on the assembly of polypeptides with defined structural, and potentially functional, properties.[1, 2] The production of a peptidyl motif designed to detect Zn^{II} in solution emphasizes the importance of tuning the metal binding affinity of such constructs.[3] The ability to modulate metal binding affinity is essential in order to operate such peptide-based sensors over a wide metal cation concentration range. Furthermore, it is necessary for the peptide to preferentially bind the metal cation of interest to exploit such peptides in sensor applications.

One approach to the construction of metallopeptides involves the use of novel multidentate metal-binding residues.[4-11] An advantage to the utilization of such residues in small peptidyl constructs is that enhanced metal binding affinities may be achieved readily. Whereas nature exploits the protein architecture to carefully position the metal-binding side chain functionalities within metalloprotein systems, unnatural metal-chelating amino acids simplify the task by simultaneously orienting more than one ligating atom. Additionally, the chemical synthesis of small peptides generally affords milligram quantities of material and allows the incorporation of the unnatural amino acids at any position in the primary sequence.

The bidentate hetereoaromatic ligands 2,2′-bipyridine and 1,10-phenanthroline are among the best known coordination agents.[12-16] These multidentate nitrogen ligands generally afford high binding affinities for metal cations due to the chelation effect and the π-accepting ability of these moieties.[17] While alkyl substitution at the 6,6′-positions of 2,2′-bipyridine and the 2,9-positions of 1,10-phenanthroline is expected to raise the basicity of the donor nitrogens, substituted ligands generally exhibit weaker metal binding affinities

than the parent heterocycle due to steric effects. Therefore, alkyl substitution can affect the metal binding preference and complex stoichiometry. Furthermore, attachment of these aromatic metal-binding functionalities to the backbone through one methylene would provide residues with conformations similar to the natural amino acids Phe, Tyr, and Trp. Adopting such a design enables facile prediction of the conformation of the unnatural residue, since there is considerable understanding of the conformation of the natural aromatic residues. Importantly, the 2,2′-bipyridine and 1,10-phenanthroline functionalities are stable under aqueous conditions, thereby allowing valid investigations of the corresponding peptides. α-Amino acids featuring these bidentate ligands as side chains can therefore be exploited to control the metal cation binding affinities and preferences of the metallopeptides (Figure 2-1).

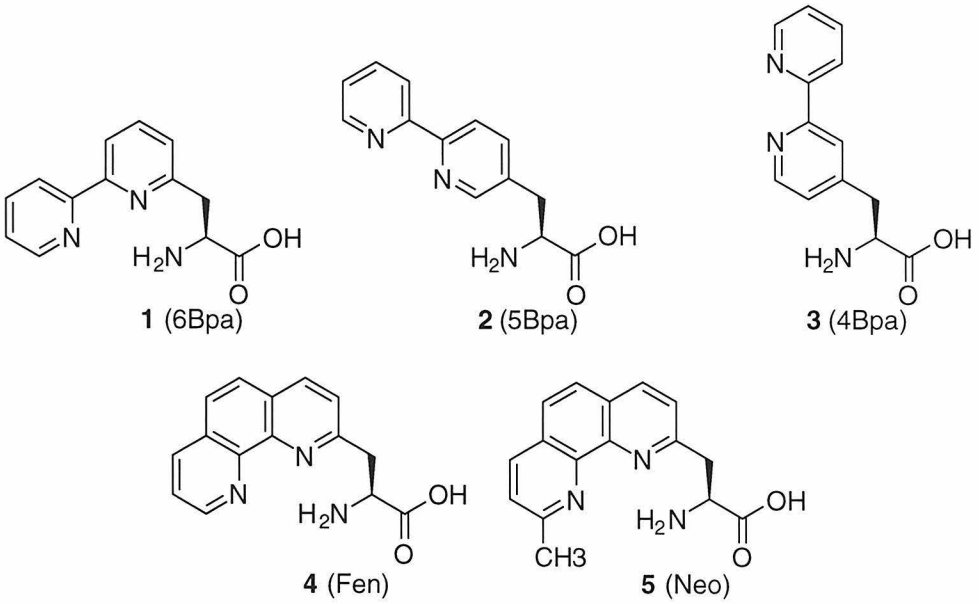

Figure 2-1 Various unnatural α-amino acids featuring the 2,2′-bipyridine, 1,10-phenanthroline and methyl-1,10-phenanthroline functionalities.

The metal-binding properties of several peptides that incorporate 2,2′-bipyridine, 1,10-phenanthroline or 2,9-dimethyl-1,10-phenanthroline (neocuproine) functionalities are described in this chapter. The syntheses and

peptide incorporation of the 6-, 5- and 4- substituted (*S*)-2-amino-3-(2,2'-bipyridyl)propanoic acids (**1**, 6Bpa; **2**, 5Bpa; **3**, 4Bpa) have been previously reported.[6-8] The utility of these residues has been highlighted in the semisynthesis of cytochrome *c* mutants with enhanced electron transfer properties.[18] Additionally, the residue (*S*)-2-amino-3-(1,10-phenanthrol-2-yl)propanoic acid (**4**, Fen) has been used in an iterative design process to form a folded, metal-independent ββα motif (for details see Chapter 3).[19, 20] The syntheses of Fen (**4**) and the novel neocuproine-containing α-amino acid, (*S*)-2-amino-3-(9-methyl-1,10-phenanthrol-2-yl)propanoic acid (**5**, Neo), are presented in this chapter. These syntheses afford multigram quantities of N^{α}-Fmoc protected α-amino acids for incorporation into polypeptides. The key step in the syntheses of these unnatural amino acids involves an enzymatic resolution with alkaline protease.[7, 21] These unnatural amino acids are completely compatible with peptide assembly using standard Fmoc-based (Fmoc, 9-Fluorenylmethyloxycarbonyl) solid phase methodology and do not require side chain protection.[22] Therefore, these bidentate unnatural residues with enviable inherent metal-binding properties can be incorporated into small peptides readily.

Naturally occurring metalloproteins frequently form metal binding sites with multiple residues to achieve the high affinity and selectivity for their native metal cations. Therefore, the incorporation of more than one metal-ligating amino acid in designed metallopeptides could enhance the affinity and selectivity of such constructs. In order for two residues to cooperatively participate in the formation of a high affinity metal binding site, it is advantageous to place the coordinating side chain functionalities in close proximity. One of the most direct methods to achieve this placement would be to situate the key residues flanking a preorganized polypeptide motif such as a

reverse turn. The chain reversal afforded by a β-turn would place residues at either end of the sequence proximal to each other and promote the cooperative binding of metal cations.[23] Judicious placement of the residues is essential to situate the two metal binding side chains on the same face of the β-hairpin motif (Figure 2-2). Molecular modeling studies reveal that two metal-binding amino acids flanking four turn-forming residues places the metal coordinating moieties on the same face of the motif and in close proximity. The type II β-turn has been studied extensively,[24-26] and therefore different peptide sequences with varying turn-forming propensities were utilized to connect the two metal-binding residues. The metal binding affinity can therefore be varied by changing the extent of structural preorganization of the motif required for high affinity and cooperative binding between two ligating residues.

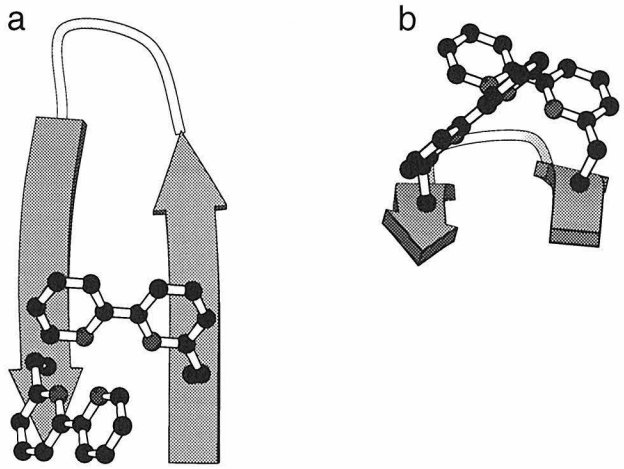

Figure 2-2 (a) Schematic diagram of the β-hairpin motif desinged to bring two 6Bpa residues into close proximity (generated using the program Molscript[27]). (b) An edge-on view of the same model.

Several hexapeptides incorporating the unnatural metal-chelating amino acids described above were synthesized and their metal-binding properties were investigated. Peptides containing only one bidentate residue and those with two bidentate amino acids display different affinities for metal cations, indicating cooperative ligation in the latter. Furthermore, constructs containing both a

bidentate residue and a naturally-occurring metal-binding residue (Asp or His) were prepared and exhibited varying metal binding affinities. Two sequences, -Val-Pro-DSer-Phe- and -Thr-Pro-DAla-Val- with different type II β-turn propensities were used to connect the metal-binding residues to probe the influence of structural preorganization on metal binding affinity.[23, 28, 29] In light of the successful utilization of a type II′ turn as a structural nucleation element in a designed ββα motif,[19, 20] an additional peptide containing the sequence -Val-DPro-Ser-Phe-, which was predicted to form a type II′ β-turn, was also investigated. For all the peptides studied, the *N*-termini were capped with an acetyl group and the *C*-termini were capped with an amide in order to avoid potential peptide conformational changes due to electrostatic interactions and competing metal cation coordination effects involving the free carboxyl or amino termini.

Results and Discussion

Synthesis of N^{α}-Fmoc-(*S*)-2-Amino-3-(1,10-phenanthrol-2-yl)propanoic Acid (Fmoc-Fen) and N^{α}-Fmoc-(*S*)-2-Amino-3-(9-methyl-1,10-phenanthrol-2-yl)propanoic Acid (Fmoc-Neo)

Syntheses of the two amino acids were accomplished using a modified version of the Sørenson method (Scheme 2-1).[30] Alkylation of diethyl acetamidomalonate[31] with the corresponding chlorides (**6**[32, 33], **7**[34]) in sodium ethoxide/ethanol solution yielded the decarboxylated alkylated adducts (**8**, **9**). In order to achieve full consumption of the chloride compounds **6** and **7**, an excess amount of diethyl acetamidomalonate was used. Exhaustive hydrolysis of the racemic alkylated adducts in refluxing 6N HCl was performed to hydrolyze the *N*-acetyl and ethyl ester groups, which yielded racemic mixtures of the fully

unprotected α-amino acids. Esterfication of the amino acids in acidic methanol produced the racemic amino acid methyl esters (**10**, **11**) for enzymatic resolution of the residues. Selective catalytic hydrolysis of the α-amino acid methyl esters by alkaline protease[7, 21] afforded the L-enantiomers in high stereoselectivity (>98% ee as determined by chiral high performance liquid chromatography). The absolute configuration of the resulting amino acids were consistent with the specificity of the enzyme to hydrolyze the L-amino acid ester, and the convention of the elution profile for the CrownPak CR (+) chiral column. Furthermore, the change of optical rotation upon lowering the pH for Neo followed the Clough-Lutz-Jirgenson rule (pH 8.8, $[\alpha]^{25}_D$ -80.3; pH 0, $[\alpha]^{25}_D$ +8.5),[35] which further confirms the configuration of the stereocenter. Subsequent protection of the L-amino acids with *N*-9-fluorenylmethylsuccinimidyl carbonate (Fmoc-OSu) yielded the fully protected phenanthroline amino acid derivatives (**12**, **13**), which were used directly for solid phase peptide synthesis. All steps leading to both α-amino acids are amenable to large scale synthesis. This further expansion in the repertoire of α-amino acid building blocks enables the construction of a wide variety of novel metal-binding peptides. These multidentate amino acids provide avid metal binding within short peptides and are also useful as structural probes due to their rich spectroscopic properties.[19, 20]

Scheme 2-1. Synthesis of Fmoc-Protected Fen and Neo Amino Acids

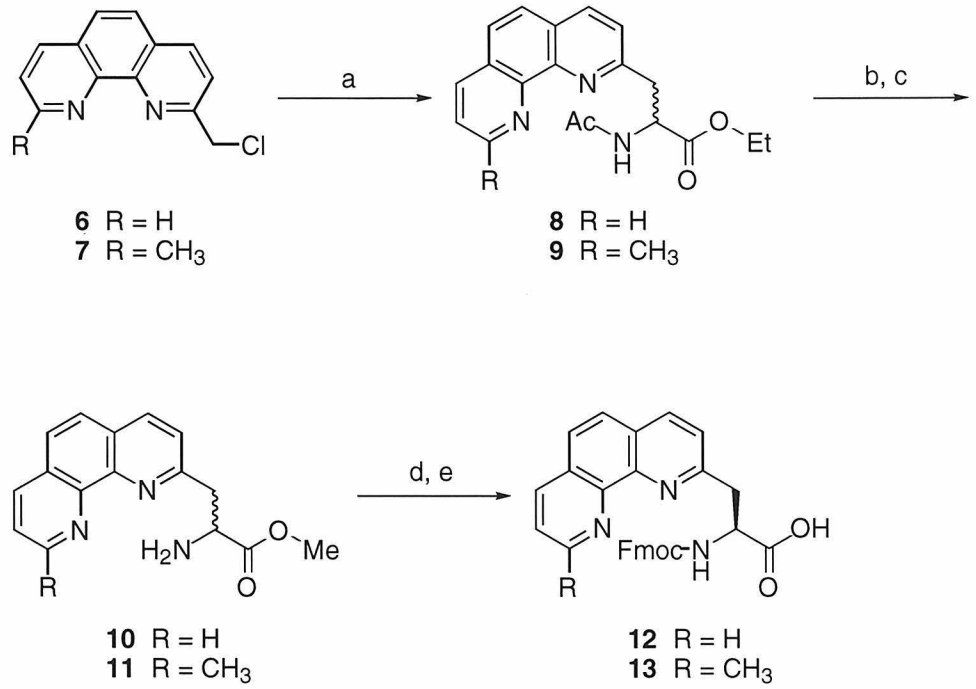

6 R = H
7 R = CH_3

8 R = H
9 R = CH_3

10 R = H
11 R = CH_3

12 R = H
13 R = CH_3

[a] Diethyl acetamidomalonate, EtONa, EtOH reflux (**8**, 67%; **9**, 69%).
[b] 6N HCl, reflux.
[c] HCl(g), MeOH, reflux to room temperature (two steps; **10**, 100%; **11**, 93%).
[d] Alkaline protease, ^{t}BuOH, 10% $NaHCO_3$, room temperature.
[e] Fmoc-OSu, dioxane, bicarbonate solution, room temperature (**12**, 85%, 92-94% ee; **13**, 92%, >98% ee)

Dissociation Constants of the Peptide-M^{II} Complexes

The hexapeptides are designated according to the residues present at positions 1 and 6. Standard three-letter abbreviations are employed for natural residues, while "6Bpa", "5Bpa" and "4Bpa" are used to designate the unnatural α-amino acids **1**, **2** and **3**, and "Fen" and "Neo" are used for residues **4** and **5** respectively. The prime (') designates that the type II' turn sequence -Val-DPro-Ser-Phe- connects the first and last residues. The subscript "w" indicates the connecting sequence -Thr-Pro-DAla-Val- which displays a limited tendency to form a turn.[29] Lack of any additional indication would refer to the intervening sequence -Val-Pro-DSer-Phe- which exhibits stronger turn propensity.[25, 28]

Bpa-Containing Peptides

The peptides 4BpaPhe$_w$ (Ac-4Bpa-Thr-Pro-DAla-Val-Phe-NH_2), 5BpaPhe$_w$ (Ac-5Bpa-Thr-Pro-DAla-Val-Phe-NH_2) and 6BpaPhe$_w$ (Ac-6Bpa-Thr-Pro-DAla-Val-Phe-NH_2) were synthesized and studied. Additionally, peptides 6Bpa6Bpa (Ac-6Bpa-Val-Pro-DSer-Phe-6Bpa-NH_2) and 6Bpa6Bpa$_w$ (Ac-6Bpa-Thr-Pro-DAla-Val-6Bpa-NH_2), which both contain two 6Bpa residues were also investigated. The metal cation titrations of these Bpa-containing peptides were monitored by absorption spectroscopy (UV-Vis) as illustrated in Figure 2-3. The $\pi \rightarrow \pi^*$ transition of the bipyridyl moiety displays a distinct red-shift upon chelation of metal cations. Clean isosbestic points were observed, supporting a two-state model equilibrium. Binding isotherms were obtained from such experiments. The apparent dissociation constants for the peptide-M^{II} complexes were determined to be the free metal cation concentration when half of the peptide was bound. The apparent dissociation constants of the peptide-M^{II} complexes for the Bpa-containing peptides are summarized in Table 2-1.

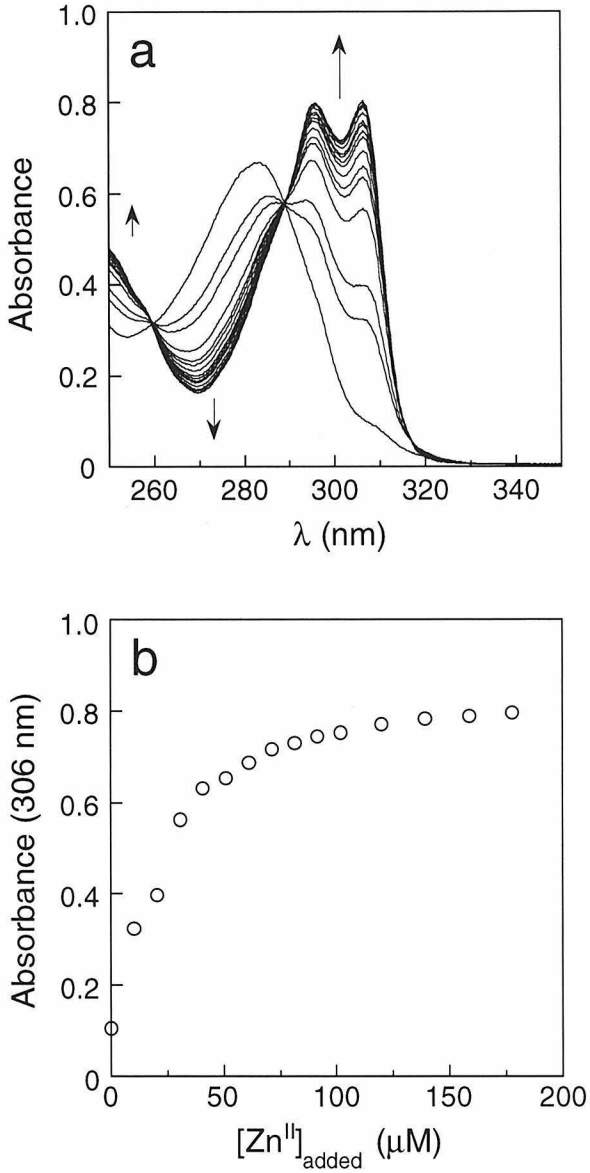

Figure 2-3 A typical metal cation titration of a Bpa-containing peptide monitored by absorption spectroscopy. (a) Absorption spectra of 52 μM $4BpaPhe_W$ upon addition of $ZnCl_2$ up to 178 μM at pH 6.8-7.0 in 0.2 M NaCl. (b) The binding isotherm obtained from the data shown in panel a at 306 nm.

Table 2-1 Apparent Dissociation Constants (μM) for Bpa-Containing Peptide-M^{II} Complexes[a]

Peptide	Sequence	Zn^{II}	Co^{II}
$4BpaPhe_W$	Ac-4Bpa-Thr-Pro-DAla-Val-Phe-NH_2	22	ND[b]
$5BpaPhe_W$	Ac-5Bpa-Thr-Pro-DAla-Val-Phe-NH_2	19	ND[b]
$6BpaPhe_W$	Ac-6Bpa-Thr-Pro-DAla-Val-Phe-NH_2	2700	1100
$6Bpa6Bpa_W$	Ac-6Bpa-Thr-Pro-DAla-Val-6Bpa-NH_2	960	110
6Bpa6Bpa	Ac-6Bpa-Val-Pro-DSer-Phe-6Bpa-NH_2	16	7

[a] Metal cation titrations performed at pH 7 in 0.2 M NaCl.
[b] Dissociation constants not determined due to stoichiometry of 2:1 peptide:metal.

Peptides $4BpaPhe_W$, $5BpaPhe_W$ and $6BpaPhe_W$ each contain only one metal-binding Bpa residue. These peptides differ only at the point of attachment to the β-carbon of the bipyridyl-containing amino acid (4Bpa, 5Bpa and 6Bpa). Since the 4 and the 6 isomers behaved differently in the construction of the bipyridyl-alanine cytochrome *c* mutants,[18] the various isomers were investigated in peptides with the same underlying sequence to evaluate their individual metal binding characteristics more carefully. The dissociation constants of the peptide-Zn^{II} complexes for $6BpaPhe_W$, $5BpaPhe_W$ and $4BpaPhe_W$ exhibit the overall trend $6BpaPhe_W > 5BpaPhe_W \sim 4BpaPhe_W$ (Table 2-1). Thus, the peptide $6BpaPhe_W$ shows the lowest affinity for Zn^{II} among the three peptides. The steric hindrance of the *ortho* substitution presumbly results in the larger dissociation constant for peptide $6BpaPhe_W$. As the substitution of the residues 5Bpa and 4Bpa does not interfere with the metal binding process, the peptides $5BpaPhe_W$ and $4BpaPhe_W$ exhibit similar affinities for Zn^{II}. Unlike all the other peptide-M^{II} complexes studied in this report, the stoichiometries of the peptide-Co^{II} complexes for $5BpaPhe_W$ and $4BpaPhe_W$ were determined to be 2:1, reflecting the

unencumbered chelation by these residues. Thus, a change in the point of attachment of the bipyridyl ring to the amino acid results in alteration of both the complex stoichiometry and the metal binding affinity.

Two bidentate metal-chelating residues were positioned at opposite ends of peptides 6Bpa6Bpa and 6Bpa6Bpa$_W$. The intervening sequences were designed to adopt a β-turn structure with different turn-forming propensities. The sequence -Val-Pro-DSer-Phe- has been shown to exhibit more turn character than -Thr-Pro-DAla-Val- by CD and NMR spectroscopies.[25, 28, 29] The affinities of peptides 6Bpa6Bpa$_W$ and 6Bpa6Bpa for Zn^{II} and Co^{II} were significantly stronger than those observed for peptide 6BpaPhe$_W$ (i.e. lower dissociation constants), indicating the cooperative participation of both bipyridyl moieties as ligands (Table 2-1). This participation of a second 6Bpa residue enhances the metal binding affinity by two orders of magnitude. The peptide 6Bpa6Bpa, which contains an intervening sequence with higher type II β-turn propensity, exhibits stronger binding for both Zn^{II} and Co^{II} than the weak turn-forming peptide 6Bpa6Bpa$_W$. This result strongly suggests that the connecting residues can serve to bring the two metal chelating residues into close proximity and therefore play a role in the process of binding metal cations (Figure 2-4). Thus, through the control of the peptidyl structure, the metal binding affinity of a peptide for a specific metal cation can be modulated by 60 fold.

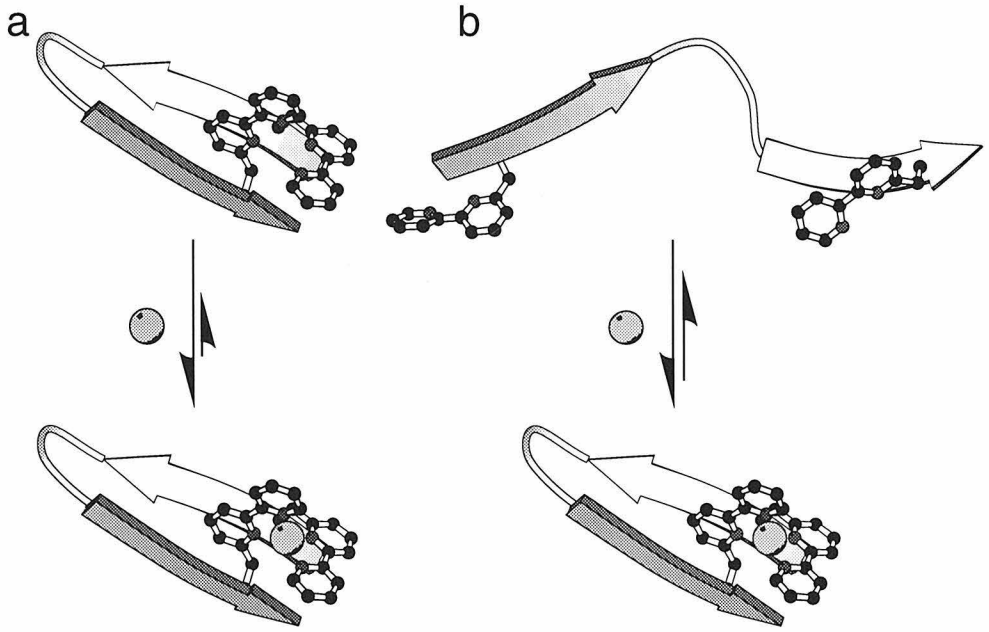

Figure 2-4 Schematic diagram of the metal binding event for (a) the hexapeptide 6Bpa6Bpa incorporating a structurally preorganized intervening sequence with high turn propensity and (b) the hexapeptide 6Bpa6Bpa$_W$ with a less structured connecting sequence (generated using the program Molscript[27]).

Fen- and Neo-Containing Peptides

Peptides $FenPhe_W$ (Ac-Fen-Thr-Pro-DAla-Val-Phe-NH_2), FenLeu (Ac-Fen-Val-Pro-DSer-Phe-Leu-NH_2), and NeoPhe (Ac-Neo-Val-Pro-DSer-Phe-Phe-NH_2), were synthesized and evaluated to assess the inherent chelation properties of the residues Fen and Neo. Additionally, five hexapeptides which were designed to cooperatively bind to a single metal cation *via* coordination of a bidentate residue (Fen or Neo) and an auxiliary natural metal binding amino acid (His or Asp) were investigated (Table 2-2). The metal cation titrations of the Fen- and Neo-containing peptides were monitored by UV-Vis spectroscopy (Figure 2-5 and 2-6). A distinct red-shift of the $\pi \rightarrow \pi^*$ transition for the phenanthrolyl moiety was observed upon binding metal cations. Binding isotherms were obtained from such titrations. Clean isosbestic points were observed for all the titrations except for experiments performed on peptide NeoPhe, in which essentially no change in the absorption spectrum was observed upon addition of Zn^{II} or Co^{II}. Fortunately, metal cation titrations monitored by circular dichroism (CD) spectroscopy showed distinct changes in the near-UV region (250 to 300 nm) attributable to the neocuproine moiety (Figure 2-7). The binding isotherms for the formation of the NeoPhe-M^{II} complexes were therefore obtained from these CD experiments. Calculations employing an iterative method based on the Scott equation[36] afforded the dissociation constants for the peptide-M^{II} complexes (Table 2-2). The final iteration from a typical analysis is shown in Figure 2-8, in which $[M^{II}]_{free}/b \cdot \Delta A$ ($[M^{II}]_{free}$ = free M^{II} concentration in solution, b = path length of cuvette, ΔA = change in absorbance at the wavelength of interest) is plotted against $[M^{II}]_{free}$ and the apparent dissociation constant is given by y-intercept/slope.

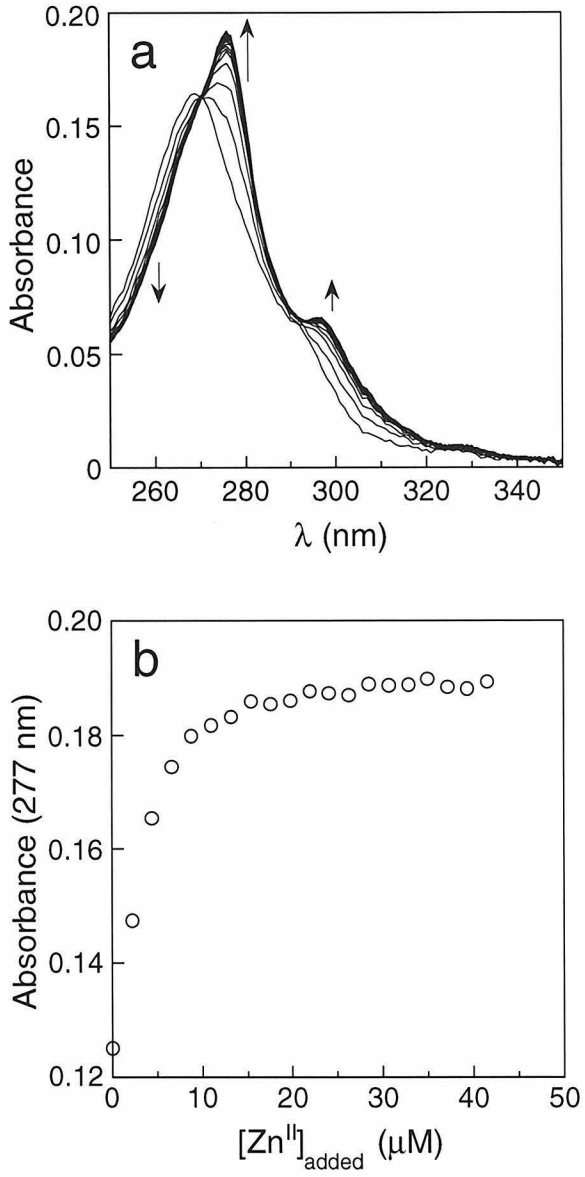

Figure 2-5 A typical metal cation titration of a Fen-containing peptide monitored by absorption spectroscopy. (a) Absorption spectra of 7.85 μM FenHis upon addition of $ZnCl_2$ up to 42 μM in 0.05 M HEPES [*N*-(2-hydroxyethyl)piperazine-*N'*-(2-ethane-sulfonic acid] buffer at pH 8.25. (b) The binding isotherm obtained from the data shown in panel a at 277 nm.

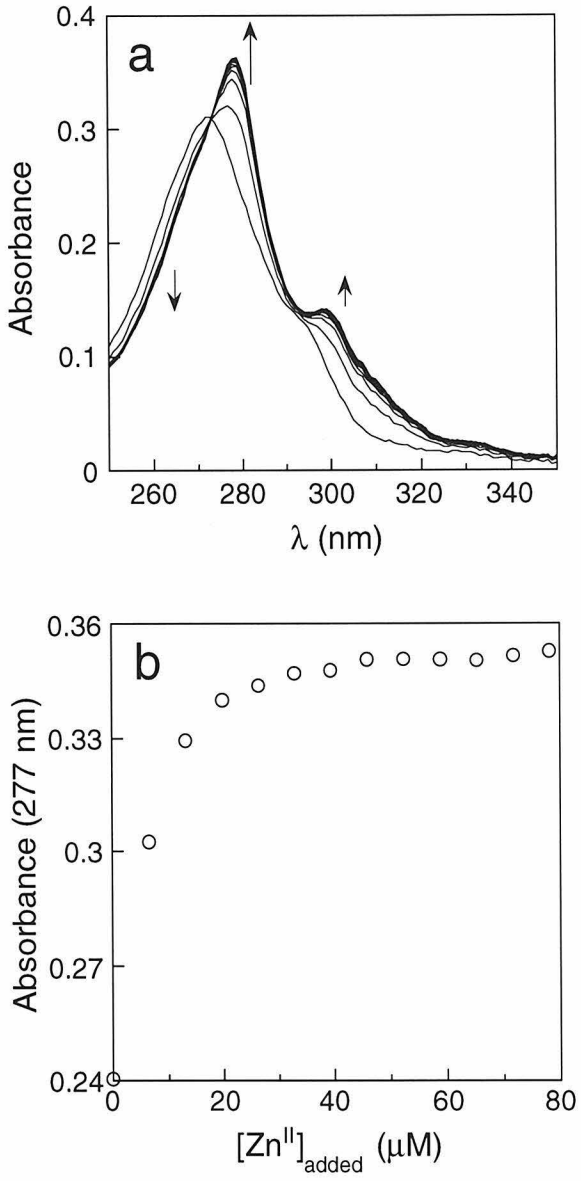

Figure 2-6 A typical metal cation titration of a Neo-containing peptide monitored by absorption spectroscopy. (a) Absorption spectra of 12.8 μM NeoHis upon addition of $ZnCl_2$ up to 123 μM in 0.05 M HEPES buffer at pH 8.25. (b) The binding isotherm obtained from the data shown in panel a at 280 nm.

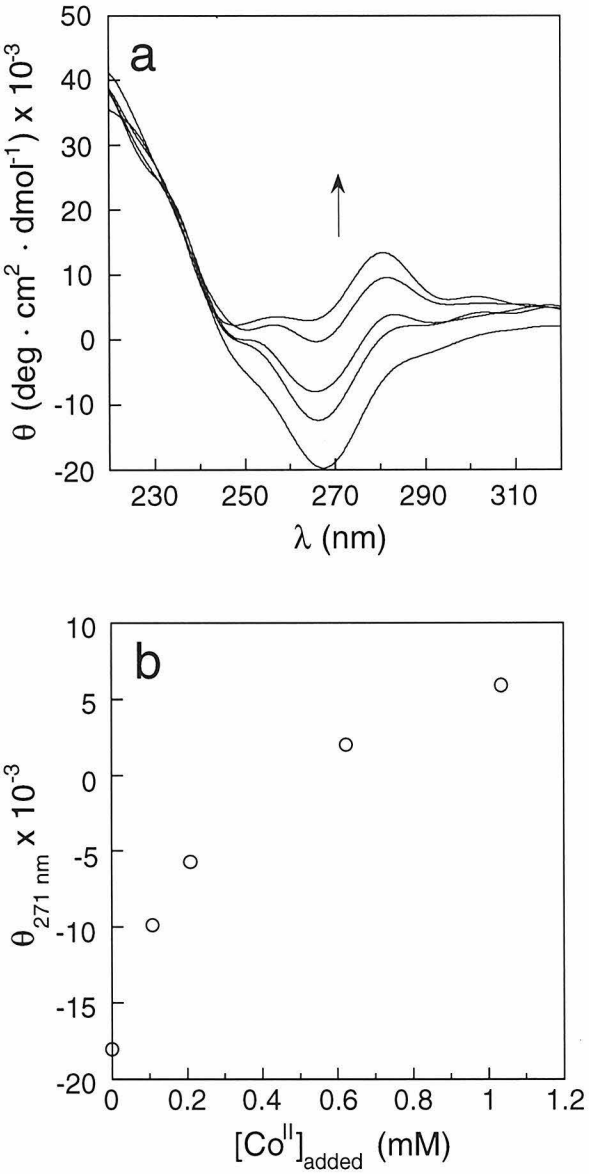

Figure 2-7 A Co^{II} cation titration of a Neo-containing peptide monitored by circular dichroism spectroscopy. (a) Circular dichroism spectra of 66 μM NeoPhe upon addition of $CoCl_2$ up to 1.0 mM in 0.01 M TRIS [2-amino-2-(hydroxymethyl)-1,3-propanediol] buffer at pH 8.25. (b) The binding isotherm obtained from the data shown in (a) at 271 nm.

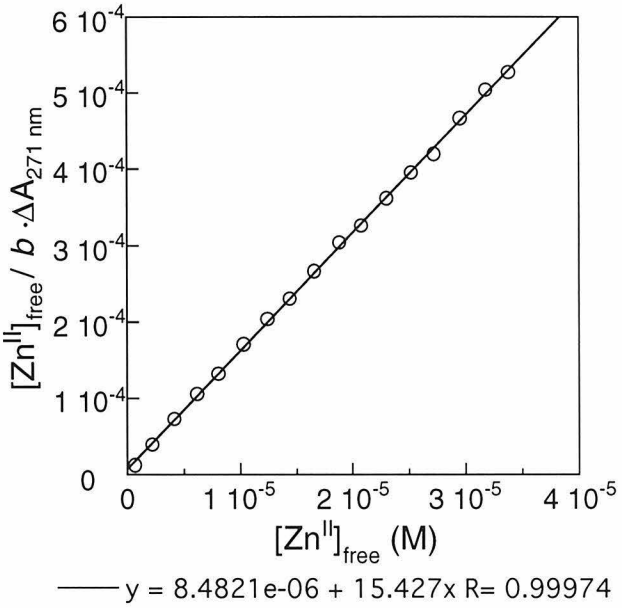

Figure 2-8 The final analysis of a typical metal cation titration to obtain the apparent dissociation constant based on the Scott equation. The data from Figure 2-5 where 7.85 μM FenHis is titrated with $ZnCl_2$ up to 42 μM. The ratio of the y-intercept and slope derived from the linear fit gives the dissociation constant of 0.55 μM.

Table 2-2 Apparent Dissociation Constants (μM) of Fen- and Neo-Containing Peptide-M^{II} Complexes[a]

Peptide	Sequence	Zn^{II}	Co^{II}
$FenPhe_W$	Ac-Fen-Thr-Pro-DAla-Val-Phe-NH_2	26.8	7.91
FenLeu	Ac-Fen-Val-Pro-DSer-Phe-Leu-NH_2	51.7	13.8
$FenHis_W$	Ac-Fen-Thr-Pro-DAla-Val-His-NH_2	1.50	2.48
FenHis	Ac-Fen-Val-Pro-DSer-Phe-His-NH_2	0.65	0.60
FenHis'	Ac-Fen-Val-DPro-Ser-Phe-His-NH_2	0.96	1.57
FenAsp	Ac-Fen-Val-Pro-DSer-Phe-Asp-NH_2	8.28	3.91
NeoPhe	Ac-Neo-Val-Pro-DSer-Phe-Phe-NH_2	110[b]	300[b]
NeoHis	Ac-Neo-Val-Pro-DSer-Phe-His-NH_2	0.69	5.45

[a] Metal cation titrations performed in 0.05 M HEPES buffer at pH 8.25.
[b] Values obtained from titrations performed in 0.01 M TRIS buffer at pH 8.25 monitored by circular dichoism (CD) spectroscopy.

Peptides $FenPhe_W$, FenLeu, and NeoPhe were analyzed to determine the inherent metal-binding properties of these residues. The peptides $FenPhe_W$ and FenLeu have stronger affinities for Zn^{II} and Co^{II} than peptide NeoPhe (Table 2-2). This demonstrates that the steric effect of the 9-methyl group of Neo interferes with metal chelation. This trend parallels that observed for the parent ligands 2-methyl-1,10-phenanthroline (Zn^{II} complex, K_D = 11.0 μM; Co^{II} complex, K_D = 7.94μM) and 2,9-dimethyl-1,10-phenanthroline (neocuproine) (Zn^{II} complex, K_D = 79.4 μM; Co^{II} complex, K_D = 63μM). [37] However, peptide NeoPhe exhibits a preference to bind Zn^{II} over Co^{II} . This observation is unusual given the opposite trends observed for Bpa and Fen peptides as well as the parent ligand neocuproine. This reversal in preference is most likely due to the steric bulk introduced by the peptide. However, the participation of functional

groups other than the Neo side chain cannot be completely ruled out. Interestingly, peptide FenPhe$_W$ exhibits higher metal-binding affinity than peptide FenLeu for both Zn^{II} and Co^{II}. This trend suggests that the sequence with higher turn propensity effectively recruits an "innocent" residue that is incapable of binding metal to the chelating functionality, which would result in masking of the metal binding functionality, and thereby diminishing the metal-binding ability of the chelating residue.

Peptides FenHis$_W$, FenHis, FenHis', and FenAsp exhibit stronger metal binding affinities than the parent "Fen only" peptides, FenPhe$_W$ and FenLeu (Table 2-2). Thus, the auxiliary naturally-occurring coordinating residues (His or Asp) incorporated in these peptides must be actively participating in the metal binding event. Furthermore, the greater metal binding affinity of peptide FenHis compared to peptide FenHis$_W$ suggests that the sequence with higher turn propensity promotes a higher metal binding affinity, which is consistent with the results obtained for peptides 6Bpa6Bpa and 6Bpa6Bpa$_W$. Additionally, FenHis' binds Co^{II} and Zn^{II} with affinities similar to FenHis. In this regard, the type II' turn does not appear to contribute a significant advantage over the type II turn in preorganizing the metal binding site.

Comparison between peptides NeoPhe and NeoHis, illustrates that incorporation of the auxiliary metal binding residue, histidine, results in a 160 fold increase in affinity for Zn^{II} (Table 2-2). Additionally, the peptide NeoHis was anticipated to have diminished metal binding properties compared to the analogous Fen-containing peptide due to the steric crowding of a bound metal cation by the 9-methyl group near a nitrogen donor atom. While this was demonstrated for the Co^{II} binding affinities of peptides NeoHis and FenHis, the K_D of the Zn^{II} complexes for the two peptides were comparable. In addition, there was one order of magnitude preference for NeoHis to bind Zn^{II} over Co^{II}.

This result highlights the potential for tuning the metal binding affinities and selectivities of short peptide motifs for future metal cation sensor designs by judicious selection of the unnatural bidentate residue and auxiliary naturally-ocurring metal-ligating amino acid. Since Co^{II} is known to favor octahedral geometry due to ligand field stabilization while Zn^{II} has no specific geometrical preference,[2, 38] it is possible that the steric effect of the 9-methyl group interferes with the formation of an octahedral complex, and results in the decrease in binding affinity for the peptide-Co^{II} complex. On the other hand, Zn^{II} does not prefer a specific geometry and therefore exhibits similar metal binding properties for FenHis and NeoHis. It should be noted that the differences in metal binding preferences between FenHis and NeoHis must be ascribed to a single methyl group.

Summary

Several guidelines for the design of short metallopeptides with high metal binding affinity can be derived from these studies. First, the novel chelating amino acids (Bpa, Fen, Neo) presented generally bind metal cations with higher affinity than naturally occurring metal-binding residues due to the bidentate nature of the side chain functionality. The selection of unnatural chelating amino acid can affect both affinity and stoichiometry of the metal complex for the designed peptide. The metal binding affinity for the hexapeptides with bipyridyl-containing amino acids follows the trend 4Bpa ~ 5Bpa > 6Bpa. However, the stoichiometries of the peptide-Co^{II} complexes for peptides $4BpaPhe_W$ and $5BpaPhe_W$ are 2:1. In contrast, high affinity and 1:1 stoichiometry can be achieved through the incorporation of the phenanthrolyl-containing amino acids (Fen, Neo). Second, further modulation of the metal binding affinity can be accomplished *via* the incorporation of auxiliary metal-binding amino acids

(6Bpa, Asp or His). The participation of an auxiliary metal-binding residue is exemplified by the 160 fold enhancement in Zn^{II} binding affinity for NeoHis over NeoPhe. Third, control of the peptide structure can be exploited to bring two residues into close proximity to either facilitate or disrupt the metal binding process. Peptide 6Bpa6Bpa which contains a sequence with high turn propensity connecting two 6Bpa residues exhibits a 80 fold higher affinity for Zn^{II} than peptide $6Bpa6Bpa_W$ which has a considerably less structured intervening sequence. Peptide FenLeu which contains a sequence with high turn propensity connecting the chelating Fen and the "innocent" Leu residue exhibits a 2 fold lower affinity for Zn^{II} and Co^{II} compared to peptide $FenPhe_W$ which has a considerably less structured intervening sequence for linking Fen and the innocent residue Phe.

Conclusion

The modulation of metal binding affinity in designed peptides has been demonstrated in this study by varying three different features: selection of unnatural bidentate residue, incorporation of auxiliary metal-binding amino acid and control of structural preorganization of the peptide architecture. Dissociation constants ranging from 10^{-3} to $<10^{-6}$ M for Zn^{II} have been achieved by altering these three features. The combination of a variety of bidentate amino acids with the structural preorganization afforded by the peptidyl template, such as a reverse turn, results in the ability to tune the metal binding affinity of metallopeptides. The availability of the novel chelating α-amino acids and the guidelines for their utilization derived in this chapter can be exploited in future metalloprotein and peptide-based sensor design.

Acknowledgments

The work in the chapter was performed in collaboration with Stewart L. Fisher (Ph.D., Caltech, 1993). Stew had synthesized and investigated the Bpa-containing peptides, pioneered the synthesis of Fen, and initiated the studies on the Fen-containing peptides $FenPhe_W$, $FenHis_W$, and FenHis. Additionally, Thomas, J. Prins (M.S., Caltech, 1992) was responsible for some of the earlier work on the Bpa-containing peptides. The bulk of the work presented in this chapter appeared in the following publication:

Cheng, R. P.; Fisher, S. L.; Imperiali, B. "Metallopeptide Design: Tuning the Metal Cation Affinities with Unnatural Amino Acids and Peptide Secondary Structure", *J. Am. Chem. Soc.* **1996**, *118*, 11349-11356.

Experimental Section

Synthesis

All reagents were obtained from Aldrich Chemical Co. and used without further purification. Protease Type VIII (Subtilisin Carlsberg, Bacterial, CA#[9014-01-1], 11.6 units/mg) was purchased from Sigma Chem. Co., and stored at 4°C. All synthetic intermediates were stored at 4°C after purification. ^1H (300 MHz)and ^{13}C (75 MHz) NMR spectra were recorded on a General Electric QE-300 spectrometer.

Racemic 2-Acetamido-3-(1,10-phenanthrol-2-yl)propanoic Acid Ethyl Ester (8). Diethyl acetamidomalonate (5.679 g, 26.1 mmol) was added to a solution of sodium (0.6077 g, 26.4 mmol) in 60 mL absolute ethanol and stirred for 30 minutes. A solution of 2-chloromethyl-1,10-phenanthroline[32, 33] (**6**, 3.033 g, 13.2 mmol) in 15 mL absolute ethanol was added dropwise to the mixture. After

16 hours at reflux, the mixture was cooled, concentrated to a thick red oil, suspended in water (150 mL), and extracted with $CHCl_3$ (3 x 150 mL). The organic fractions were combined and concentrated to a red oil. The oil was suspended in 0.05 M HCl and washed with ethyl acetate. The aqueous phase was neutralized with Na_2CO_3(s) over ice and extracted with $CHCl_3$ (5 x 150 mL). The organic fractions were combined, dried over Na_2SO_4 and then concentrated to a red oil (2.96 g, 67%). The crude product was taken on to the next step without further purification. An analytical sample was purified using a neutral Al_2O_3 column (2:1 CH_2Cl_2:EtOAc) to yield a white solid; mp(d): 182.5-184.3 °C; TLC (Al_2O_3; 2:1 CH_2Cl_2:EtOAc, UV detection) R_f = 0.23; HRMS: calculated for $[MH]^+$ $C_{19}H_{20}N_3O_3$ [338.1505]; observed [338.1504]; ^1H NMR ($CDCl_3$) δ: 1.14 (t, 3H, J = 7.19 Hz), 2.11 (s, 3H), 3.63 (d, 2H, J = 5.54 Hz), 4.10 (q, 2H, J = 7.15 Hz), 5.08 (dt, 1H, J = 7.82, 5.54 Hz), 7.54 (d, 1H, J = 8.20 Hz), 7.64 (dd, 1H, J = 8.09, 4.38 Hz), 7.78 (s, 2H), 8.20 (d, 1H, J = 8.21 Hz), 8.26 (dd, 1H, J = 8.10, 1.76 Hz), 8.51 (d, 1H, J = 7.35 Hz), 9.15 (dd, 1H, J = 4.35, 1.74 Hz); ^{13}C NMR ($CDCl_3$) δ: 14.2, 23.3, 38.9, 52.2, 61.4, 123.3, 123.5, 126.3, 126.4, 127.3, 136.2, 137.0, 150.3, 158.1, 170.6; IR ($CHCl_3$) cm^{-1} : 3425, 3295, 3002, 1743, 1666, 1508, 1396, 1373, 1232, 1196, 1032, 850.

Racemic 2-Acetamido-3-(9-methyl-1,10-phenanthrol-2-yl)propanoic Acid Ethyl Ester (9). Diethyl acetamidomalonate (1.4350 g, 6.61 mmol) was added to a solution of sodium (0.1504 g, 6.54 mmol) in 10 mL absolute ethanol and stirred for 30 minutes. A solution of 2-chloromethyl-9-methyl-1,10-phenanthroline[34] (**7**, 0.7866 g, 3.24 mmol) in 6 mL absolute ethanol was added dropwise to the mixture. After 12 hours at reflux, the mixture was cooled, concentrated to a thick red oil, suspended in water (50 mL), and extracted with $CHCl_3$ (3 x 50 mL). The organic fractions were combined and concentrated to a red oil. The oil was suspended in 0.05 M HCl and washed with ethyl acetate. And then the aqueous phase was basified with Na_2CO_3(s) over ice and extracted with $CHCl_3$ (5 x 50

mL). The organic fractions were combined, dried over Na_2SO_4 and then concentrated to a red oil (0.7804 g, 69%). The crude product was taken on to the next step without further purification. An analytical sample was purified using a neutral Al_2O_3 column (2:1 CH_2Cl_2:EtOAc) to yield a white solid; mp(d): 166.7-168.9 °C; TLC (Al_2O_3; 2:1 CH_2Cl_2:EtOAc, UV detection) R_f = 0.30; HRMS: calculated for $[MH]^+$ $C_{20}H_{21}N_3O_3$ [351.1583]; observed [351.1584]; ^1H NMR ($CDCl_3$) δ: 1.09 (t, 3H, J = 7.15 Hz), 2.19 (s, 3H), 2.87 (s, 3H), 3.58 (m, 2H), 4.05 (q, 2H, J = 7.14 Hz), 5.08 (dt, 1H, J = 7.79, 4.74 Hz), 7.46 (d, 1H, J = 8.16 Hz) , 7.48 (d, 1H, J = 8.21 Hz), 7.66 & 7.70 (ABX, 2H, J = 8.81 Hz), 8.10 (d, 1H, J = 8.22 Hz), 8.14 (d, 1H, J = 8.20 Hz), 9.09 (d, 1H, J = 7.69 Hz); ^{13}C NMR ($CDCl_3$) δ: 14.2, 23.4, 25.7, 38.4, 52.1, 61.2, 123.4, 123.8, 125.3, 126.3, 127.0, 127.3, 136.3, 136.9, 158.0, 170.6, 171.5; IR ($CHCl_3$) cm^{-1} : 3307, 3002, 1743, 1666, 1496, 1373, 1196, 1038, 850.

Racemic 2-Amino-3-(1,10-phenanthrol-2-yl)propanoic Acid Methyl Ester (10). A solution of **8** (10.21 g, 30 mmol) in 300 mL 6N HCl was heated to 90 °C with stirring for 10 hr. The reaction was cooled and concentrated *in vacuo* to a thick red oil. The oil was then resuspended in water (50 mL) and concentrated *in vacuo* twice to remove excess HCl. The mixture of amino acid and sodium salts was dried over P_2O_5 under vacuum overnight. The molecular weight of the product, racemic 2-amino-3-(1,10-phenanthroline-2-yl)propanoic acid, was confirmed by mass spectrometry. HRMS : calculated for $[MH]^+$ $C_{15}H_{14}N_3O_2$ [268.1086]; observed [268.1101]. The solid mixture was then suspended in 250 mL of freshly distilled MeOH, and anhydrous HCl was passed through the mixture for 10 min. After stirring overnight the reaction was complete as shown by chiral-HPLC analysis, the solid suspension was concentrated *in vacuo*. The solid was resuspended in MeOH (250 mL) and concentrated *in vacuo* twice to remove excess acid. The solid residue was neutralized with saturated Na_2CO_3 and extracted with $CHCl_3$ (3 x 250 mL). The organic fractions were combined,

dried over Na_2SO_4, and concentrated to yield a yellow oil (9.17 g, quantitative). HRMS : calculated for $[MH]^+$ $C_{15}H_{14}N_3O_2$ [268.1086]; observed [268.1101]; ^1H NMR ($CDCl_3$) δ: 3.43 (m, 1H), 3.72 (m, 4H), 4.26 (m, 1H), 7.53 (m, 2H), 7.67 (s, 2H), 8.08 (d, 1H, J=8.1 Hz), 8.15 (d, 1H, J=8.0 Hz), 9.08 (d, 1H, J=3.8 Hz); ^{13}C NMR (CD_3OD) δ: 43.8, 52.8, 55.3, 119.5, 123.4, 124.3, 126.6, 126.9, 127.8, 129.3, 136.5, 137.0, 146.3, 150.7, 159.1, 175.6; IR (thin film) cm^{-1} : 3373, 2944, 1732, 1590, 1556, 1506, 1494, 1454, 1394, 1277, 1206, 1139, 1015, 855.

Racemic 2-Amino-3-(9-methyl-1,10-phenanthrol-2-yl)propanoic Acid Methyl Ester (11). A solution of **9** (0.7804 g, 2.22 mmol) in 25 mL 6N HCl was heated to 90 °C with stirring for 10 hr. The reaction was cooled and concentrated *in vacuo* to a thick red oil. The oil was then resuspended in water (25 mL) and concentrated *in vacuo* twice to remove excess HCl. The mixture of amino acid and sodium salts was dried over P_2O_5 under vacuum overnight. The molecular weight of the product, racemic 2-amino-3-(9-methyl-1,10-phenanthroline-2-yl)propanoic acid, was confirmed by mass spectrometry. HRMS : calculated for $[MH]^+$ $C_{16}H_{16}N_3O_2$ [282.1243]; observed [282.1255]. The solid mixture was then suspended in 25 mL of freshly distilled MeOH, and anhydrous HCl was passed through the mixture for 10 min. After refluxing for 1 hour and stirring overnight at room temperature the reaction was complete as shown by chiral-HPLC analysis, the solid suspension was concentrated *in vacuo*. The solid was resuspended in MeOH (25 mL) and concentrated *in vacuo* twice to remove excess acid. The solid residue was neutralized with saturated Na_2CO_3 and extracted with $CHCl_3$ (3 x 25 mL). The organic fractions were combined, dried over Na_2SO_4, and concentrated to yield a yellow oil (0.5806 g, 93%). HRMS : calculated for $[MH]^+$ $C_{17}H_{18}N_3O_2$ [296.1399]; observed [296.1399]; ^1H NMR ($CDCl_3$) δ: 2.91 (s, 3H), 3.43 (dd, 1H, J = 14.0, 8.2 Hz), 3.68 (dd, 1H, J = 14.1, 4.5 Hz), 3.81 (s, 3H), 4.26 (dd, 1H, J = 8.4, 4.5 Hz), 7.49 (d, 1H, J = 8.3 Hz), 7.53 (d, 1H,

J = 8.2 Hz), 7.71 (s, 2H), 8.11 (d, 1H, J = 8.2 Hz), 8.12 (d, 1H J = 8.2 Hz), 8.16 (d, 1H, J = 8.2 Hz); ^{13}C NMR ($CDCl_3$) δ: 25.9, 43.4, 52.4, 107.4, 123.5, 123.6, 123.7, 125.4, 126.1, 127.4, 136.3, 136.6, 159.4, 175.7; IR (thin film) cm^{-1} : 3225, 3013, 2954, 1725, 1684, 1661, 1625, 1608, 1590, 1502, 1437, 1425, 1373, 1349, 1279, 1232, 1143, 867, 850.

Determination of Enantiomeric Excess by CrownPak CR Column Analysis. Characterization was obtained through HPLC analysis using a CrownPak CR (+) column (J.T. Baker), on an Isco Model 2350 HPLC equipped with an Isco Model V4 Absorbance detector using the following conditions the conditions as described. 2-Amino-3-(1,10-phenanthrol-2-yl)propanoic acids and methyl esters (**10**): Flow rate 1.0 mL/min.; 25 °C, monitored at 278 nm; eluent 10% MeOH / 0.1 M $HClO_4$. Methyl esters: D-**10** 11.50 min., L-**10** 12.25 min.; amino acids: D 7.75 min., L 8.25 min. 2-Amino-3-(9-methyl-1,10-phenanthrol-2-yl)propanoic acids and methyl esters: Flow rate 0.6 mL/min.; 25 °C, monitored at 280 nm; eluent 10% MeOH / 0.1 M $HClO_4$. Methyl esters: D-**11** 15.73 min., L-**11** 18.10 min.; amino acids: D 11.87 min., L 12.61 min.

***N*$^{\alpha}$-(9-Fluorenylmethyloxycarbonyl)-(*S*)-2-amino-3-(1,10-phenanthrol-2-yl)propanoic Acid (12).** A solution of racemic 2-amino-3-(1,10-phenanthrol-2-yl)propanoic acid methyl ester (**10**, 3.6587 g, 16.0 mmol) was dissolved in 45 mL *t*-butanol and added to 445 mL 10% $NaHCO_3$. A sample of alkaline protease (125 mg, 800 - 2000 units) in 120 mL of 0.2 M $NaHCO_3$ was added to the amino acid methyl ester **10** (8 mmol) in a 1L Erlenmeyer flask. The mixture was rotated at 120-200 rpm and monitored by HPLC at 20 minute intervals. When the ratio of the D-amino acid methyl ester to the L-amino acid methyl ester was >50:1 (about 40 min.), the mixture was extracted with $CHCl_3$ (6 x 150 mL). The aqueous phase was reduced in volume to remove any chloroform and then lyophilized yielding a mixture of amino acid and carbonate salts. The combined organic layers were

dried over Na_2SO_4 and the solvent was evaporated. HPLC analysis of the aqueous phase showed a 92-94% ee of the L-amino acid based on conventions of the elution profiles on the CrownPak(+) column and the specificity of alkaline protease. The amino acid/carbonate salt mixture was dissolved in 25 mL of 10% Na_2CO_3. The 9-Fluorenylmethylsuccinimidyl carbonate (1.2 eq) was dissolved in 15 mL dioxane and added dropwise to the amino acid solution. The reaction mixture was shaken periodically for 1.5 hours and then transferred to a separatory funnel and diluted with 100 mL water. This mixture was washed with ether (4 x 60 mL), and transferred to a 250 mL Erlenmeyer flask. After cooling to 0 °C and adjusting to pH <2 with concentrated HCl, the precipitate was isolated by centrifugation if necessary and washed with water (3 x 100 mL). The residue was transferred to a round bottom flask with methanol (200 mL). The methanol was removed under reduced pressure and toluene (80 mL) was added. The resulting toluene/water mixture was azeotropically removed under reduced pressure. The residue was rubbed with ether to obtain a solid which was dried *in vacuo* to yield the Fmoc-protected amino acid (**10**, 85% based on the amount of L-amino acid methyl ester. mp = 187°C (dec.); HRMS: calculated $[MH]^+$ for $C_{30}H_{24}N_3O_4$ [490.1767]; observed [490.1749]; TLC (SiO_2; 4:1 $CHCl_3$:MeOH; UV); R_f = 0.55; ^1H NMR (DMSO-*d6*) δ: 3.45 (m, 1H), 3.65 (m, 1H), 4.10 (m, 3H), 4.40 (m, 1H), 4.80 (d, 2H, J=5.8 Hz), 7.05 (m, 2H), 7.35 (m, 2H), 7.50 (m, 2H), 7.68 (d, 1H, J=7.2Hz), 7.80 (d, 1H, J=7.6 Hz), 7.93 (m, 2H), 8.10 (m, 2H), 8.64 (d, 1H, J=8.3Hz), 9.00 (d, 1H, J=4.6 Hz), 9.25 (d, 1H, J=4.85 Hz); ^{13}C NMR (DMSO-*d6*) δ: 47.5, 55.1, 66.6, 121.0, 124.3, 125.0, 126.0, 126.1, 127.2, 127.3, 127.4, 128.0, 128.6, 128.8, 129.6, 137.2, 137.6, 141.6, 144.7, 144.8, 150.9, 159.4, 174.2; IR (mineral oil mull) cm^{-1} : 3307, 1690, 1601, 1537, 1454, 1372, 1337, 1261, 1150, 1102, 1078, 1037, 850, 761, 732; $[\alpha]_D^{25}$ -67.9° (c = 0.35, DMSO); UV (MeOH, nm) λ_{max} = 299 (11,000), 268 (32,000), 224 (38,900).

***N*-(9-Fluorenylmethoxycarbonyl)-(*S*)-2-amino-3-(9-methyl-1,10-phenanthrol-2-yl)propanoic Acid (13).** A solution of racemic 2-amino-3-(9-methyl-1,10-phenanthrol-2-yl)propanoic acid methyl ester (**11**, 0.5733 g, 2.04 mmol) was dissolved in 20 mL *t*-butanol and added to 200 mL 10% $NaHCO_3$. A sample of alkaline protease (55.4 mg, 400 - 1000 units) was added to the amino acid methyl ester in a 1L Erlenmeyer flask. The mixture was rotated at 150 rpm and monitored by HPLC at 20 minute intervals. When the ratio of the D-amino acid methyl ester to the L-amino acid methyl ester was >50:1 (about 40 min.), the mixture was extracted with $CHCl_3$ (6 x 150 mL). The aqueous phase was reduced in volume to remove any $CHCl_3$ and then lyophilized yielding a mixture of amino acid and carbonate salts. HPLC analysis of the aqueous phase generally shows a 98% ee of the L-amino acid based on conventions of the elution profiles on the CrownPak(+) column and the specificity of alkaline protease. The resulting product L-Neo had $[\alpha]_D^{25}$ -80.3 at pH 8.8 and $[\alpha]_D^{25}$ +8.5 at pH 0, which is consistent with the Clough-Lutz-Jirgenson rule, confirming the configuration of the stereocenter. The amino acid/carbonate salt mixture was suspended in 200 mL of water. The 9-fluorenylmethylsuccinimidyl carbonate (0.5508 g, 1.63 mmol) was dissolved in 20 mL dioxane and added dropwise to the amino acid solution. The reaction mixture was stirred at room temperature for 1.5 hours. To the reaction, a solution of 9-fluorenylmethylsuccinimidyl carbonate (0.3431 g, 1.02 mmol) dissolved in 15 mL dioxane was added dropwise. After stirring overnight, this mixture was washed with ether (4 x 100 mL). After cooling to 0 °C and adjusting to pH < 2 with concentrated HCl, the precipitate was isolated by centrifugation and washed with water (3 x 100 mL). The residue was transferred to a round bottom flask with methanol (150 mL). The methanol was removed under reduced pressure and toluene (80 mL) was added. The resulting toluene/water mixture was azeotropically removed under reduced pressure.

The residue was rubbed with ether to yield a solid which was dried *in vacuo* (0.4726 g, 92% yield based on the amount of L-amino acid methyl ester). mp = 131.4-132.7°C (dec.); HRMS: calculated for $[MH]^+$ $C_{31}H_{26}N_3O_4$ [504.1923]; observed [504.1931]; TLC (SiO_2; 4:1 $CHCl_3$:MeOH; UV); R_f = 0.36; ^1H NMR (DMSO-*d6*) δ: 2.76 (s, 3H), 3.45 (m, 1H), 3.55 (m, 1H), 4.18 (m, 3H), 4.61 (m, 1H), 7.15 (t, 1H, J = 7.4 Hz), 7.21 (t, 1H, J = 7.4 Hz), 7.35 (m, 3H), 7.61 (m, 2H), 7.70 (d, 1H, J = 8.2 Hz), 7.84 (d, 2H, J = 7.6 Hz), 7.90 (s, 2H), 8.17 (d, 1H, J = 8.3 Hz), 8.36 (d, 1H, J = 8.2 Hz), 8.40 (d, 1H, J = 8.3 Hz); ^{13}C NMR (DMSO-*d6*) δ: 40.8, 47.0, 47.2, 54.2, 66.2, 120.5, 120.6, 125.6, 126.3, 127.3, 127.5, 127.6, 128.0, 128.1, 137.5, 141.2, 144.4, 156.6, 158.7, 173.7; IR (KBr) cm^{-1} : 3316, 3063, 3043, 2946, 1728, 1694, 1538, 1446, 1372, 1261, 1222, 1149, 1105, 1080, 1046, 857, 759, 740; $[\alpha]_D^{25}$ -71.4°.

Peptide Synthesis

All peptides were synthesized on a 0.084 to 0.168 mmole scale by solid phase methods using N^{α}-9-fluorenylmethyloxycarbonyl (Fmoc) amino acid with BOP/HOBT activated-ester chemistry on a Milligen 9050 automated peptide synthesizer, except for the Neo-containing peptides and FenHis'. These peptides were synthesized on macrocrowns purchased from Chiron Mimotopes. Commercially available starting materials and reagents were purchased from MilligenBiosearch, EM Science, NovaBiosearch or Aldrich Chemical Co.

Solid Phase Peptide Synthesis. Fmoc-PAL-PEG-PS resin (0.21mmol/g) was used to afford carboxyl terminus primary amides. Typical protocols for coupling a residue involved 30 to 90 minute coupling cycles with three or four equivalents of amino acid. However, for the bipyridyl and phenanthrolyl amino acids, a double coupling protocol was employed, where 2.5 equivalents was used for the first coupling followed by a similar acylation with 1.5 equivalents of the residue with 60 minute coupling times for both. Activated esters were formed *in*

situ using benzotriazole-1-yloxy-tris(dimethylamino)-phosphoniumhexafluorophosphate (BOP), 1-hydroxybenzotriazole (HOBt) and *N*-methylmorpholine or diisopropylcarbodiimide (DIPCDI), HOBt and diisopropylethylamine (DIEA). Due to poor solubility of the bipyridyl and phenanthrolyl amino acid activated esters, the amino acid ester solutions were filtered manually through a 0.45 μm nylon syringe filter (Gelman Scientific) prior to manual injection onto the column. Deprotection of FMOC-protected amine groups were performed using either a 7 minute 20% piperidine/dimethylformamide (DMF) wash or a 5 minute 2% 1,7-diazabicyclo[5,4,0]-undec-7-ene (DBU)/DMF wash. Peptides were *N*-acylated on the resin using either 7 equivalents of acetic anhydride and 7 equivalents of triethylamine (TEA) or 21 equivalents of acetic anhydride and 5 equivalents of triethylamine in 3 mL of DMF for 2 hours. The resin was then washed with DMF and dichloromethane and lyophilized overnight.

The peptides were then deprotected and cleaved from the resin by treatment with trifluoroacetic acid (TFA)/phenol/H_2O/thioanisole/ethanedithiol (82.5:5:5:5:2.5) or TFA/thioanisole/ethanedithiol/anisole (90:5:3:2) for two hours.[39] The resin was filtered, washed with TFA and the combined filtrates were concentrated to 2 mL and precipitated with ether/hexane 1:1 or 2:1 (20 mL). The supernatant was decanted and the peptides were triturated with ether/hexane 1:1 (5 x 20 mL) or ether/hexane 2:1 (3 x 20 mL). The peptides were lyophilized overnight and purified by reverse-phase C_{18} HPLC. All peptides were confirmed by mass spectrometry (Table 2-3).

Peptide Synthesis on Macrocrowns. A typical full coupling cycle involves the following steps. A 30 minute soak in 20% (v/v) piperidine/DMF suspended in DMF followed by a 5 minute wash with DMF and three rinses with methanol. After air drying for 10 minutes and 5 minutes soaking in DMF, the pin is submitted to the coupling cocktail. Typical couplings were performed 2 hours

with Fmoc protected amino acid pentafluorophenyl esters and HOBt at 80 mM concentration each with 450 μL of activated amino acid ester solution per pin. After coupling, the pins were then washed once with DMF and thrice with methanol. The pins were then air dried for 10 minutes to complete a full cycle. The residues Neo and Fen were coupled with three equivalents of amino acid and *O*-(7-azabenzotriazol-1-yl)-1,1,3,3-tetramethyluronium hexafluorophosphate (HATU) /1-hydroxy-7-azabenzotriazole (HOAt)/DIEA mediated chemistry in N-methylpyrrolidinone (NMP).[40-42] These cycles were repeated until the synthesis was complete. Peptides were *N*-acetylated on the solid support using 450 μL of DMF/Ac_2O/TEA (43:1:1) in place of a typical coupling solution. The peptides synthesized were deprotected and removed from the solid support by treatment with trifluoroacetic acid (TFA)/phenol/H_2O/thioanisole/ethanedithiol (82.5:5:5:5:2.5) for 4 hours.[39] The resulting solution was concentrated to 2 mL volume and precipitated with ether/hexane 1:1. The supernatant was decanted and the peptides were triturated with ether/hexane 1:1 (5 x 10 mL). The peptides were lyophilized overnight and purified by reverse-phase C_{18} HPLC. The peptides were confirmed by mass spectrometry (Table 2-3).

Table 2-3 The Calculated and Observed High Resolution Mass Values for the Synthesized Hexapeptides

Peptide	Formula	Calcd. [MH$^+$]	Obsd. [MH$^+$]
4BpaPhe$_W$[a]	$C_{41}H_{53}N_9O_8$	800.4095	800.4055
5BpaPhe$_W$[a]	$C_{41}H_{53}N_9O_8$	800.4095	800.4057
6BpaPhe$_W$[a]	$C_{41}H_{53}N_9O_8$	800.4095	800.4153
6Bpa6Bpa$_W$[a]	$C_{45}H_{55}N_{11}O_8$	878.4313	878.4285
6Bpa6Bpa[a]	$C_{50}H_{57}N_{11}O_8$	940.4470	940.4459
FenPhe$_W$[a]	$C_{43}H_{53}N_9O_8$	824.4095	824.4117
FenLeu[a]	$C_{45}H_{58}N_9O_8$	852.4408	852.4418
FenHis$_W$[a]	$C_{40}H_{51}N_{11}O_8$	814.4000	814.3983
FenHis[a]	$C_{45}H_{53}N_{11}O_8$	876.4156	876.4140
FenAsp[a]	$C_{43}H_{51}N_9O_{10}$	854.3837	854.3841
FenHis′[b]	$C_{45}H_{53}N_{11}O_8$	898.3976[c]	898.4031[d]
NeoPhe[b]	$C_{49}H_{57}N_9O_8$	900.4408	900.4422
NeoHis[b]	$C_{46}H_{55}N_{11}O_8$	890.4302	890.4313

[a] Peptides synthesized on the automated peptide synthesizer.
[b] Peptides synthesized on the macrocrowns.
[c] Calculated [MNa$^+$].
[d] Observed [MNa$^+$].

Absorption Spectroscopy (UV-Vis) Studies

The absorption spectra were obtained on a Shimadzu UV-160U in 10 mm path length cuvettes. The concentrations of the peptide solutions were determined spectrophotometrically using the characteristic absorption band of the bipyridyl (λ_{max} = 285 nm, ε_{max} = 12800) or phenanthrolyl (Fen, λ_{max} = 268 nm, ε_{max} = 20890; Neo, λ_{max} = 274 nm, ε_{max} = 24150) moiety. The aqueous solutions of known peptide concentrations were then titrated with standard metal cation solutions at room temperature. For the bipyridyl containing peptides, the pH of the solution was monitored by a glass electrode and held within the pH range of 7.0 to 7.5 through small additions of 0.1 N NaOH or 0.1 N HCl in the presence of 200 mM NaCl. For the peptides containing Fen or Neo,

the titrations were performed in 50 mM *N*-(2-hydroxyethyl)piperazine-*N'*-(2-ethane-sulfonic acid) (HEPES) buffer, pH 8.25. The distinct red-shift of the bipyridyl or phenanthrolyl π-π^* transition upon binding metal cations was monitored by absorption (UV-Vis) spectroscopy. With peptide concentrations ranging from 1 to 500 μM, the metal binding constants were determined by calculations carried out using KaleidaGraph version 3.0 (Abelbeck Software, CA). A minimum of three titrations were performed for each peptide-metal cation complex. The binding isotherms were assumed to follow a two state equilibrium when well defined isosbestic points associated with the addition of metal cations were observed. The dissociation constants (K_D) were obtained using an iterative process based on the Scott equation:[36]

$$\frac{b \cdot [M]}{\Delta A} = \frac{[M]}{[Pep]_t \cdot \Delta\varepsilon} + \frac{K_D}{[Pep]_t \cdot \Delta\varepsilon}$$

where b = path length, [M] = free metal cation concentration, ΔA = change in absorbance due to complex formation, $[Pep]_t$ = total peptide in solution, $\Delta\varepsilon$ = change in molar absorptivity due to complex formation. Initial estimations of [M] were achieved by using data where $[M]_{total} >> [Pep]_t$. An analysis was performed where $\frac{b \cdot [M]}{\Delta A}$ was plotted against [M]. The $\Delta\varepsilon$ thus generated was used to calculate [M] more accurately ($[M] = [M]_{total} - (\Delta A/\Delta\varepsilon)$) for every iteration until $\Delta\varepsilon$ values converges. When the $\Delta\varepsilon$ converge, the dissociation constants (K_D) were calculated from the last iterations as:

$$K_D = \frac{\text{y - intercept}}{\text{slope}}$$

Circular Dichroism Spectroscopy Studies

Circular dichroism spectra were recorded on a Jasco J600 Circular Dichroism Spectrometer. The concentration of the peptide solutions was

determined spectrophotometrically using the characteristic absorption band of the phenanthrolyl (Neo, λ_{max} = 274 nm, ε_{max} = 24150) moiety. The spectra were baseline corrected and noise reduced using the Jasco J600 System Software, and were then further analyzed using KaleidaGraph version 3.0 (Abelbeck Software). Metal cation titrations were performed with peptide concentrations ranging from 65 μM to 70 μM in 0.01M TRIS buffer (pH 8.25) in a 1 mm path-length cuvette. The change in CD signature where the phenanthrolyl moiety absorbs was monitored, and the binding isotherms were thus obtained. The dissociation constants were calculated as described in the UV-Vis experiments.

References

1. Rabanal, F.; DeGrado, W. F.; Dutton, P. L. *J. Am. Chem. Soc.* **1996**, *118*, 473-474.
2. Regan, L. *Trends Biochem. Sci.* **1995**, *20*, 280-285 and references therein.
3. Walkup, G. K.; Imperiali, B. *J. Am. Chem. Soc.* **1996**, *118*, 3053-3054.
4. Kazmierski, W. M. *Int. J. Pept. Protein Res.* **1995**, *45*, 241-247.
5. Gilbertson, S. R.; Chen, G.; McLoughlin, M. *J. Am. Chem. Soc.* **1994**, *116*, 4481-4482.
6. Imperiali, B.; Prins, T. J.; Fisher, S. L. *J. Org. Chem.* **1993**, *58*, 1613-1616.
7. Imperiali, B.; Fisher, S. L. *J. Org. Chem.* **1992**, *57*, 757-759.
8. Imperiali, B.; Fisher, S. L. *J. Am. Chem. Soc.* **1991**, *113*, 8527-8528.
9. Rana, T. M.; Ban, M.; Hearst, J. E. *Tetrahedron Lett.* **1992**, *33*, 4521-4524.
10. Wilson, S. R.; Yasmin, A.; Wu, Y. *J. Org. Chem.* **1992**, *57*, 6941-6945.
11. Ruan, F.; Chen, Y.; Hopkins, P. B. *J. Am. Chem. Soc.* **1990**, *112*, 9403-9404.
12. Summers, L. A. *Adv. Heterocyclic Chem.* **1978**, *22*, 1-69.
13. McWhinnie, W. R.; Miller, J. D. *Adv. Inorg. Chem. Radiochem.* **1969**, *12*, 135-213.
14. König, E. *Coord. Chem. Rev.* **1968**, *3*, 471-495.

15. Lindoy, L. F.; Livingstone, S. E. *Coord. Chem. Rev.* **1967**, *2*, 173-193.

16. Brandt, W. W.; Dwyer, F. P.; Gyarfas, E. C. *Chem. Rev.* **1954**, *54*, 959-1017.

17. Cotton, F. A.; Wilkinson, G. *Advanced Inorganic Chemistry*; Jonh Wiley & Sons, Inc: Singapore, 1988 .

18. Wuttke, D. S.; Gray, H. B.; Fisher, S. L.; Imperiali, B. *J. Am. Chem. Soc.* **1993**, *115*, 8455-8456.

19. Struthers, M. D.; Cheng, R. P.; Imperiali, B. *Science* **1996**, *271*, 342-345.

20. Struthers, M. D.; Cheng, R. P.; Imperiali, B. *J. Am. Chem. Soc.* **1996**, *118*, 3073-3081.

21. Chen, S.-T.; Wang, K.-T.; Wong, C. H. *J. Chem. Soc., Chem. Comm.* **1986**, 1514.

22. Fields, G. B.; Noble, R. L. *Int. J. Pept. Protein Res.* **1990**, *35*, 161-214.

23. Imperiali, B.; Kapoor, T. M. *Tetrahedron* **1993**, *49*, 3501-3510.

24. Hutchinson, E. G.; Thornton, J. M. *Protein Science* **1994**, *3*, 2207-2216.

25. Imperiali, B.; Fisher, S. L.; Moats, R. A.; Prins, T. J. *J. Am. Chem. Soc.* **1992**, *114*, 3182-3188.

26. Dyson, H. J.; Rance, M.; Houghten, R. A.; Lerner, R. A.; Wright, P. E. *J. Mol. Biol.* **1988**, *201*, 161-200.

27. Kraulis, P. J. *J. Appl. Crystallogr.* **1991**, *24*, 946-950.

28. Fisher, S. L. **1993** PhD. Thesis, California Institute of Technology.

29. Prins, T. J. **1992** M. S. Thesis, California Institute of Technology.

30. Albertson, N. F. *J. Am. Chem. Soc.* **1946**, *68*, 450-453.

31. Coulter, A. W.; Talalay, P. *J. Biol. Chem.* **1968**, *243*, 3238-3247.

32. Weijnen, J. G. J.; Koudijs, A.; Schellekens, G. A.; Engbersen, J. F. J. *J. Chem. Soc., Perkin Trans. 2* **1992**, 829-834.

33. Weijnen, J. G. J.; Koudijs, A.; Engbersen, J. F. J. *J. Chem. Soc., Perkin Trans. 2* **1991**, 1121-1126.

34. Newkome, G. R.; Theriot, K. J.; Gupta, V. K.; Fronczek, F. R.; Baker, G. R. *J. Org. Chem.* **1989**, *54*, 1766-1769.

35. Greenstein, J. P.; Winitz, W. D. "*Chemistry of the Amino Acids*" in John Wiley & Sons, New York, 1961; pp 1879-2155.

36. Connors, K. A. *Binding Constants : the Measurement of Molecular Complex Stability*; Wiley: New York, 1987 .

37. Smith, R. M.; Martell, A. E. "*Critical Stability Constants, Volume 2, Amines*" in Plenum Press, New York, 1975; pp 235-262.

38. Lippard, S. J.; Berg, J. M. *Principles of Bioinorganic Chemistry*; University Science Books: Mill Valley, 1994 .

39. King, D. S.; Fields, C. G.; Fields, G. B. *Int. J. Pept. Protein Res.* **1990**, *36*, 255-266.

40. Carpino, L. A.; El-Faham, A.; Minor, C. A.; Albericio, F. *J. Chem. Soc., Chem. Commun.* **1994**, 201-203.

41. Carpino, L. A. *J. Am. Chem. Soc.* **1993**, *115*, 4397-4398.

42. Kuroda, H.; Chen, Y.-N.; Kimura, T.; Sakakibara, S. *Int. J. Pept. Protein Res.* **1992**, *40*, 294-299.

Chapter 3

Evolution of a ββα Motif Based on the Zinc Finger Domains

Reprinted in part with permission from Struthers, M. D.; Cheng, R. P.; Imperiali, B. *J. Am. Chem. Soc.* **1996**, *118*, 3073-3081. Copyright 1996 American Chemical Society.

Introduction

The exploitation of metal-chelating amino acids for the design of metallopeptides with high metal-binding affinity has been demonstrated by the short hexapeptides described in Chapter 2. However, the corresponding peptide-M^{II} complexes of these hexapeptides exhibited limited rate enhancement for esterase activity.[1] This is consistent with the fact that both the primary ligand sphere (ligating residues) and the secondary ligand sphere (the surrounding protein matrix) are responsible for modulating the reactivity of the metal center (for details see Chapter 1), and these hexapeptides are unable to impose such modulations on the bound metal cation. Furthermore, the metal-binding site for these peptides seemed to be exposed to the surrounding solvent, forming a nest-like construct (Figure 3-1). However, the natural zinc hydrolases such as carbonic anhydrase and carboxypeptidase have metal-binding sites with a more cage-like construct. For these natural metalloenzymes, the entire protein architecture serves to orient the ligands to form the appropriate primary ligand sphere and to provide the optimal secondary ligand sphere for performing catalysis. Therefore, a metallopeptide much larger than six residues is necessary to engulf the metal center and enable catalytic activity. Furthermore, these peptides would need to be readily accessible by chemical synthesis (< 50 residues) to enable facile modulation and incorporation of the chelating unnatural residues.

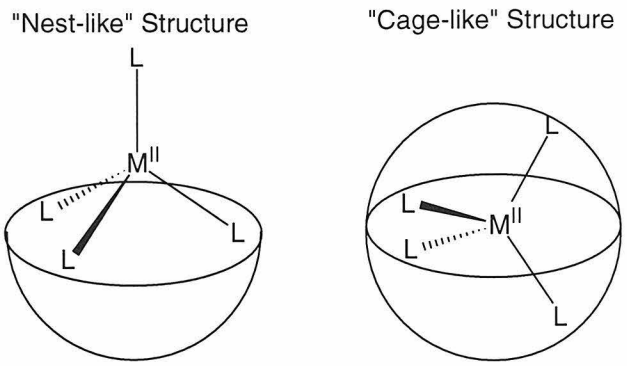

Figure 3-1 Schematic diagram of the nest-like construct and the cage-like structure.

To facilitate the design of zinc metallopeptides, the corresponding natural proteins were carefully examined. There are two different metal binding sites for zinc metalloproteins: structural sites and catalytic sites (Table 3-1).[2] Structural Zn^{II} sites are required to maintain the architecture of the protein. Catalytic Zn^{II} sites are required only to enable catalysis. The structures of the apo-form of the catalytic Zn^{II} sites have ligands already positioned in optimal orientations for the binding of Zn^{II}. Accordingly, a peptide motif that folds independent of metal cations would be an optimal structural scaffold for implementation of Zn^{II} dependent catalysis. Full structural characterization of such a motif would enable detailed evaluations of the functional metallopeptides.

Table 3-1 Characteristics of Structural and Catalytic Zn^{II} Sites[2]

Characteristics	Structural Sites	Catalytic Sites
Number of Zn^{II}-Binding Residues	Four	Three
Zn^{II} Binding Residues	Cys, His	His, Glu, Asp, Cys
Water as Ligand	No	Yes
Structure in the Absence of Zn^{II}	Random Coil	Nicely Folded
Structure in the Presence of Zn^{II}	Folded and Very Rigid	Well Folded but Flexible

For the implementation of hydrolase activity into a structural template, the catalytic machinery of the natural Zn^{II} dependent hydrolase carbonic anhydrase were examined more carefully (Figure 3-2). Carbonic anhydrase is responsible for the hydration of CO_2 to form carbonic acid and the reverse reaction to regulate the pH of blood serum in humans.[3-5] This enzyme is a single polypeptide of 260 residues containing a catalytically-required Zn^{II}. Three metal-binding histidines and a Zn^{II} bound water form the coordination sphere with a distorted tetrahedral geometry.

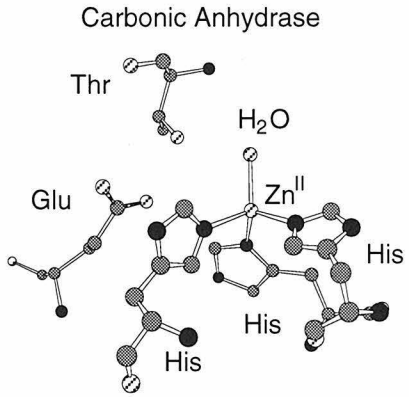

Figure 3-2 The structure of the Zn^{II}-binding site of carbonic anhydrase. The hydrogens are omitted for clarity.

The mechanism for CO_2 hydration catalyzed by carbonic anhydrase is depicted in Figure 3-3. The Zn^{II} bound water is deprotonated to give a Zn^{II} bound hydroxide which is the active species.[3, 5, 6] This deprotonation step has been demonstrated to be the rate limiting step in the catalytic cycle. Additionally, the Zn^{II} bound water has a pK_a of 7.5 which is crucial for forming the active species. Furthermore, a hydrogen bonding network involving residues Thr^{199} and Glu^{106} is responsible for facilitating the deprotonation process.[7, 8] The residue Thr^{199} has been called the proton abstractor due to its direct interaction with the Zn^{II} bound water. The active Zn^{II}-bound hydroxide nucleophilically attacks the enzyme bound CO_2 to

form a penta-coordinate intermediate involving bicarbonate. The bicarbonate is then released and a water molecule binds to the Zn^{II} to complete the cycle.

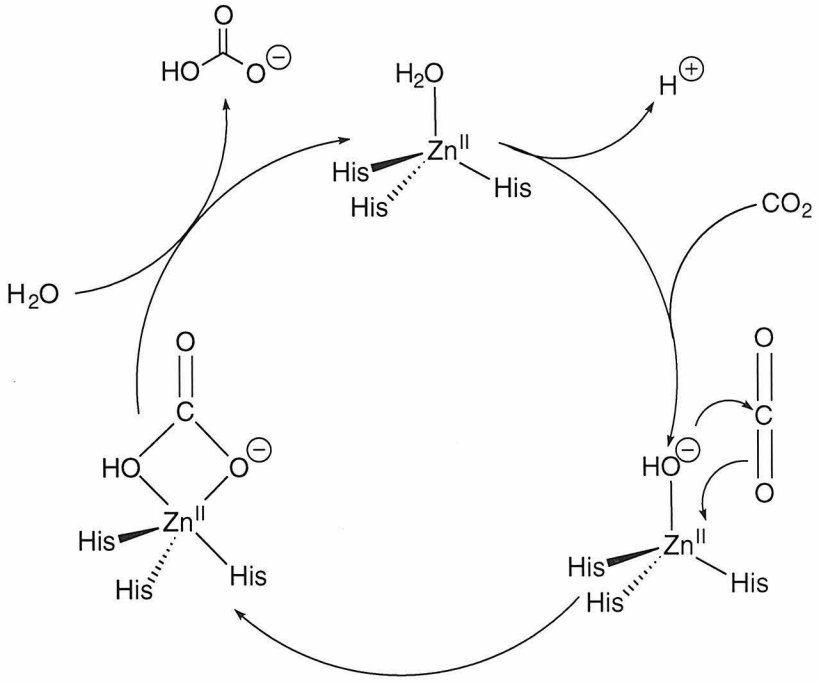

Figure 3-3 The mechanism for CO_2 hydration catalyzed by carbonic anhydrase.

A suitable structural scaffold must be small, robust and capable of emulating the metal-binding site found in natural Zn^{II} hydrolases. Considerable research has focused on the design of specific peptide sequences that adopt a predictable three-dimensional structure.[9-14] However, the most successful designs are too large to synthesize chemically (>60 residues)[15, 16] or multimeric (thereby complicating structural analysis),[10, 17-19] and many require crosslinks such as disulfide bonds[17, 18, 20] or metal ligation[21-23]. Since none of these currently available motifs were optimal for the incorporation of function, construction of a small monomeric peptidyl motif (<30 residues) was necessary.

One ideal target is the ββα motif, which is exemplified by the zinc finger domains (Figure 3-4). Natural zinc finger peptides are small independently

folded domains consisting of approximately 30 residues which adopt a ββα super-secondary structure. Atypical loops connect the two β-strands and the α-helix to the β-sheet. The consensus sequence for these peptides is Tyr/Phe-Xaa-Cys-Xaa_4-Cys-Xaa_3-Phe-Xaa_5-Leu-Xaa_2-His-Xaa_{3-5}- with conserved hydrophobic and metal-binding residues.[24, 25] Rigorous structural characterization has been achieved on individual zinc finger domains by both two-dimensional nuclear magnetic resonance (2D-NMR) spectroscopy and crystallography.[26-28] The circular dichroism (CD) signature of natural zinc fingers has been well characterized (Figure 3-5),[29-31] and serves to enable facile assessment of the designs.

Additionally, many alterations in the sequences have been investigated including the minimalist zinc finger.[25] In this minimalist design, almost all residues besides the conserved hydrophobic core and metal-binding amino acids were replaced with alanine residues. These conserved residues enable the peptide to fold into the desired structure upon addition of Zn^{II}. Thus, this motif exhibits great flexibility for incorporating different residues at varying positions, which would be crucial for future implementation of catalysis. However, these peptides adopt well-defined solution structures only in the presence of specific metal cations such as Zn^{II}, Co^{II}, or Cd^{II}.[31-33] Uncoupling the tertiary structure of the peptide from metal binding would allow an increased versatility for the design of a catalytic metal center.

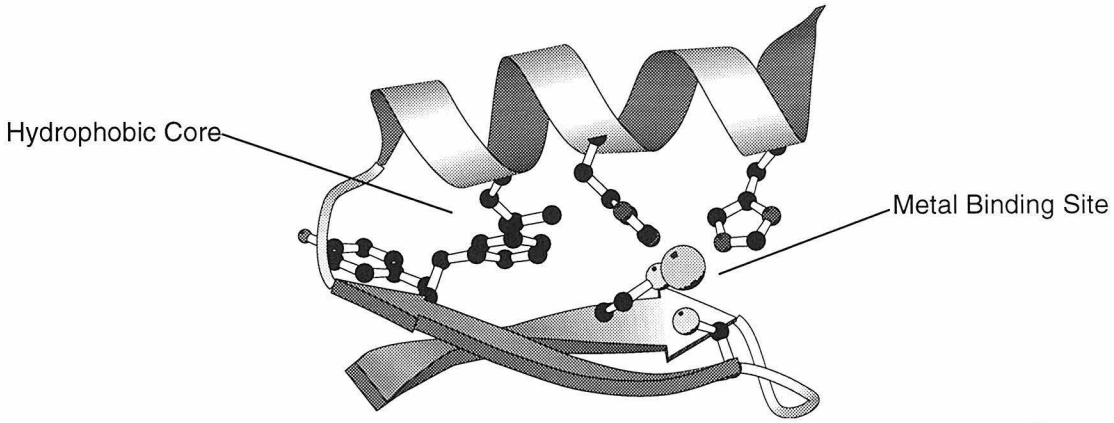

Figure 3-4 The structure of a natural zinc finger peptide bound to Zn^{II}.

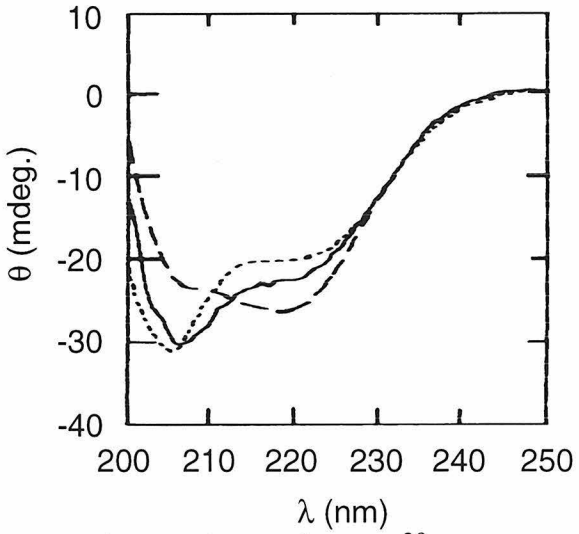

Figure 3-5 CD spectra of typical zinc fingers.[30] Reprinted with permission from Weiss, M. A.; Mason, K. A.; Dahl, C. E.; Keutmann, H. T. *Biochemistry* **1990**, *29*, 5660-5664. Copyright 1990 American Chemical Society.

For the design of a functional metallopeptides patterned after zinc finger domains, the first step involves removing the metal dependence of the ββα fold (Scheme 3-1). This may be achieved by introducing heterochiral turn sequences designed to promote β-hairpin formation in place of the atypical loop linking the two strands. Furthermore, the replacement of the two sulfhydryl metal-binding residues with nitrogen ligating amino acids would eliminate the need for special handling techniques normally required to prevent the oxidation of these residues to the corresponding disulfide.[34] The

second stage focuses on the implementation of the catalytic machinery. One of the four metal-binding amino acids could then be replaced by a hydroxyl residue to introduce a potential proton abstractor, thereby mimicking the minimal catalytic machinery of carbonic anhydrase.

Scheme 3-1 Schematic Diagram of the Iterative Design Process to Generate a Zinc Metallopeptide with Hydrolase Activity

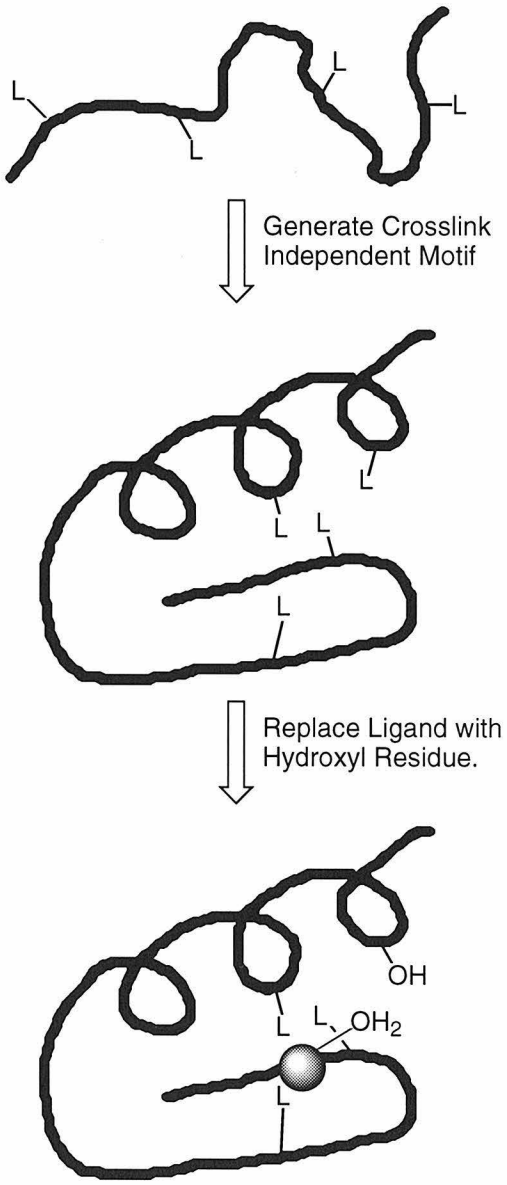

Results and Discussion

The iterative design process for creating the metal independent ββα motif patterned after the consensus zinc finger sequence[24] and Zif268[27] is outlined in Figure 3-6. Seven sequences containing the unnatural chelating amino acid Fen [(*S*)-2-amino-3-(1,10-phenanthrol-2-yl)propionic acid] were investigated by circular dichroism spectroscopy (CD). Three distinct CD experiments were performed to study the structural effect upon addition of Zn^{II}, change in pH, and peptide concentration. The structural changes that resulted from the addition of Zn^{II} indicated the dependence of structure on binding metal. Since the phenanthroline moiety on the residue Fen exhibits a CD signal when situated in a chiral environment, this region of the CD spectra was monitored as well. The pH dependence studies were performed to ensure that the structures would not differ significantly between hydrolysis assay conditions (neutral to basic pH) and nuclear magnetic resonance (NMR) spectroscopy conditions (pH 4.5). The concentration dependence studies established that no significant aggregation would occur at concentrations used for NMR analysis. Additionally, the Zn^{II} binding properties of these metallopeptides were characterized by absorption (UV-vis) spectroscopy according to the procedures established in Chapter 2.

For the first generation peptide, **ZF01**, a type II reverse turn was incorporated into the β-hairpin. Additionally, the metal coordination sphere was altered from Cys_2His_2 to $FenHis_2$ to form a four coordinate system using nitrogen ligands. Amino acids with strong β-sheet (Thr, Val) and α-helix (Ala, Leu) propensities[35] were incorporated to increase the inherent secondary structure in the peptide **ZF02**. The type II β-turn was then replaced with a type II′ β-turn for peptide, **ZF03**. NMR analysis of this peptide by Mary

Struthers revealed the presence of slowly interconverting *cis-trans* proline isomers, which was further investigated in a series of short peptides, the **Fens**. Based on these studies, replacement of the histidine residue at position 3 with either valine or threonine remediated this problem in peptides **ZF04** and **ZF05**, respectively. Both peptides were investigated by NMR. While peptide **ZF05** exhibited only limited structure, secondary and tertiary structure appeared to be present in peptide **ZF04**. However, degeneracy in the chemical resonances precluded a full structural analysis. Therefore a minor alteration in the sequence for peptide **ZF06** facilitated the analysis of the NMR data. An additional control peptide was studied to probe the role of turn type (type II vs. type II') upon the establishment of defined secondary and tertiary structure.

Figure 3-6 (following page) Sequences of the peptides in the iterative design process that are intended to adopt a ββα super-secondary structure. The sequence of peptide **ZF01** was based on the three natural zinc finger domains in Zif268 as well as the consensus sequence.

Peptide **Sequence**

β-hairpin — loop — α-helix

Zif268 Fingers

-Pro-Tyr-Ala-Cys-Pro-Val-Glu-Ser-Cys-Asp-Arg-Arg-Phe-Ser-Arg-Ser-Asp-Glu-Leu-Thr-Arg-His-Ile-Arg-Ile-His-Thr-Gly-Gln-Lys

-Pro-Phe-Gln-Cys-Arg-Ile----------Cys-Met-Arg-Asn-Phe-Ser-Arg-Ser-Asp-His-Leu-Thr-Thr-His-Ile-Arg-Thr-His-Thr-Gly-Glu-Lys

-Pro-Phe-Ala-Cys-Asp-Ile----------Cys-Gly-Arg-Lys-Phe-Ala-Arg-Ser-Asp-Glu-Arg-Lys-Arg-His-Thr-Lys-Ile-His-Leu-Arg-Gln-Lys

Consensus:

-Xaa-Phe-Xaa-Cys-Xaa-Xaa-Xaa-Xaa-Cys-Xaa-Xaa-Xaa-Phe-Xaa-Xaa-Xaa-Xaa-Xaa-Leu-Xaa-Xaa-His-Xaa-Xaa-Xaa-His-Xaa-

⇩ • Incorporation of Type II Turn
• $Cys_2His_2 \rightarrow FenHis_2$

β-hairpin — loop — α-helix

5 10 15 20

ZF01: Ac-Phe-Ala-His-Pro-DSer-Fen-Ala-Phe-Ser-Gln-Ser-Asp-Glu-Leu-Thr-Lys-Ala-Ile-Arg-Thr-His-Thr-NH_2

⇩ • Stabilization of Secondary Structure
• Incorporation *C*-Terminal Helix Cap - Gly^{23}

ZF02: Ac-Phe-Thr-His-Pro-DSer-Fen-Thr-Phe-Ser-Arg-Ser-Asp-Glu-Leu-Ala-Lys-Leu-Leu-Arg-Leu-His-Ala-Gly-NH_2

⇩ • Incorporation of Type II' Turn to Replace the Type II Turn

ZF03: Ac-Phe-Thr-His-DPro-Ser-Fen-Thr-Phe-Ser-Arg-Ser-Asp-Glu-Leu-Ala-Lys-Leu-Leu-Arg-Leu-His-Ala-Gly-NH_2

⇩ • Incorporation of Val^3 (**ZF04**) and Thr^3 (**ZF05**) to Stabilize the Type II' Conformation

ZF04: Ac-Phe-Thr-Val-DPro-Ser-Fen-Thr-Phe-Ser-Arg-Ser-Asp-Glu-Leu-Ala-Lys-Leu-Leu-Arg-Leu-His-Ala-Gly-NH_2

ZF05: Ac-Phe-Thr-Thr-DPro-Ser-Fen-Thr-Phe-Ser-Arg-Ser-Asp-Glu-Leu-Ala-Lys-Leu-Leu-Arg-Leu-His-Ala-Gly-NH_2

⇩ • Incorporation of Tyr1 (**ZF06**) to Enable Complete NMR Assignment
• Generation of Corresponding Control Peptide (**ZF07**) with Type II Turn

ZF06: Ac-Tyr-Thr-Val-DPro-Ser-Fen-Thr-Phe-Ser-Arg-Ser-Asp-Glu-Leu-Ala-Lys-Leu-Leu-Arg-Leu-His-Ala-Gly-NH_2

ZF07: Ac-Tyr-Thr-Val-Pro-DSer-Fen-Thr-Phe-Ser-Arg-Ser-Asp-Glu-Leu-Ala-Lys-Leu-Leu-Arg-Leu-His-Ala-Gly-NH_2

Peptide Synthesis

The designed peptides were synthesized by Fmoc (9-fluorenylmethyloxycarbonyl)-based solid phase peptides synthesis (SPPS). Initial syntheses utilized standard coupling procedures for Fmoc-protected amino acids using diisopropylcarbodiimide/1-hydroxybenzotrazole (DIPCDI/HOBt) mediated chemistry. The results were unsatisfactory with many truncation peptides and the coupling efficiencies were exceptional low at residues between the α-helix and the β-hairpin (Figure 3-7a). Furthermore, the desired peptide and the truncation peptide lacking the Fen residue were present in equal amounts (not shown), indicating the coupling of Fmoc-Fen-OH proceeded only up to 50% with double couple. Since activated pentafluorophenyl (Pfp) esters are known to be more efficient in synthesizing peptides,[36] these esters were utilized for coupling most of the residues. In these syntheses, the coupling of Fmoc-Fen-OH was performed using *O*-(7-azabenzotriazol-1-yl)-1,1,3,3,-tetramethyluronium hexafluorophosphate /1-hydroxy-7-azabenzotriazole (HATU/HOAt) mediated chemistry in *N*-methylpyrrolidinone (NMP).[37] Although low coupling efficiencies were still observed in the loop region mentioned above, results indicated considerable improvement of the synthesis and the coupling of Fmoc-Fen-OH was quantitative with single couplings (Figure 3-7b).

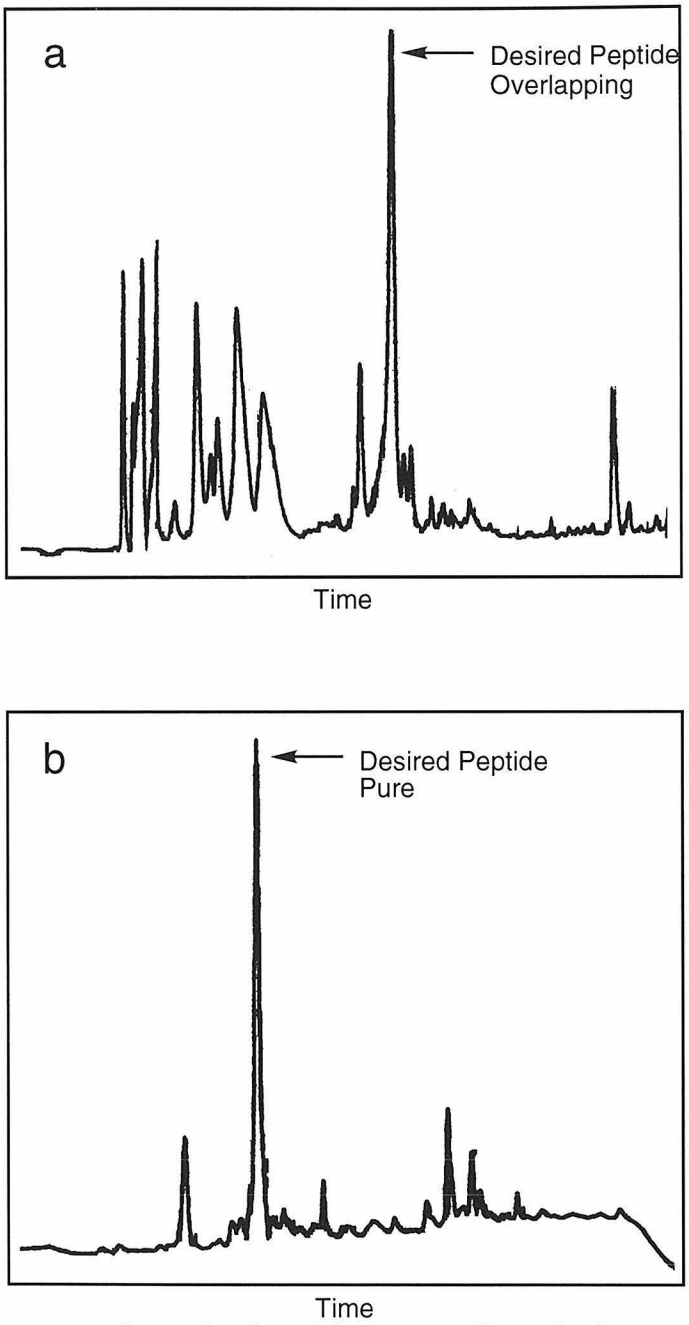

Figure 3-7 Reverse phase high performance liquid chromatography (RP-HPLC) traces for the peptide synthesis products involving (a) free acid chemistry and (b) activated pentafluorophenyl ester chemistry.

Peptide ZF01

*Design of Peptide **ZF01***

The sequence of peptide **ZF01** was based on the sequences of the three fingers of Zif268[27] as well as the zinc finger consensus sequence (Figure 3-5).[24] Conformational studies of proteins and polypeptides have indicated that the β-turn may serve as a nucleating element in the folding process.[38-43] Furthermore, recent computational[44-46] and spectroscopic studies[47-49] have focused on establishing the stability of the various β-turn types. In particular, heterochiral type II turns have exhibited an inherent stability in theoretical and experimental investigations.[44, 47, 48] Thus, the β-hairpin region was engineered to incorporate a heterochiral type II β-turn forming sequence Pro-DSer in the first generation design, peptide **ZF01**. Additionally, the two conserved hydrophobic aromatic amino acids in the natural system were incorporated at either end of the β-hairpin. It has been shown that alanine substitutions are widely tolerated in the natural zinc finger motif with the exception of the metal binding ligands and the three conserved hydrophobic core residues (Phe^1, Phe^8, and Leu^{14} in **ZF01**),.[25] Thus, the central residues of this β-hairpin (positions 2 and 7) were alanines. Furthermore, the helix of peptide **ZF01** was based on the sequences of Zif268.[28]

The metal binding site of peptide **ZF01** is a four coordinate system involving an exclusively nitrogen ligand sphere $FenHis_2$. This modification required the replacement of the two Cys ligands within the β-hairpin of Zif268 with His and Fen respectively. The central histidine residue of the α-helix was replaced with alanine (position 17) to retain a four coordination site. After a rigid structural scaffold is constructed, one of the ligands may be replaced with a hydroxyl residue to serve as the proton abstractor of a catalytic

Zn^{II} site.[7] Furthermore, the removal of the cysteines avoids special handling techniques required to prevent oxidation of these residues to the corresponding disulfide.[34] The resulting sequence for peptides **ZF01** was Ac-Phe-Ala-Val-Pro-DSer-Fen-Ala-Phe-Ser-Gln-Ser-Asp-Glu-Leu-Thr-Lys-Ala-Ile-Arg-Thr-His-Thr-NH_2.

*Circular Dichroism Studies on Peptide **ZF01***

While the CD signature of peptide **ZF01** in the absence of metal was largely random coil,[50] the addition of Zn^{II} increased the overall secondary structure (Figure 3-8a). The resulting spectroscopic signature of the peptide-Zn^{II} complex, although considerably weaker, is reminiscent of that of natural zinc fingers.[29, 31] Concurrent with the increase in secondary structure, the addition of Zn^{II} also produced a significant CD signal in the near-UV (250-300 nm) region (Figure 3-8b). This signal was indicative of the formation of a chiral metal complex involving the Fen residue. The CD spectra of uncomplexed peptide **ZF01** were invariant with pH (4.0-7.0) and peptide concentration (21 μM-1.9 mM) demonstrating the absence of aggregation behavior (not shown).

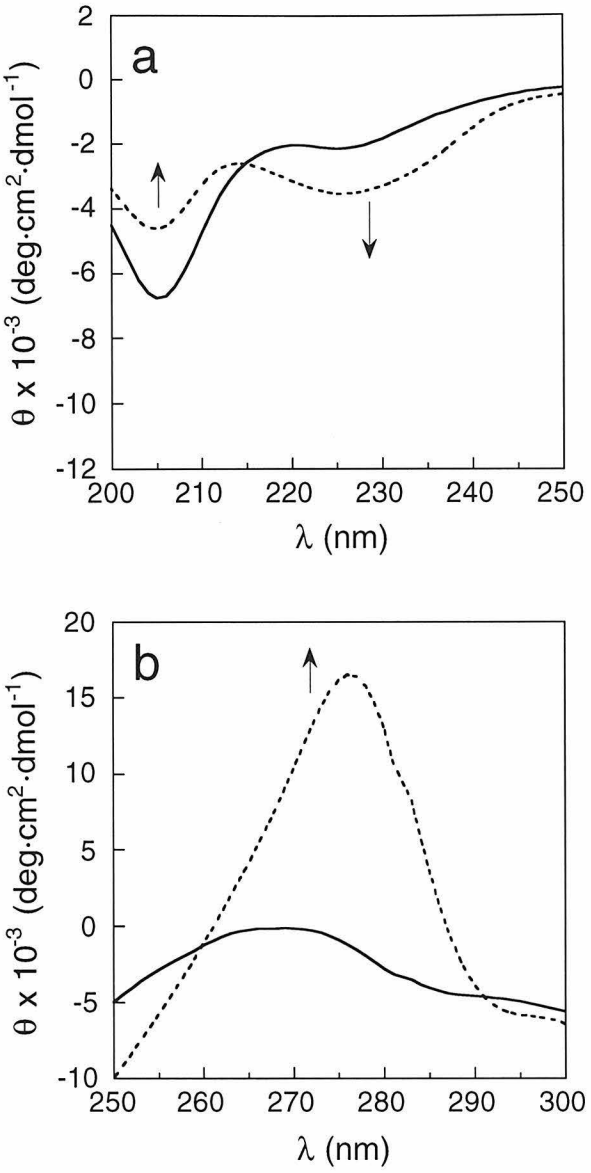

Figure 3-8 CD spectra of peptide **ZF01**. (a) The far-UV spectra reported in mean residue ellipticity. (b) The near-UV spectra normalized to the concentration of the phenanthroline chromophore. The solid lines represents the spectra in the absence of Zn^{II}, and the dashed lines are the spectra upon addition of Zn^{II}.

Peptide ZF02

*Design of Peptide **ZF02***

The second generation design, **ZF02**, included amino acid substitutions intended to increase inherent secondary structure.[35] The alanine residues in the β-hairpin region (positions 2, and 7) were replaced with the β-branched amino acid threonine, which has a higher propensity to adopt an extended or sheet-like conformation.[35] These positions are located on the solvent exposed exterior of the sheet and threonine also imparts hydrophilicity to this face. Additionally, the β-branched amino acids in the α-helix were replaced with residues exhibiting high helical propensities (Leu or Ala), and the sequence was lengthened by one residue to include a glycine at the end of the helix. This residue is often found at the C-terminus of helices and is thought to serve as a helix "stop signal" or helix "cap".[51, 52] The sequence of peptide **ZF02** was designed to be Ac-Phe-Thr-Val-Pro-DSer-Fen-Thr-Phe-Ser-Arg-Ser-Asp-Glu-Leu-Ala-Lys-Leu-Leu-Arg-Leu-His-Ala-Gly-NH_2.

*Circular Dichroism Studies on Peptide **ZF02***

CD studies suggested that the structure of **ZF02** was more preorganized than that of **ZF01**. The increased negative ellipticity of this peptide at 222 nm was consistent with greater inherent helicity in the absence of metal (Figure 3-9a). Nevertheless, addition of metal resulted in spectral changes consistent with the formation of a more structured peptide. The CD signature was not dependent on peptide concentration (23 μM-2.2 mM) or pH (4.5-8.0). Appearance of a distinct CD signal in the near-UV range (250-350 nm) upon addition of Zn^{II} indicated the formation of a chiral complex involving the Fen residue similar to peptide **ZF01** (Figure 3-9b).

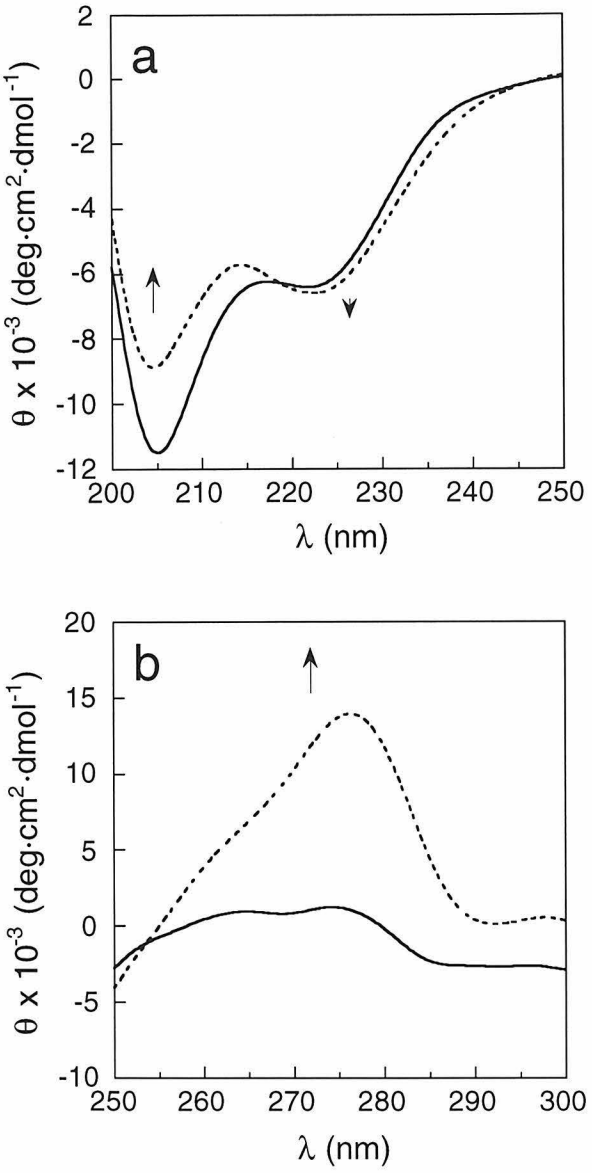

Figure 3-9 CD spectra of peptide **ZF02**. (a) The far-UV spectra reported in mean residue ellipticity. (b) The near-UV spectra normalized to the concentration of the phenanthroline chromophore. The solid lines represents the spectra in the absence of Zn^{II}, and the dashed lines are the spectra upon addition of Zn^{II}.

Peptide ZF03

*Design of Peptide **ZF03***

Although the results of the CD studies of peptide **ZF02** were encouraging, it was evident that the structure of **ZF02** still required metal coordination. To create a metal independent structural motif, the design of peptide **ZF03** targeted the β-hairpin region. Specifically the incorporation of a type II′ turn was investigated. Studies of the protein database[53] have found that tight β-hairpins include almost exclusively type I' or type II' β-turns, despite a general prevalence of type I and type II turns in protein structures.[54] Modeling studies performed by Ranabir Sinha Roy have revealed that a type II′ turn leads to convergent β-strands, while the type II turn affords divergent strands that cannot effectively form a β-sheet (Figure 3-10).[55] These results prompted the incorporation of a type II′ reverse turn into peptide **ZF03**. Since the (ϕ, ψ) dihedral angles associated with the central two residues of the type II′ turn [(60°, -120°), (-80°, 0°)] are the inverse of those required for type II turn formation [(-60°, 120°), (80°, 0°)],[53] the two turn types exhibit opposite chirality preferences. Specifically, the Pro^4-DSer^5 sequence present in peptide **ZF02** was replaced with DPro^4-Ser^5 for peptide **ZF03**.

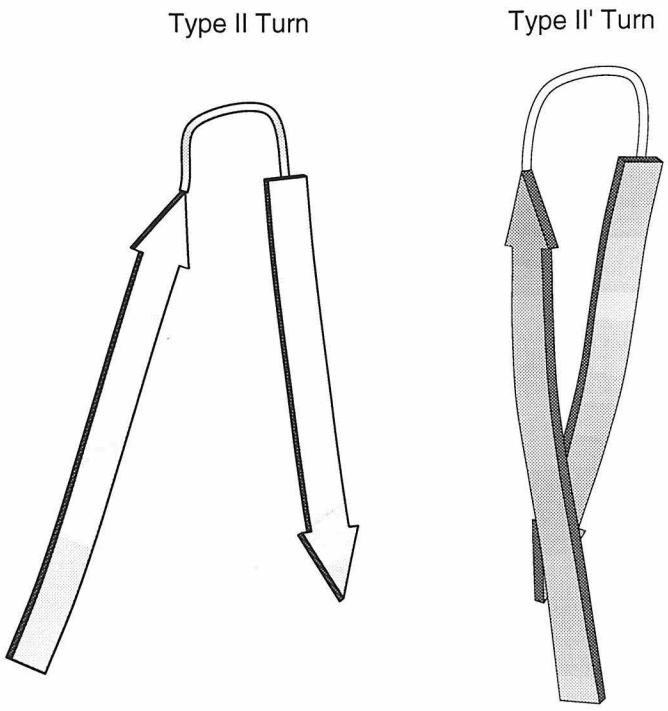

Figure 3-10 Results from molecular modeling to illustrate the effects of type II turn and type II′ turn on β-sheet formation.

*Circular Dichroism Studies on Peptide **ZF03***

Uncomplexed peptide **ZF03** exhibited a CD signature similar to that seen for peptide **ZF02**. However, it was notable that this CD spectrum changed very little upon addition of Zn^{II}, indicating that the secondary structure for **ZF03** was not metal dependent (Figure 3-11a). As with previous designs, the CD spectra in the absence of metal was invariant with changes in pH (pH 4.5-8.0) and peptide concentration (22 μM-2.1 mM). However, examination of the Zn^{II} induced changes in the near-UV CD spectrum suggested that the structural changes encountered by the phenanthroline chromophore were different compared to those observed for peptides **ZF01** and **ZF02**.

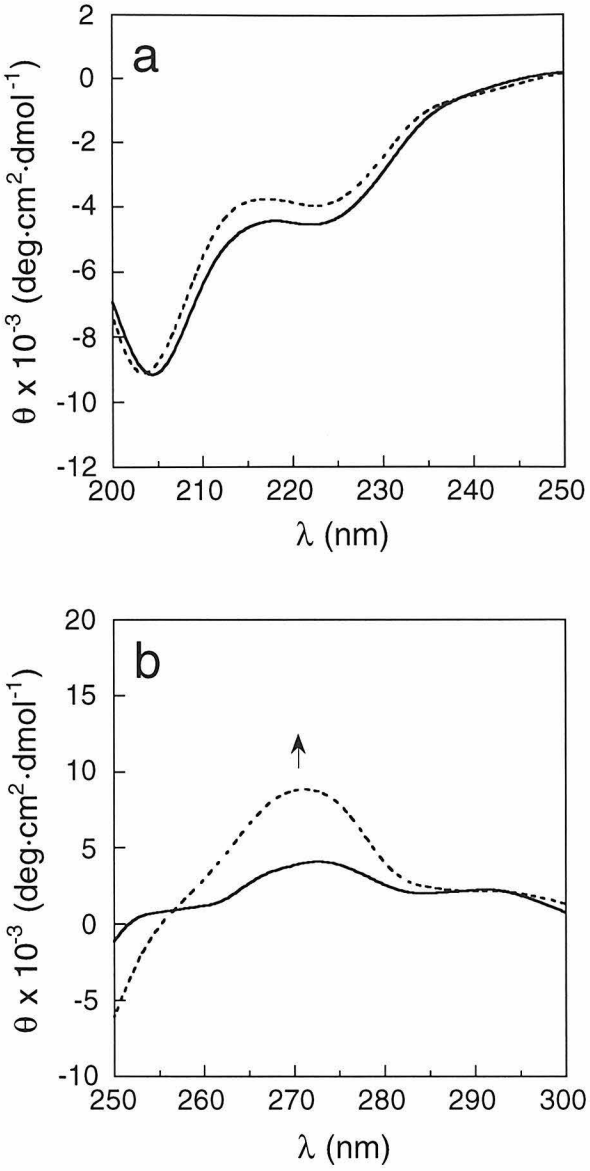

Figure 3-11 CD spectra of peptide **ZF03**. (a) The far-UV spectra reported in mean residue ellipticity. (b) The near-UV spectra normalized to the concentration of the phenanthroline chromophore. The solid lines represents the spectra in the absence of Zn^{II}, and the dashed lines are the spectra upon addition of Zn^{II}.

NMR Analysis on Peptide ***ZF03***

Peptide **ZF03** was further analyzed by Mary Struthers using 2D-NMR spectroscopy in the absence of metal cations. Observation of more than 35 spin systems, rather than the 23 expected for this peptide in this analysis suggested the presence of slowly interconverting conformers. These additional spin systems greatly complicated the spectral analysis, precluding complete sequence specific assignment. Dual spin systems that exhibited vastly different chemical shifts were observed for residues in the β-hairpin region containing DPro^4. In contrast, residues in the helical region (Leu^{14}-Gly^{23}) exhibited dual spin systems with nearly overlapping chemical shifts. These results suggested that the two conformers were the *cis-trans* isomers of the amide bond of DPro^4. While this peptide exhibited a CD spectrum that changed very little upon addition of metal, a detailed structural analysis by NMR revealed the presence of approximately a 40/60 ratio of slowly interconverting *cis-trans* amide isomers of DPro^4. This unexpected result highlights the importance of complementary CD and NMR studies in the analysis of designed polypeptides.

Examining the *cis-trans* Isomerization of DPro in Type II' Turns with the Fens Peptides

In order to manipulate the *cis-trans* proline amide isomer ratio, a series of tetrapeptides was prepared. Since the nature of the residue immediately preceding proline has been shown to influence the proline amide geometry,[56, 57] peptides containing the sequence DPro-Ser (positions *i+1* and *i+2* respectively) and various amino acids (Thr, Val, and Ala) at position (*i*) were analyzed. The peptides studied are listed in Table 3-2. The *cis* amide

bond between residue (*i*) and Pro (*i+1*) results in a large downfield shift in the resonances for protons associated with residue (*i*). The *cis-trans* isomer ratio could therefore be quantified by integration of the 1D-NMR signals of the methyl side chain protons of residue (*i*). The *trans* amide isomer dominated by greater than 90% for all sequences investigated. The peptides were further examined by ROESY and amide proton variable temperature (VT) NMR analyses to determine the propensity of each sequence to adopt a type II′ turn conformation in solution. The results of these studies are summarized in Table 3-2. The spectroscopic signature of type II' turn formation includes the NOEs[58] illustrated in Figure 3-12 and a low VT coefficient ($-\Delta\delta/\Delta T$) for the Fen amide proton. In the series of tetrapeptides studied, peptides **VFen** and **TFen** exhibited lower Fen amide temperature coefficients, as well as the NOEs characteristic of turn formation (Table 3-2). As a result of this study, the optimal turn sequences Val-DPro-Ser-Fen and Val-DPro-Ser-Fen were included in the peptides **ZF04** and **ZF05** respectively.

Table 3-2 Conformational Analysis on the **Fens** Peptides

Peptide	Sequence	% *trans*	NOE[a] Observed	-Δδ/ΔT (ppb/K)		
				Xaa	Ser	Fen
AFen	Ac-Ala-DPro-Ser-Fen-NH_2	92	1,2,3,5	9.10	8.83	4.53
TFen	Ac-Thr-DPro-Ser-Fen-NH_2	94	1,2,3,5	8.18	9.51	3.59
VFen	Ac-Val-DPro-Ser-Fen-NH_2	94	1,2,3,4,5	9.36	8.03	3.52

[a] NOE crosspeaks present in the ROESY experiment for the *trans* amide conformation of DPro[2]. The identities are presented in Figure 3-12.

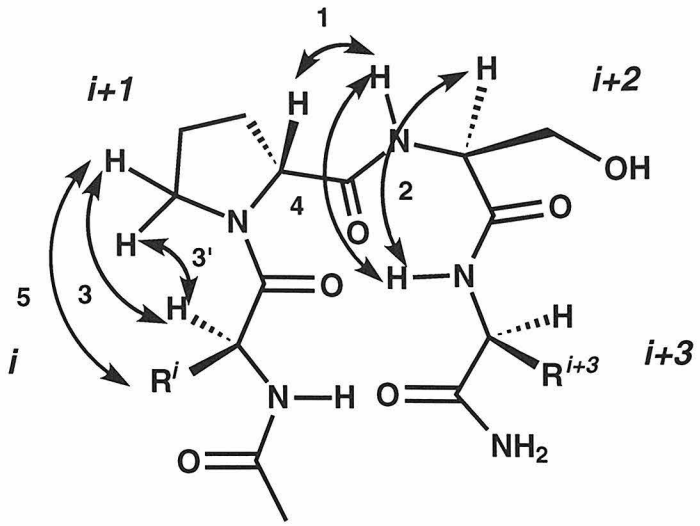

Figure 3-12 Expected NOE interactions in the heterochiral type II' reverse turn. 1, $d_{\alpha,N}$(Pro,Ser); 2, $d_{\alpha,N}$(Ser,Fen); 3 and 3', $d_{\alpha,\delta}$(Xaa,Pro); 4, d_{NN}(Ser, Fen); $d_{\beta,\delta}$(Xaa,Pro). The *i* through *i+1* amides are shown in the trans conformation.

Peptides ZF04 and ZF05

The peptides **ZF04** and **ZF05** incorporated the type II' β-turns that had been determined to contain minimum amounts of the *cis* DPro isomer. The two sequences, Val-DPro-Ser-Fen and Thr-DPro-Ser-Fen, were introduced in the turn region of peptides **ZF04** and **ZF05**, respectively. Furthermore, the turn sequence for peptide **ZF05** incorporates a hydroxyl residue that may serve as a proton abstractor. Peptide **ZF04** was investigated by Mary Struthers and will not be discussed in detail.[59]

*Circular Dichroism Studies on Peptide **ZF05***

The CD signature of uncomplexed peptide **ZF05** resembles those of natural zinc finger peptides. Unlike previous designs, the additions of Zn^{II} resulted in a slight increase of the ellipticity at 222 nm, indicating loss of secondary structure (Figure 3-13a). The CD spectrum was invariant with peptide concentration (15 μM - 1.2 mM) and pH (4.5-8.0). Similar to earlier

designs, changes in the near-UV CD spectrum upon addition of Zn^{II} indicated the formation of a chiral complex involving the Fen residue (Figure 3-13b).

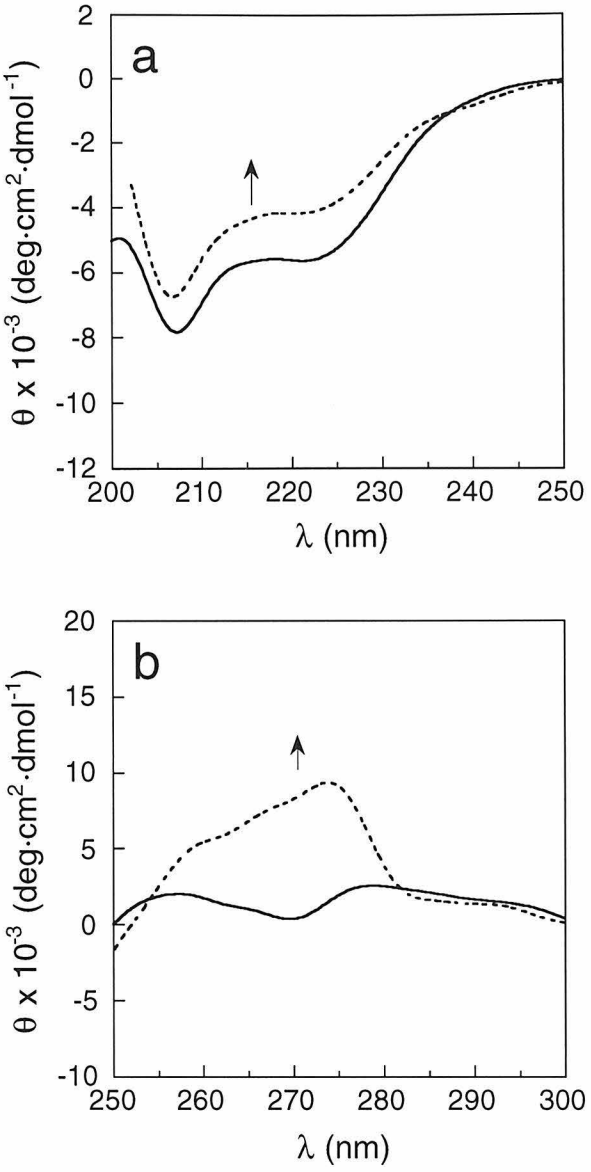

Figure 3-13 CD spectra of peptide **ZF05**. (a) The far-UV spectra reported in mean residue ellipticity. (b) The near-UV spectra normalized to the concentration of the phenanthroline chromophore. The solid lines represents the spectra in the absence of Zn^{II}, and the dashed lines are the spectra upon addition of Zn^{II}.

NMR Analysis on Peptide ***ZF05***

The complete sequence assignment of peptide **ZF05** revealed the expected 23 spin systems (Table 3-3). However, analysis of the NOESY spectra revealed the presence of limited local secondary structure. Although a few NOE crosspeaks indicated of α-helix and β-hairpin formation , no crosspeaks indicative of super-secondary structure were observed (Figure 3-14a). In contrast, the NMR analysis of peptide **ZF04** indicated that this peptide contained both secondary and super-secondary structures (Figure 3-14b).[59] Furthermore, long range NOE crosspeaks indicative of super-secondary structure were also present. It is interesting that substitution of threonine with valine at position 3 drastically influences the overall peptide structure. Thus, future elaboration of the ββα motifs must avoid replacing the valine residue at position 3 to retain the overall super-secondary structure. Further studies focused on this topic would be necessary to elucidate the interactions that are governing this interesting behavior.

Assignment of several key NOE crosspeaks for peptide **ZF04** was hindered by overlapping resonances for the aromatic rings of Phe^{8} and Phe^{1}. This ambiguity resulted in difficulties for obtaining a three dimensional structure by simulated annealing protocols.[59] Therefore, peptide **ZF06** with tyrosine incorporated at position 1 was synthesized and studied.

Table 3-3 Sequence Specific Assignments for Peptide **ZF05**

Residue	Amide	Alpha	Beta	Other Side Chain Protons
Ac	N/A	1.92	N/A	N/A
Phe^{1}	8.290	4.591	2.998, 2.759	7.073, 7.165
Thr^{2}	8.262	4.463	4.122	γ1.087
Thr^{3}	8.299	4.600	4.179	γ1.222
Pro^{4}	N/A	4.398	2.162, 1.737	γ1.880, 1.843; δ3.731
Ser^{5}	8.344	4.377	3.768, 3.733	N/A
Fen^{6}	8.760	5.283	3.644, 3.529	7.747, 8.369, 8.020, 7.971, 8.820, 8.036, 9.093
Thr^{7}	8.372	4.330	4.021	γ1.061
Phe^{8}	8.258	4.350	2.747, 2.667	7.003, 7.174,
Ser^{9}	8.449	4.391	3.872, 3.781	N/A
Arg^{10}	8.597	4.221	1.885	γ1.763, 1.621; δ3.136, 3.129; NH7.371
Ser^{11}	8.455	4.241	3.903, 3.839	N/A
Asp^{12}	8.351	4.505	2.679	N/A
Glu^{13}	8.182	4.074	2.089	γ2.337
Leu^{14}	8.156	4.124	1.702	γ1.603; δ0.886, 0.865
Ala^{15}	8.013	4.097	1.469	N/A
Lys^{16}	7.853	4.011	1.891	γ1.363; δ1.658, 1.554; ε2.914; NH7.663
Leu^{17}	7.868	4.130	1.820	γ1.708, 1.607; δ0.922, 0.868
Leu^{18}	8.035	4.177	1.761	γ1.589; δ0.894, 0.863
Arg^{19}	7.844	4.201	1.880	γ1.715, 1.624; δ3.205; NH7.298
Leu^{20}	7.963	4.211	1.686	γ1.507; δ0.901, 0.842
His^{21}	8.275	4.667	3.339, 3.197	7.297, 8.624
Ala^{22}	8.298	4.327	1.428	N/A
Gly^{23}	8.481	3.920	N/A	N/A

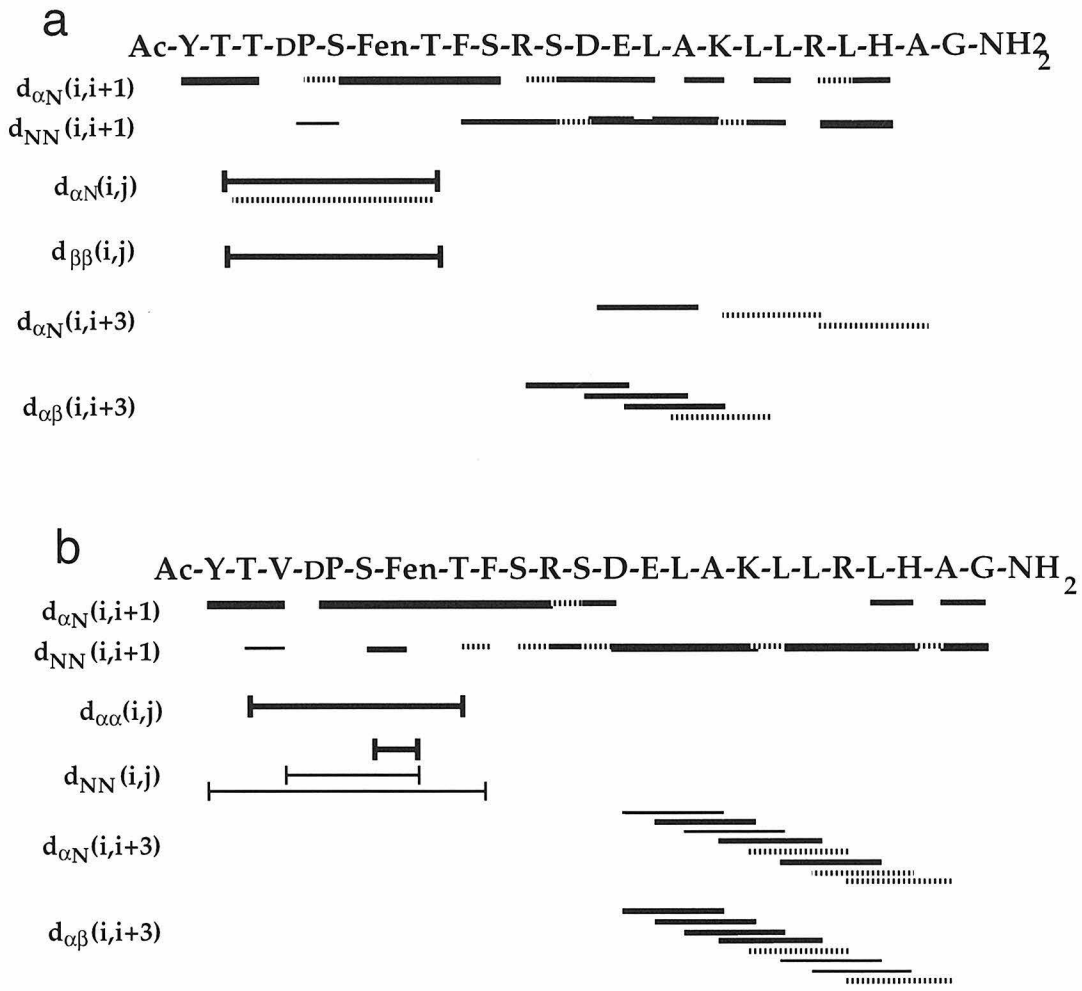

Figure 3-14 NOE crosspeaks indicative of structure for peptide **ZF05** (a) and **ZF04** (b). The width of the lines represent the relative strength of the crosspeak, a dashed line indicates that the NOE could not be identified due to overlap.

Peptide ZF06

*Circular Dichroism Studies on Peptide **ZF06***

The CD spectrum of **ZF06** resembles that of the natural zinc fingers.[30, 31] The addition of Zn^{II} results in only a slight change in the CD spectrum in the far-UV range, indicating that secondary structure is metal independent (Figure 3-15a). Furthermore, a much weaker CD signal is observed in the near UV-region for peptide **ZF06**, consistent with the idea that addition of Zn^{II} no longer dominates secondary and super-secondary structure (Figure 3-15b). The CD spectrum of uncomplexed **ZF06** was invariant with pH (4.0-8.0) and peptide concentration (20 μM-2 mM), indicating the absence of aggregation effects. The NMR data was analyzed by Mary Struthers. Complete sequence assignment was performed for peptide **ZF06**, and NOE crosspeaks indicative of secondary and super-secondary structure were observed. The solution structure of peptide **ZF06** was solved through the use of an NOE-restrained simulated annealing (Figure 3-16).[60] Interestingly, peptide **ZF06** exhibits a more open structure compared to natural zinc finger domains due to the removal of the structurally required metal binding site. This creates an accessible cleft between the α-helix and the β-hairpin which may be exploited in future designs to incorporate function. As the first successfully designed metal independent ββα motif, this peptide was renamed **BBA1**.

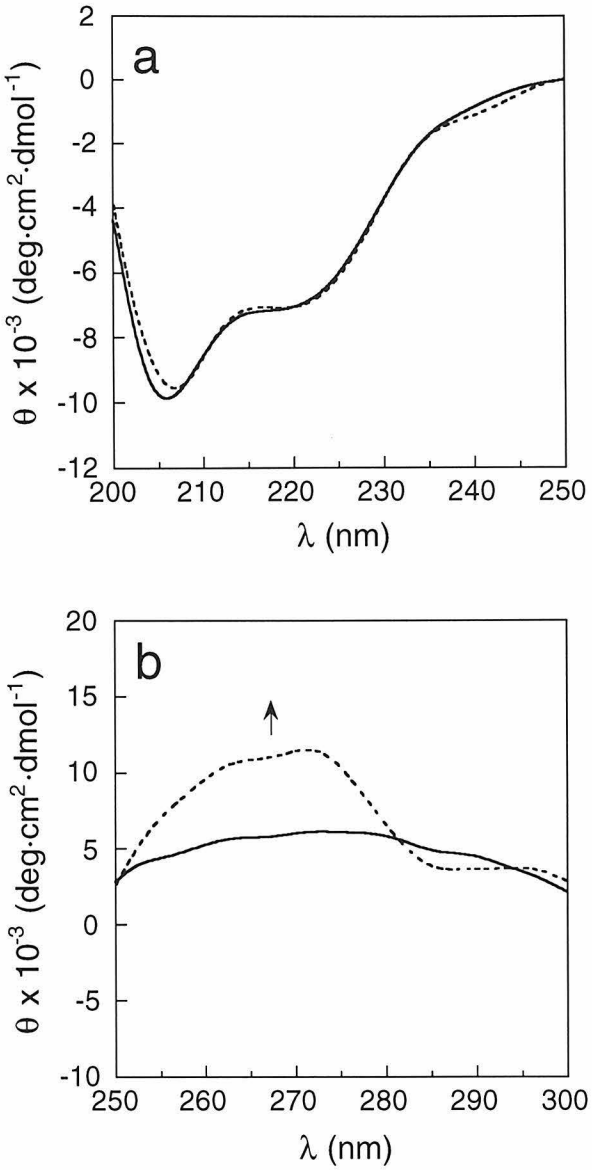

Figure 3-15 CD spectra of peptide **ZF06 (BBA1)**. (a) The far-UV spectra reported in mean residue ellipticity. (b) The near-UV spectra normalized to the concentration of the phenanthroline chromophore. The solid lines represents the spectra in the absence of Zn^{II}, and the dashed lines are the spectra upon addition of Zn^{II}.

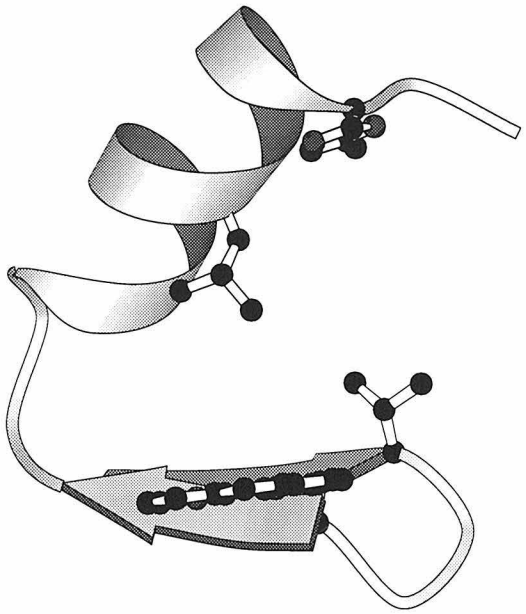

Figure 3-16 The structure of peptide **ZF06** (**BBA1**) solved by NOE-restrained simulated annealing (generated using the program Molscript[61]).

Peptide ZF07

In order to further establish the importance of the type II' β-turn in the metal independent structure exhibited by **BBA1**, a control peptide was synthesized and analyzed. The type II' turn used in peptide **BBA1** was replaced with a type II turn to in peptide **ZF07**. This peptide has an identical primary sequence to **BBA1**, differing only in the chirality of the central turn residues (Pro^4, Ser^5).

The structure of peptide **ZF07** was evaluated by Mary Struthers using NMR.[59] These analyses revealed that while the helical structure was largely maintained, both the β-hairpin and the super-secondary structure observed in **BBA1** were absent. Thus, although **ZF07** and **BBA1** differ only in the type of β-turn employed, the effects on secondary and tertiary structure are dramatic.

The β-turns have been extensively studied because of their structural and functional role in peptides and proteins. These structures have been

shown to be critical in the bioactivity of small naturally occurring peptides and have been implicated in the process of protein folding.[62] This study highlights the potential of using these small motifs as structural nucleation elements in protein design. The use of the type II' β-turn in concert with the judicious selection of amino acids to enhance inherent secondary structure have resulted in the successful design of a stable, well-defined ββα motif that folds in the absence of metal.

The Zn^{II}-Binding Properties of the Metallopeptides

The Zn^{II}-binding properties of the peptides mentioned above were investigated by monitoring metal cation titrations using absorption (UV-vis) spectroscopy according to the procedures described in Chapter 2. Calculations employing an iterative method afforded the apparent dissociation constants for the peptide-Zn^{II} complexes (Table 3-4).

The peptides **ZF01**, **ZF02**, and **ZF03** all have a putative $FenHis_2$ coordination sphere. The intended ligation sphere for peptides **ZF05**, **BBA1** and **ZF07** is FenHis. The peptides **HF01** (Ac-Ala-His-Pro-DSer-Fen-Ala-NH_2) and **HF03** (Ac-Thr-His-DPro-Ser-Fen-Thr-NH_2) are truncated version of the β-hairpins in peptides **ZF01** and **ZF03**, thereby serving as controls to probe the participation of the histidine on the α-helix in metal binding. Similarly, the sequences of peptides **TFen** and **VFen** are the sequences for the reverse turns incorporated in peptides **ZF05** and **ZF06**, respectively.

Table 3-4 Apparent Dissociation Constants (μM) for the Peptide-Zn^{II} Complexes[a]

Peptide	Intended Ligating Residues[b]	K_D
ZF01	$His^3Fen^6His^{21}$	0.65
ZF02	$His^3Fen^6His^{21}$	0.89
ZF03	$His^3Fen^6His^{21}$	0.99
ZF05	Fen^6His^{21}	3.95
BBA1	Fen^6His^{21}	4.56
ZF07	Fen^6His^{21}	6.28
HF01	Ac-Ala-**His**-Pro-DSer-**Fen**-Ala-NH_2	0.90
HF03	Ac-Thr-**His**-DPro-Ser-**Fen**-Thr-NH_2	2.62
AFen	Ac-Ala-DPro-Ser-**Fen**-NH_2	8.23
TFen	Ac-Thr-DPro-Ser-**Fen**-NH_2	16.2
VFen	Ac-Val-DPro-Ser-**Fen**-NH_2	22.8

[a] Metal cation titrations performed in 0.05 M HEPES buffer at pH 8.25.
[b] The full sequences of the **ZF** peptides are presented in Figure 3-6. The full sequences are shown for the hexapeptides **HF01** and **HF03**, and the tetrapeptides **AFen**, **TFen**, and **VFen**. Furthermore, the intended ligating residues are represented in bold.

Peptides **ZF01**, **ZF02**, and **ZF03** show higher Zn^{II} binding affinity compared to peptides **ZF05**, **BBA1** and **ZF07**. This suggests that the histidine at position 3 is actively participating in binding Zn^{II}. The Zn^{II} binding affinity of peptides **ZF01** and **ZF02** is similar to peptide **HF01**, indicating that the histidine at position 21 is not binding Zn^{II} effectively in the two ββα peptides. However, peptides **ZF03**, **ZF05**, and **BBA1** exhibit higher Zn^{II} affinity compared to **HF03**, **TFen**, and **VFen**, which can be attributed to the participation of His^{21} in Zn^{II} binding for the three ββα peptides. The

participation of His^{21} in ligation appears to parallel the existence of peptide structure. The peptide architecture of the more structured peptides **ZF03**, **ZF05** and **BBA1** is responsible for positioning the intended metal ligating residues in close proximity, thereby exhibiting enhanced metal binding compared to the corresponding tetrapeptides. The less structured peptides **ZF01** and **ZF02** are incapable of recruiting the intended ligating amino acids, therefore exhibit similar Zn^{II} binding affinities compared to the corresponding β-hairpins. Interestingly, the **Fens** peptides exhibit the following trend for Zn^{II} binding affinity: **AFen** > **TFen** > **VFen**. This trend appears to correlate with the size of the residue incorporated at position 1. The larger the "innocent" non-participating residue incorporated at position 1, the lower the Zn^{II} binding affinity. These results are consistent with the results presented in Chapter 2, which demonstrated that the modulation of metal binding affinity in designed peptides can be achieved by varying the metal-binding amino acids and the peptide architecture.

The exploitation of the peptide construct to affect metal binding affinity of metallopeptides has been expanded to include the ββα motifs. In all cases, the peptides were designed to recruit several metal binding residues to the metal binding site. In some instances, the peptide architecture served to position an "innocent" residue near the intended metal binding site to diminish the metal binding ability. These results demonstrates that the guidelines for designing metallopeptides derived from studies on hexapeptides presented in Chapter 2 can be exploited in larger constructs, and that the guidelines are universal.

Conclusions

Crucial to the *de novo* design of functional polypeptides is the availability of synthetic motifs with well defined structure in the absence of crosslinks such as disulfide bonds and metal cations. The development of such a ββα motif patterned after zinc finger domains has been demonstrated by an iterative design approach. Appropriate structural nucleation elements have been incorporated to compensate for the stability originally afforded by the metal binding in natural zinc finger peptides. The ββα topology of the resulting peptide, **BBA1,** is reminiscent of the zinc finger domains. Interestingly, the elimination of the zinc binding site results in a more open structure. This creates an accessible cleft between the α-helix and the β-hairpin which may be exploited as a small molecule substrate binding site in future designs. The template resulting from these efforts therefore provides a well-defined structural scaffold for the development of functional polypeptides.

Furthermore, the peptide architecture has been exploited in affecting the metal binding ability of these ββα peptides. This expands the applicability of the guidelines derived earlier for hexapeptides to include larger constructs such as the ββα motif. These results should be useful for future implementation of zinc dependent hydrolase activity.

Acknowledgments

The later stages of the project was performed in collaboration with Mary Struthers (Ph. D., Caltech, 1996). She is responsible for the NMR studies on peptides **ZF03**, **ZF04**, **BBA1**, **ZF07**, and the **Fens** peptides (details were not presented in this chapter). Ranabir Sinha Roy performed the molecular modeling for the type II and type II' turns. Dr. Jane Sanders is responsible for the PD-MS that was important for development of the synthetic protocols for obtaining the peptides. A portion of the work described in this chapter appeared in the following publications:

Struthers, M. D.; Cheng, R. P.; Imperiali, B. "Economy in Protein Design: Evolution of a Metal-Independent ββα Motif Based on the Zinc Finger Domains" *J. Am. Chem. Soc.* **1996**, *118*, 3073-3081.

Struthers, M. D.; Cheng, R. P.; Imperiali, B. "Design of a Monomeric 23-Residue Polypeptide with Defined Tertiary Structure" *Science* **1996**, *271*, 342-345.

Experimental Section

Peptide Synthesis

All peptides were synthesized by solid phase methods using N^{α}-9-fluorenylmethyloxycarbonyl (Fmoc) amino acid pentafluorophenyl esters on a Milligen 9050 automated peptide synthesizer. Commercially available starting materials and reagents were purchased from Milligen Biosearch, EM Science, and Aldrich Chemical Company. Fmoc-PAL-PEG-PS resin (substitution 0.21 mmol/g) was used to afford C-terminal primary amides.

The Fen residue was coupled off-line with three equivalents of Fmoc-Fen ((*S*)-*N*$^{\alpha}$-fluorenylcarboxymethyl-2-amino-3-(1,10-phenanthrol-2-yl)propionic acid[63] and four equivalents of 1-hydroxy-7-azabenzotriazole (HOAT) and *O*-(7-azabenzotriazol-1-yl)-1,1,3,3,-tetramethyluronium hexafluorophosphate (HATU)[37] in *N*-methylpyrrolidinone (NMP) for 2.5 hours. Peptides were *N*-acylated on the resin using 7 equivalents of acetic anhydride and 7 equivalents of triethylamine in 3 mL of DMF for 2 hours.

The peptides were deprotected and cleaved from the resin by treatment with Reagent K (trifluoroacetic acid/phenol/H_2O/thioanisole/ethanedithiol, 82.5:5:5:2.5)[64] for 2 hours. Trituration with 1:1 ether/hexane afforded the crude peptide. The peptides were purified by reverse-phase HPLC on a C_{18} semipreparative column. The purity of the peptides was confirmed by analytical HPLC and capillary zone electrophoresis (CZE). Identity of all peptides was confirmed by matrix-assisted laser desorption ionization mass spectrometry (MALDI-MS), plasma desorption mass spectroscopy (PDMS), electrospray mass spectrometry (ES-MS) or fast atom bombardment mass spectrometry (FAB) (Table 3-5).

Absorption Spectroscopy (UV/Vis) Studies

Absorption spectra were obtained on a Shimadzu UV-110 spectrophotometer using 1.0 cm path length quartz cuvettes. The concentrations of the peptide solutions were determined spectrophotometrically using the characteristic absorption band of the phenanthrolyl moiety (λ_{max} = 268 nm, ε_{max} = 13,950 $M^{-1}cm^{-1}$). The Zn^{II} binding studies were carried out according to procedures presented in Chapter 2. In brief, aqueous solutions of known peptide concentrations (1-20 μM) were titrated with standardized metal cation solutions at room temperature

in 0.05 M HEPES buffer at pH 8.25. The dissociation constants (K_D) were calculated using an iterative process based on the Scott equation[65]:

$$\frac{b \cdot [M]}{\Delta A} = \frac{[M]}{[Pep]_t \cdot \Delta\varepsilon} + \frac{K_D}{[Pep]_t \cdot \Delta\varepsilon}$$

where b = cell path length, [M] = free metal cation concentration, ΔA = change in absorbance due to complex formation, $[Pep]_t$ = total peptide in solution, $\Delta\varepsilon$ = change in molar absorptivity due to complex formation.

Table 3-5 The Calculated and Observed Mass Values for the Synthetic Peptides[a]

Peptide	Formula	Species Observed	Calculated	Observed
ZF01	$C_{120}H_{172}N_{34}O_{34}$	MH^+	2635.9	2635.9
ZF02	$C_{128}H_{189}N_{37}O_{33}$	MH^+	2775.2	2775.7
ZF03	$C_{128}H_{189}N_{37}O_{33}$	MH^+	2775.2	2775.1
ZF04	$C_{127}H_{191}N_{35}O_{33}$	MH^+	2737.1	2737.5
ZF05	$C_{126}H_{189}N_{35}O_{34}$	MH_3^{3+}	913.07	913.4
BBA1	$C_{126}H_{191}N_{35}O_{34}$	MH^+	2753.1	2752.8
ZF07	$C_{126}H_{191}N_{35}O_{34}$	MH^+	2753.9	2753.1
HF01	$C_{37}H_{45}N_{11}O_8$	MH^+	772.3531	772.3537
HF03	$C_{39}H_{49}N_{11}O_{10}$	MH^+	832.3742	832.3740
AFen	$C_{28}H_{33}N_7O_6$	MH^+	564.2571	564.2552
TFen	$C_{29}H_{35}N_7O_7$	MH^+	594.2676	594.2706
VFen	$C_{30}H_{37}N_7O_6$	MH^+	592.2884	592.2881

[a] The short peptides were analyzed using FAB and high resolution data is presented. Peptide **ZF05** was analyzed by ES-MS, and peptides **ZF01** through **ZF03** were analyzed using PD-MS. Peptides **ZF04**, **BBA1**, and **ZF07** were analyzed by MALDI-MS.

Circular Dichroism Spectroscopy Studies

Circular dichroism spectra were recorded on a Jasco J600 Circular Dichroism Spectrometer. The concentration of the peptide solutions was determined spectrophotometrically using the characteristic absorption band of

the phenanthrolyl moiety. The spectra were processed using the Jasco J600 System Software, and subsequently analyzed using KaleidaGraph. Metal cation titrations were performed with peptide concentrations ranging from 20 μM to 250 μM in 0.01 M TRIS buffer (pH 8.25) in either a 1.0 cm or a 0.1 cm path-length quartz cell. Aggregation properties were investigated with peptide concentrations ranging from 10 μM to 2 mM at pH 4.5 in cuvettes of appropriate path-length.

NMR Studies

Two dimensional NMR spectroscopy of peptides **VFen**, **AFen**, **TFen**, and **ZF05** were performed on a Bruker AMX500 500 MHz spectrometer. The NOESY ^{1}H NMR spectrum of peptide **ZF05** was obtained in 90% H_2O/ 10% D_2O at 7 °C on a Varian Unity Plus 600 MHz instrument. Complete sequence specific assignments were accomplished using total correlation spectroscopy (TOCSY),[66] rotating-frame nuclear Overhauser effect spectroscopy (ROESY),[67] and nuclear Overhauser spectroscopy (NOESY).[58, 68] Suppression of the water signal was accomplished by presaturation. Processing and analysis of the spectra were done using Felix 2.3 software (Biosym Technologies, CA).

References

1. Cheng, R. P.; Imperiali, B. unpublished results.
2. Vallee, B. L.; Auld, D. S. *Acc. Chem. Res.* **1993**, *26*, 543-551.
3. Lindskog, S.; Liljas, A. *Curr. Opin. Struct. Biol.* **1993**, *3*, 915-920.
4. Eriksson, A. E.; Jones, T. A.; Liljas, A. *Proteins* **1988**, *4*, 274-282.
5. Bertini, I.; Luchinat, C. *Acc. Chem. Res.* **1983**, *16*, 272-279.
6. Vallee, B. L.; Auld, D. S. *Proc. Natl. Acad. Sci. USA* **1990**, *87*, 220-224.

7. Argos, P.; Garavito, R. M.; Evenstoff, W.; Branden, C. I. *J. Mol. Biol.* **1978**, *126*, 141-158.

8. Xue, Y.; Liljas, A.; Jonsson, B.-H.; Lindskog, S. *Proteins* **1993**, *17*, 93-106.

9. Regan, L.; DeGrado, W. F. *Science* **1988**, *241*, 976-978.

10. Osterhout, J. J.; Handel, T.; Na, G.; Toumadje, A.; Long, R. C.; Connolly, P. J.; Hoch, J. C.; Johnson Jr., W. C.; Live, D.; DeGrado, W. F. *J. Am. Chem. Soc.* **1992**, *114*, 331-337.

11. Hecht, M. H. *Proc. Natl. Acad. Sci. U.S.A.* **1994**, *91*, 8729-8730.

12. Betz, S. F.; Raleigh, D. P.; DeGrado, W. F. *Curr. Opin. Struct. Biol.* **1993**, *3*, 601-610.

13. Fezoui, Y.; Weaver, D. L.; Osterhout, J. J. *Proc. Natl. Acad. Sci. U.S.A.* **1994**, *91*, 3675-3679.

14. Raleigh, D. P.; Betz, S. F.; DeGrado, W. F. *J. Am. Chem. Soc.* **1995**, *117*, 7558-7559.

15. Smith, D. D. S.; Pratt, K. A.; Sumner, I. G.; Heneeke, C. M. *Protein Eng.* **1995**, *8*, 13-20.

16. Pessi, A.; Bianchi, E.; Crameri, A.; Venturini, S.; Tramontano, A.; Sollazzo, M. *Nature* **1993**, *362*, 367-369.

17. Quinn, T. P.; Tweedy, N. B.; Williams, R. W.; Richardson, J. S.; Richardson, D. C. *Proc. Natl. Acad. Sci. U.S.A.* **1994**, *91*, 8747-8751.

18. Yan, Y.; Erickson, B. W. *Protein Science* **1994**, *3*, 1069-1073.

19. Lovejoy, B.; Choe, S.; Cascio, D.; McRorie, D. K.; DeGrado, W. F.; Eisenberg, D. *Science* **1993**, *259*, 1288-1293.

20. Kuroda, Y. *Protein Eng.* **1995**, *8*, 97-101.

21. Handel, T. M.; Williams, S. A.; DeGrado, W. F. *Science* **1993**, *261*, 879-885.

22. Lieberman, M.; Sasaki, T. *J. Am. Chem. Soc.* **1991**, *113*, 1470-1471.

23. Ghadiri, M. R.; Soares, C.; Choi, C. *J. Am. Chem. Soc.* **1992**, *114*, 4000-4002.

24. Berg, J. M. *Annu. Rev. Biophys. Biophys. Chem.* **1990**, *19*, 405-421.

25. Michael, S. F.; Kilfoil, V. J.; Schmidt, M. H.; Amann, B. T.; Berg, J. M. *Proc. Natl. Acad. Sci. U.S.A.* **1992**, *89*, 4796-4800.

26. Pavletich, N. P.; Pabo, C. O. *Science* **1993**, *261*, 1701-1707.

27. Pavletich, N. P.; Pabo, C. O. *Science* **1991**, *252*, 809-817.

28. Lee, M. S.; Gippert, G. P.; Soman, K. V.; Case, D. A.; Wright, P. E. *Science* **1989**, *245*, 635-637.

29. Weiss, M. A.; Mason, K. A.; Dahl, C. E.; Keutmann, H. T. *Biochemistry* **1990**, *29*, 5660-5664.

30. Weiss, M. A.; Keutmann, H. T. *Biochemistry* **1990**, *29*, 9808-9813.

31. Parraga, G.; Horvath, S.; Eisen, A.; Taylor, W.; Hood, L.; Young, E.; Klevit, R. E. *Science* **1988**, *241*, 1489-1492.

32. Eis, P. S.; Lakowicz, J. R. *Biochemistry* **1993**, *32*, 7981-7993.

33. Frankel, A. D.; Berg, J. M.; Pabo, C. O. *Proc. Natl. Acad. Sci. U.S.A.* **1987**, *84*, 4841-4845.

34. Krizek, B. A.; Amann, B. T.; Kilfoil, V. J.; Merkle, D. L.; Berg, J. M. *J. Am. Chem. Soc.* **1991**, *113*,

35. Fasman, G. D. "*The Development of the Prediction of Protein Structure*" in *Prediction of Protein Structure and the Principles of Protein Conformation*, Plenum Press, New York, 1989; pp 193-316.

36. Fields, G. B.; Noble, R. L. *Int. J. Pept. Protein Res.* **1990**, *35*, 161-214.

37. Carpino, L. A.; El-Faham, A.; Minor, C. A.; Albericio, F. *J. Chem. Soc. Chem. Comm.* **1994**, 201-203.

38. Blanco, F. J.; Rivas, G.; Serrano, L. *Nat. Struct. Biol.* **1994**, *1*, 584-589.

39. Viguera, A. R.; Blanco, F. J.; Serrano, L. *J. Mol. Biol.* **1995**, *247*, 670-681.

40. Stroup, A. N.; Gierasch, L. M. *Biochemistry* **1990**, *29*, 9765-9771.

41. Mantelione, G. T.; Arnold, E.; Meinwald, Y. C.; Stimson, E. R.; Denton, J. B.; Huang, S.-G.; Clardy, J.; Scheraga, H. A. *J. Am. Chem. Soc.* **1984**, *106*, 7946-7958.

42. Wright, P. E.; Dyson, H. J.; Lerner, R. A. *Biochemistry* **1988**, *27*, 7167-7175.

43. Blanco, F. J.; Jiménez, A.; Rico, M.; Santoro, J.; Heranz, J.; Nieto, L. *Eur. J. Biochem.* **1991**, *200*, 345-351.

44. Yan, Y.; Erickson, B. W.; Tropsha, A. *J. Am. Chem. Soc.* **1995**, *117*, 7592-7599.

45. Chalmers, D. K.; Marshall, G. R. *J. Am. Chem. Soc.* **1995**, *117*, 5927-5937.

46. Yan, Y.; Tropsha, A.; Hermans, J.; Erickson, B. W. *Proc. Natl. Acad. Sci. U.S.A.* **1993**, *90*, 7898-7902.

47. Aubry, A.; Cung, M. T.; Marraud, M. *J. Am. Chem. Soc.* **1985**, *105*, 7640-7647.

48. Imperiali, B.; Fisher, S. L.; Moats, R. A.; Prins, T. J. *J. Am. Chem. Soc.* **1992**, *114*, 3182-3188.

49. Dyson, H. J.; Rance, M.; Houghten, R. A.; Lerner, R. A.; Wright, P. E. *J. Mol. Biol.* **1988**, *201*, 161-200.

50. Johnson, J., W. C. *Proteins: Struct. Func. Gen.* **1990**, *7*, 205-214.

51. Richardson, J. S.; Richardson, D. C. *Science* **1988**, *240*, 1649-1652.

52. Presta, L. G.; Rose, G. D. *Science* **1988**, *240*, 1632-1641.

53. Wilmot, C. M.; Thornton, J. M. *J. Mol. Biol.* **1988**, *203*, 221-232.

54. Sibanda, B. L.; Thornton, J. M. *Nature* **1985**, *316*, 170-174.

55. Antiparallel β-strands were generated using the dihedral angles ϕ = -139°, ψ = 135°. A β-hairpin connecting these strands was created by adjusting the dihedrals of the central two turn residues (type II: ϕ_1 = -60°,ψ_1 = 120°; ϕ_2 = 80°,ψ_2= 0°; type II′: ϕ_1 = 60°,ψ_1 =-120°; ϕ_2 =-80°,ψ_2 = 0°).

56. Yao, J.; Feher, V. A.; Espejo, B. F.; Reymond, M. T.; Wright, P. E.; Dyson, H. J. *J. Mol. Biol.* **1994**, *243*, 736-753.

57. Grathwohl, C.; Wüthrich, K. *Biopolymers* **1976**, *15*, 2025-2041.

58. Wüthrich, K. *NMR of Proteins and Nucleic Acids*; John Wiley and Sons: New York, 1986 .

59. Struthers, M. **1996** Ph. D. Thesis, California Institute of Technology.

60. Nilges, M.; Clore, G. M.; Gronenborn, A. M. *FEBS Lett.* **1988**, *239*, 129-136.

61. Kraulis, P. J. *J. Appl. Crystallogr.* **1991**, *24*, 946-950.

62. Rose, G. D.; Gierasch, L. M.; Smith, J. A. *Adv. Prot. Chem.* **1985**, *37*, 1-105.

63. Cheng, R. P.; Fisher, S. L. *J. Am. Chem. Soc.* **1996**, *118*, 11349-11356.

64. King, D. S.; Fields, C. G.; Fields, G. B. *Int. J. Pept. Protein Res.* **1990**, *36*, 255-266.

65. Connors, K. A. *Binding Constants: The Measurement of Molecular Complex Stability*; John Wiley and Sons: New York, 1987 .

66. Bax, A.; Davis, D. G. *J. Magn. Res.* **1985**, *65*, 355-360.

67. Bax, A.; Davis, D. G. *J. Magn. Res.* **1985**, *63*, 207-213.

68. States, D. J.; Haberkorn, R. A.; Ruben, D. J. *J. Magn. Res.* **1982**, *48*, 286-292.

Chapter 4

Design of Zinc Metallopeptides Based on a ββα Motif

Introduction

Toward the design of a functional metallopeptide, an iterative design approach has been adopted which involves two distinct stages: the construction of a structural scaffold and the incorporation of the catalytic function. The successful design of a 23-residue monomeric ββα motif that folds into a well defined super-secondary structure in the absence of crosslinks has been described in Chapter 3 (Figure 4-1). This motif is crucial as a structural scaffold for generating functional Zn^{II} metallopeptides, since it provides a more "nest-like" construct compared to the hexapeptides described in Chapter 2 (see Chapter 3 for details). Furthermore, the folding of this ββα motif is independent of crosslinks such as a metal cation. This characteristic resembles the apo-forms of natural zinc enzymes that bear catalytic zinc sites.

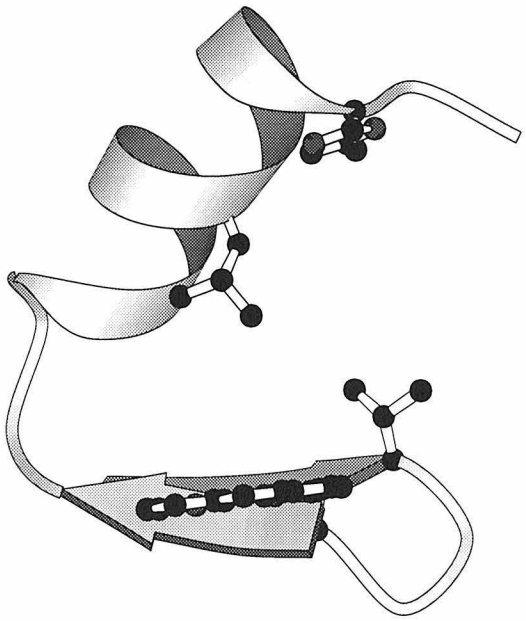

Figure 4-1 The structure of peptide **BBA1** which folds into a well defined structure in the absence of crosslinks (generated using the program Molscript[1]).

After the construction of a rugged structural motif, implementation of the Zn^{II} dependent hydrolase activity into the peptides can be achieved

through incorporating metal-binding residues and other amino acids related to the catalytic function. Hydrolase activity was chosen to be the target due to the simplicity as well as its prevalence in nature. The catalytic machinery of the natural Zn^{II} dependent hydrolases carbonic anhydrase and carboxypeptidase were examined more carefully (Figure 4-2).

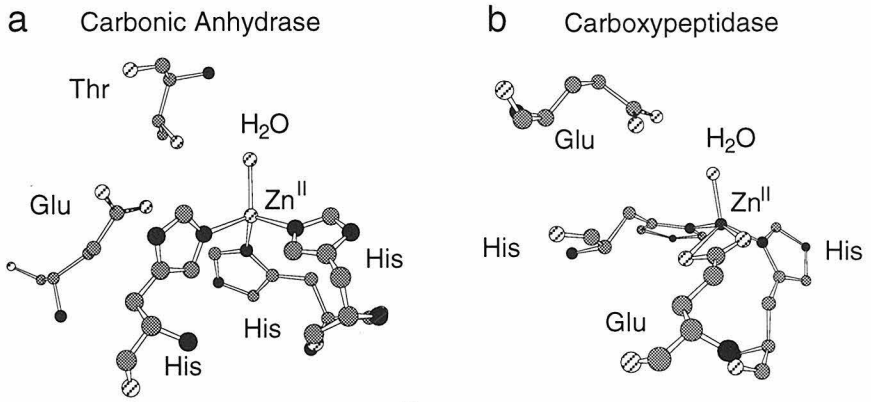

Figure 4-2 The structure of the Zn^{II}-binding site of carbonic anhydrase (a) and carboxypeptidase (b). The hydrogens are omitted for clarity.

The coordination sphere of carbonic anhydrase comprises three metal-binding histidines and a Zn^{II} bound water with a distorted tetrahedral geometry (Figure 4-2a).[2] The mechanism for CO_2 hydration catalyzed by carbonic anhydrase is depicted in Figure 4-3 (for detail description see Chapter 3). The rate limiting step has been demonstrated to be the deprotonation of the Zn^{II} bound water.[3-6] The Zn^{II} bound water has a pK_a of 7.5 which is crucial for forming the active species. Furthermore, a hydrogen bonding network involving residues Thr^{199} and Glu^{106} is responsible for facilitating the deprotonation process. The key residue Thr^{199} has been called the proton abstractor due to its direct interaction with the Zn^{II} bound water.

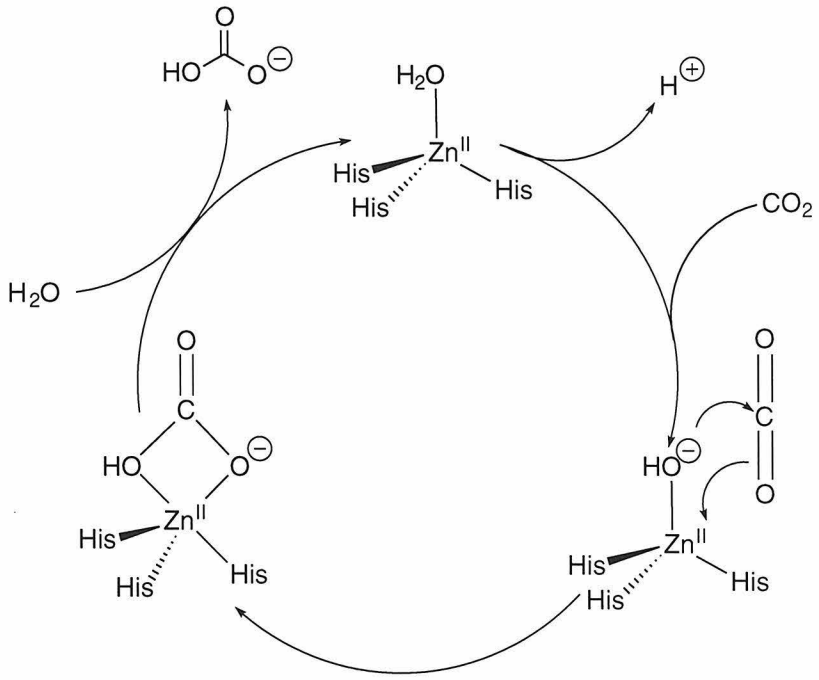

Figure 4-3 The mechanism for CO_2 hydration catalyzed by carbonic anhydrase.

Carboxypeptidase is a Zn^{II} dependent enzyme with 307 residues.[7] This enzyme hydrolyzes amide bonds with considerable rate enhancement. The Zn^{II} in this enzyme is coordinated to two histidines, a glutamic acid and a Zn^{II} bound water (Figure 4-2b). Similar to carbonic anhydrase, the Zn^{II} bound water has a pK_a around 7 and there is a proton abstractor Glu^{270} to facilitate the deprotonation of the Zn^{II} bound water. The catalytic mechanism for performing hydrolase activity is similar to that of carbonic anhydrase.

An ideal model for carbonic anhydrase would have a tetrahedral zinc binding site and a pK_a of 7 for the Zn^{II}-bound water. Many model systems have been developed for carbonic anhydrase.[8-10] One of the well characterized aqueous model complexes to date has been the Zn^{II} complex of 1,5,9,-triazacyclododecane ([12]aneN3) developed by Kimura and coworkers (Figure 4-4).[11-13] The crystal structure establishes the tetrahedral geometry of

the complex. Furthermore, the pK_a is 7.3 which is closer to the pK_a of the enzyme than any of the other models that has shown activity.

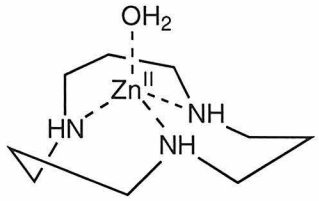

Figure 4-4 A model for carbonic anhydrase, $Zn^{II}[12]aneN_3(OH_2)$

The goal is to construct a metal-binding site that mimics carbonic anhydrase or carboxypeptidase in the ββα motif. Small peptidyl models would have more potential to demonstrate selectivity due to the ease of incorporating different amino acids to facilitate selectivity. Non-peptidyl systems require the chemical synthesis of the appropriate ligands which would prove arduous and time consuming. Since the overall fold of our peptide scaffold is still small compared to the natural enzymes (23 versus > 250), the focus lies with establishing the metal-binding site which is responsible for the reactivity.

Results and Discussion

The sequences of all peptides investigated in this chapter are depicted in Figure 4-5. These peptides were designed to form Zn^{II}-binding sites that mimic those of carbonic anhydrase (His_3) or carboxypeptidase (His_2Glu). The designs were patterned after the structural scaffold, peptide **BBA1**, which adopts a ββα fold and contains a putative metal-binding site (Fen^6His^{21}). Peptide **ZF05** contains Thr^3 in place of Val^3 found in peptide **BBA1**. This hydroxyl residue may serve as a proton abstractor to facilitate the deprotonation of the putative Zn^{II} bound water. The **CA-I** peptides (**CA01**, **CA02**, and **CA03**) were intended to bind Zn^{II} with residues 3, 6 and 17. Additionally, homoserine (Hse) has been incorporated at position 21 as a potential proton abstractor in these peptides. The Zn^{II}-binding site for peptide **CA01** (His_3) resembles that of carbonic anhydrase, while the coordination sphere for metal complexes of peptides **CA02** (His_2Asp) and **CA03** (His_2Glu) were patterned after carboxypeptidase. The **CA-II** peptides (**CA04**, **CA05**, and **CA06**) were designed to form Zn^{II}-binding sites with metal-binding residues at positions 6, 17, and 21. The Zn^{II}-binding site of peptide **CA04** comprises three histidines, while those of peptides **CA05** and **CA06** involve two histidines with a lysine and ornithine (Orn) residue, respectively. The **CA-III** peptides incorporated combinations of unnatural residues (*S*)-2-amino-3-(pyrid-3-yl)propionic acid (**3Pyr**) and (*S*)-2-amino-3-(pyrid-4-yl)propionic acid (**4Pyr**) at positions 6, 18 and 21 (Figure 4-20).

Figure 4-5 (following page) Sequences of the metallopeptides patterned after the ββα structural scaffold, peptide **BBA1**. The sequence for peptide **BBA1** is shown for comparison. The putative metal-binding residues are presented in bold face. Standard three letter codes are employed except for Fen ((*S*)-2-amino-3-(1,10-phenanthrol-2-yl)propanoic acid), Hse (homoserine), Orn (ornithine), and Pyr ((*S*)-2-amino-3-(pyridyl)propionic acid).

Peptide	Sequence	Designed Proton Abstractor
	← β-hairpin → loop ← α-helix → (5 10 15 20)	
ZF05:		
BBA1:	Ac-Tyr-Thr-Val-DPro-Ser-**Fen**-Thr-Phe-Ser-Arg-Ser-Asp-Glu-Leu-Ala-Lys-Leu-Leu-Arg-Leu-**His**-Ala-Gly-NH_2	N/A
	Ac-Phe-Thr-Thr-DPro-Ser-**Fen**-Thr-Phe-Ser-Arg-Ser-Asp-Glu-Leu-Ala-Lys-Leu-Leu-Arg-Leu-**His**-Ala-Gly-NH_2	Thr^3
CA-I Peptides		
CA01:	Ac-Tyr-Thr-**His**-DPro-Ser-**His**-Thr-Phe-Ser-Arg-Ser-Asp-Glu-Leu-Ala-Lys-**His**-Leu-Arg-Leu-Hse-Ala-Gly-NH_2	Hse^{21}
CA02:	Ac-Tyr-Thr-**Asp**-DPro-Ser-**His**-Thr-Phe-Ser-Arg-Ser-Asp-Glu-Leu-Ala-Lys-**His**-Leu-Arg-Leu-Hse-Ala-Gly-NH_2	Hse^{21}
CA03:	Ac-Tyr-Thr-**Glu**-DPro-Ser-**His**-Thr-Phe-Ser-Arg-Ser-Asp-Glu-Leu-Ala-Lys-**His**-Leu-Arg-Leu-Hse-Ala-Gly-NH_2	Hse^{21}
CA-II Peptides		
CA04:	Ac-Tyr-Thr-Val-DPro-Ser-**His**-Thr-Phe-Ser-Arg-Ser-Asp-Glu-Leu-Ala-Lys-**His**-Leu-Arg-Leu-**His**-Ala-Gly-NH_2	N/A
CA05:	Ac-Tyr-Thr-Val-DPro-Ser-**Lys**-Thr-Phe-Ser-Arg-Ser-Asp-Glu-Leu-Ala-Lys-**His**-Leu-Arg-Leu-**His**-Ala-Gly-NH_2	N/A
CA06:	Ac-Tyr-Thr-Val-DPro-Ser-**Orn**-Thr-Phe-Ser-Arg-Ser-Asp-Glu-Leu-Ala-Lys-**His**-Leu-Arg-Leu-**His**-Ala-Gly-NH_2	N/A
CA-III Peptides		
CA07:	Ac-Tyr-Thr-Val-DPro-Ser-**3Pyr**-Thr-Phe-Ser-Arg-Ser-Asp-Glu-Leu-Ala-Lys-Leu-**3Pyr**-Arg-Leu-**3Pyr**-Ala-Gly-NH_2	N/A
CA08:	Ac-Tyr-Thr-Val-DPro-Ser-**4Pyr**-Thr-Phe-Ser-Arg-Ser-Asp-Glu-Leu-Ala-Lys-Leu-**3Pyr**-Arg-Leu-**3Pyr**-Ala-Gly-NH_2	N/A

CA-I Peptides

*Design of the **CA-I** Peptides*

The **CA-I** peptides were designed based on the sequence of peptide **BBA1** to ensure that the super-secondary structure was present. Earlier designs of the ββα motif suggested that positions 3, 6, and 21 were capable of forming a metal-binding site (see Chapter 3). These residues are located on the β-hairpin (positions 3 and 6) and the α-helix (position 21). However, molecular modeling revealed that the putative Zn^{II} bound water is directed away from the peptide into the solvent, making the incorporation of auxiliary residues for catalysis difficult (Figure 4-6). Designing the metal-binding site closer to the hydrophobic core could shield the putative Zn^{II} bound water from bulk solvent and provide opportunity for further elaboration. Therefore, the metal-binding histidine at position 21 was moved to position 17, which is closer to the hydrophobic center (Figure 4-7). Furthermore, homoserine was incorporated at position 21 as a potential proton abstractor. Additionally, placement of metal-binding residues Asp or Glu at position 3 would serve to mimic the Zn^{II}-binding site of carboxypeptidase.

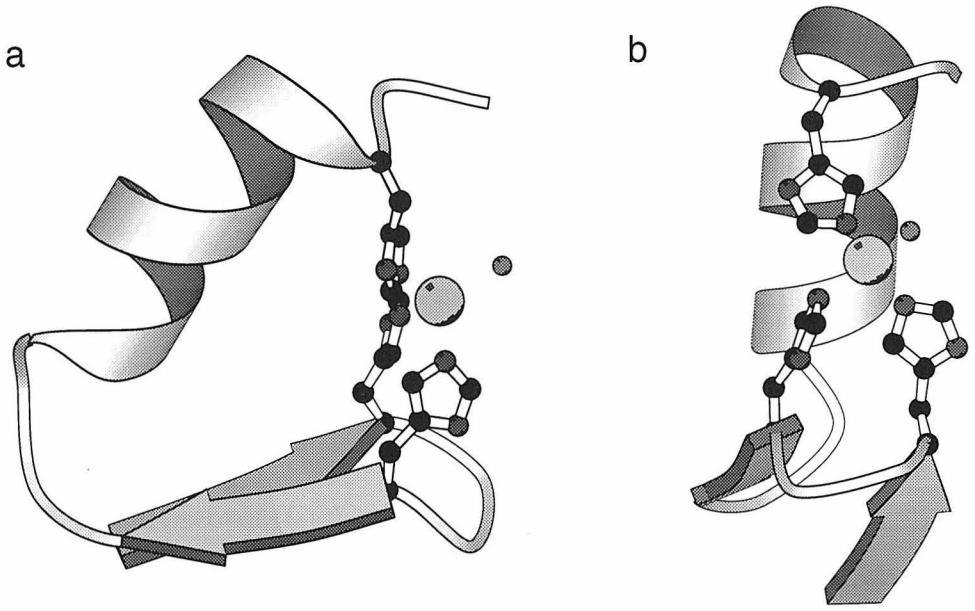

Figure 4-6 (a) Proposed structure of the Zn^{II} complex of a ββα motif with metal-binding histidines at positions 3, 6, and 21. (b) The complex in panel a viewed from a different angle (generated using the program Molscript[1]).

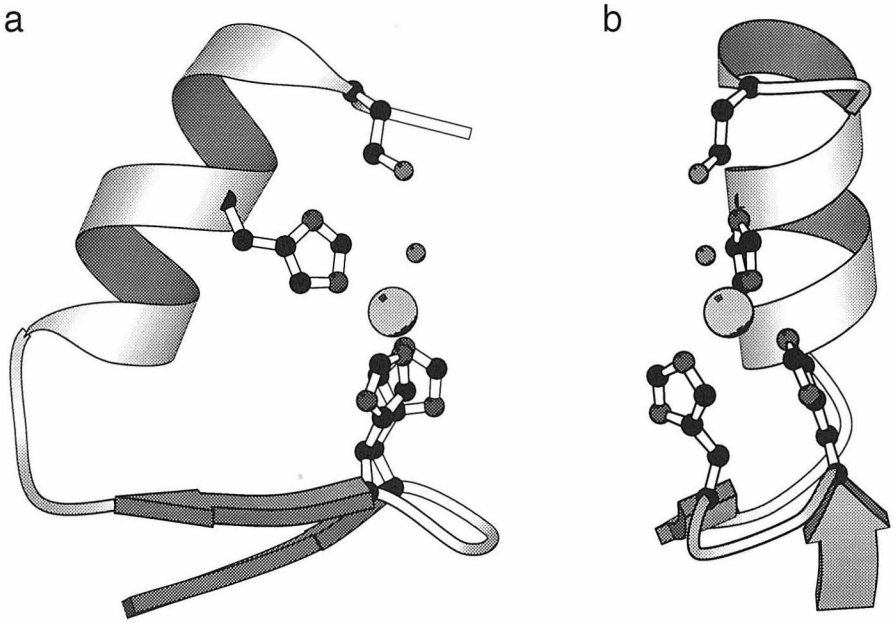

Figure 4-7 (a) Proposed structure of the Zn^{II} complex of a ββα motif with metal-binding histidines at positions 3, 6, and 17 and a potential proton abstractor homoserine at position 21. (b) The complex in panel a viewed from a different angle (generated using the program Molscript[1]).

The **CA-I** peptides therefore shared the common sequence Ac-Tyr-Thr-**Xaa^3**-DPro-Ser-**His^6**-Thr-Phe-Ser-Arg-Ser-Asp-Glu-Leu-Ala-Lys-**His^{17}**-Leu-Arg-Leu-**Hse^{21}**-Ala-Gly-NH_2 with various metal-binding residues incorporated at position 3 (Xaa^3 = His, peptide **CA01**; Xaa^3 = Asp, peptide **CA02**; Xaa^3 = Glu, peptide **CA03**) (Figure 4-5) as well as a Hse located at position 21 as a potential proton abstractor.

*Circular Dichroism Studies on **CA-I** Peptides*

The Zn^{II} titrations of **CA-I** peptides were monitored by circular dichroism spectroscopy (CD) to obtain the apparent dissociation constants for the peptide-Zn^{II} complexes and to probe the effect of Zn^{II} on the structure of peptides. Although there has been no direct evidence that spectral changes resulting from these titration are due to the formation of the peptide-Zn^{II} complex. A variety of evidence suggests that this is a reasonable assumption. The CD spectrum of the peptides were fully restored upon addition of ethylenediamminetetraacetate (EDTA) at the end of the titrations. This reversibility suggests that the spectral changes observed can be attributed to Zn^{II} binding. Furthermore, changing the ionic strength did not alter any of the CD spectra significantly (not shown). Therefore, the spectral changes observed in the Zn^{II} titrations are not due to non-specific interactions or changes in the ionic strength.

The Zn^{II} titrations were monitored by CD to obtain the apparent dissociation constants of the peptide-Zn^{II} complexes according to procedures described in Chapter 2 (Figure 4-8). The apparent dissociation constants for the peptide-Zn^{II} complexes of the **CA-I** peptides are summarized in Table 4-1.

Table 4-1 Apparent Dissociation Constants for the Zn^{II} Complexes of the **CA-I** Peptides[a]

Peptide	Putative Ligating Residues	K_D (μM)
CA01	$His^3His^6His^{17}$	8.53
CA02	$Asp^3His^6His^{17}$	29.8
CA03	$Glu^3His^6His^{17}$	13.8

[a] The Zn^{II} titrations were performed in 0.01 M TRIS buffer at pH 8.25 and monitored by CD.

Peptide **CA01** exhibits the highest Zn^{II}-binding affinity among the **CA-I** peptides. This can be attributed to the higher metal binding affinity of histidine at position 3 for peptide **CA01**, while Asp in peptide **CA02** and Glu in peptide **CA03** do not show such metal binding characteristics. Peptide **CA03** exhibits a higher Zn^{II}-binding affinity than peptide **CA02** most likely because peptide **CA03** incorporates glutamate, which has a longer side chain than aspartate for peptide **CA02**. This longer side chain appears to enable the histidine on the helix to bind Zn^{II} effectively, while the shorter aspartate incorporated in peptide **CA02** may be too short to allow His^{17} from the helix to participate in the ligand sphere without compromising the stability of the resulting Zn^{II} complex.

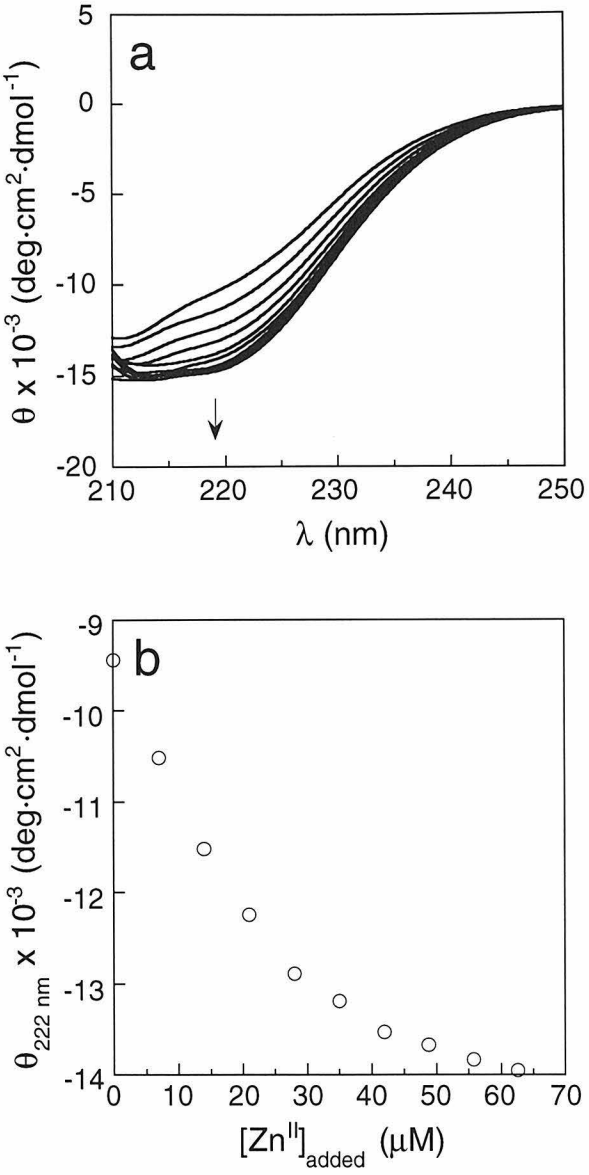

Figure 4-8 A typical Zn^{II} titration of a **CA-I** peptide monitored by CD. (a) The CD spectra of 20.6 μM of peptide **CA01** upon addition of $ZnCl_2$ up to 62.6 μM in 0.01 M TRIS buffer at pH 8.25. (b) The binding isotherm obtained from the experiment illustrated in panel a at 222 nm.

Overall, the CD spectra of the **CA-I** peptides resemble those of ββα motifs such as the individual natural zinc fingers and the **ZF** peptides reported in Chapter 3. Furthermore, the secondary structure of **CA-I** peptides appeared to increase upon binding Zn^{II} by CD (Figures 4-9, 4-10 and 4-11a). While the CD spectra of peptides **CA01** and **CA02** show more structure than the parent structural scaffold peptide **BBA1**, peptide **CA03** exhibits a CD spectrum with comparable intensity compared to peptide **BBA1**. The Zn^{II} complexes of all the **CA-I** peptides appear to have more structure compared to peptide **BBA1** by CD. Interestingly, there is a distinct CD signal in the near-UV region for the **CA03**-Zn^{II} complex (Figure 4-11b). This signal may originate from the tyrosine at position 1, which is the only residue with absorbance in this region. The signal suggests that the tyrosine is experiencing a chiral environment which is provided by the peptide construct. Although peptide **CA02** only lacks a methylene group at position 3 (Asp versus Glu), such a CD signal was not observed for this peptide. These different CD characteristics suggests that the longer side chain can allow a unique metal bound conformation.

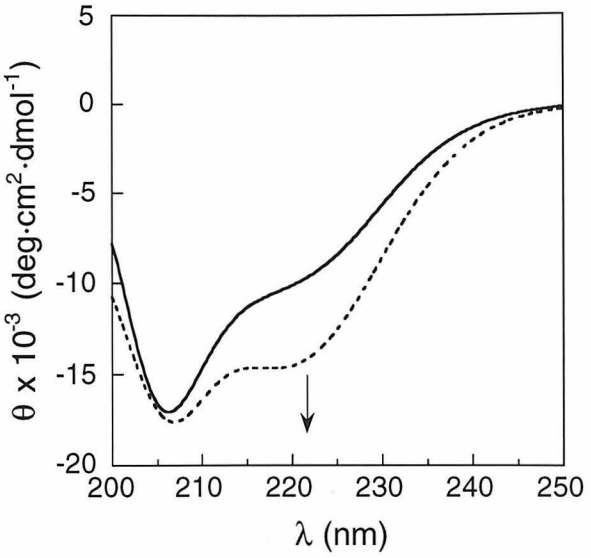

Figure 4-9 CD spectra of peptide **CA01**. The solid line represents the spectrum in the absence of Zn^{II}, and the dashed line is the spectrum upon addition of Zn^{II}. The spectra are reported in mean residue ellipticity.

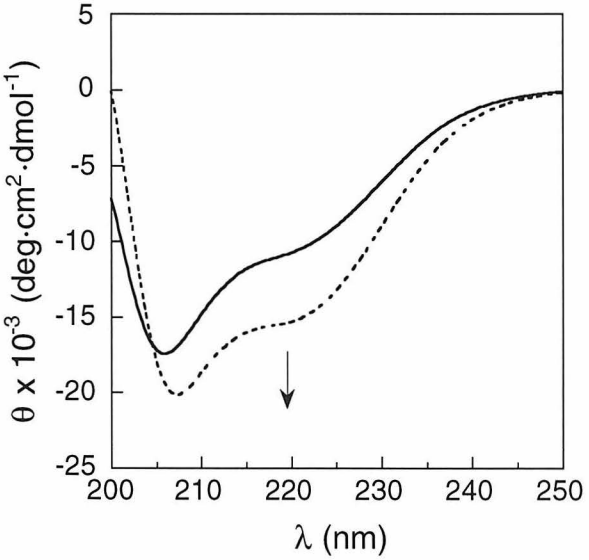

Figure 4-10 CD spectra of peptide **CA02**. The solid line represents the spectrum in the absence of Zn^{II}, and the dashed line is the spectrum upon addition of Zn^{II}. The spectra are reported in mean residue ellipticity.

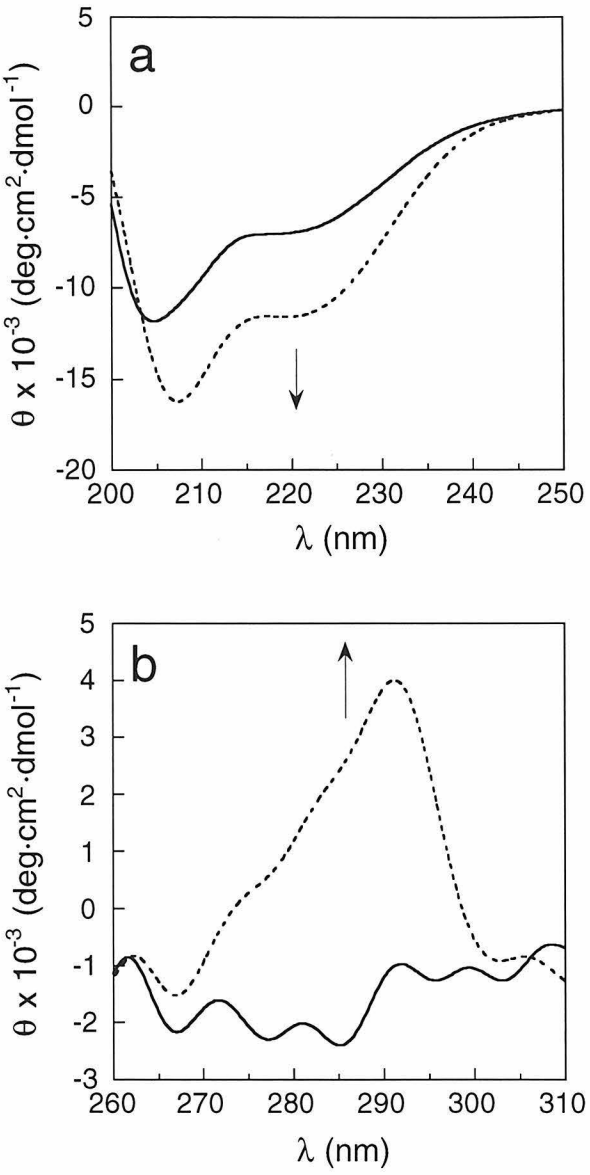

Figure 4-11 The CD spectra of peptide **CA03**. The solid lines represent the spectra in the absence of Zn^{II}, and the dashed lines are the spectra upon addition of Zn^{II}. (a) The far-UV region reported in mean residue ellipticity. (b) The near-UV region normalized to the concentration of the phenol functionality on tyrosine.

Ac-Gly-ONp Hydrolysis with M^{II} Complexes of the ***CA-I*** *Peptides*

After establishing metal binding ability, hydrolase activity was examined with activated esters. To insure there would be no interference with the formation of the peptide-Zn^{II} complex, neither the esters investigated nor their corresponding acids should bind Zn^{II} significantly under assay conditions. Amino acid esters would be convenient to study because if any rate enhancement were observed, a quick assessment of selectivity could be established by varying the side chain or the chirality of the amino acid. Although the simplest amino acid glycine binds Zn^{II} (Table 4-2), *N*-acetylglycine (Ac-Gly-OH) does not. Furthermore, the ester of the amino acid exhibits two orders of magnitude lower Zn^{II} binding affinity compared to the corresponding amino acid. The hydrolysis of *p*-nitrophenyl esters can be monitored readily by observing the formation of the conjugate base of *p*-nitrophenol using absorption (UV-vis) spectroscopy (Scheme 4-1). Therefore, *N*-acetylglycine *p*-nitrophenyl ester (Ac-Gly-ONp) was chosen as the initial substrate for probing the hydrolase activity of the peptide-Zn^{II} complexes for the **CA-I** peptides (Scheme 4-1).

Table 4-2 Dissociation Constants for Zn^{II} Complexes of Glycine Derivatives

Glycine Derivative	K_D (μM)[a]
Glycine	11
N-Methylglycine	30
N-Acetylglycine	138,000
Glycine methyl ester	1,700

[a] Smith, R. M.; Martell, A. E. *Critical Stability Constants, Vol. 2, Amines*; Plenum Press: New York, **1975**; pp235-266.

Scheme 4-1 Hydrolysis of the *p*-Nitrophenyl Ester of *N*-Acetylglycine

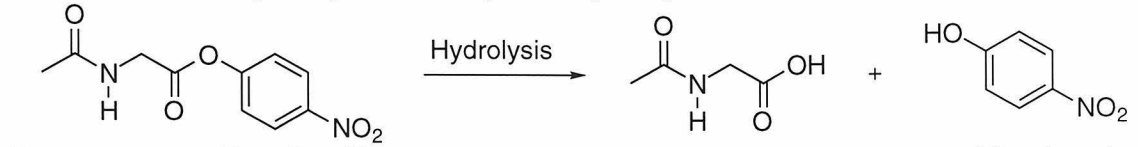

N-Acetylglycine *p*-Nitrophenyl Ester (Ac-Gly-ONp)

N-Acetylglycine (Ac-Gly-OH)

p-Nitrophenol

The hydrolysis of Ac-Gly-ONp was investigated at various pH values for the Zn^{II} complexes of the **CA-I** peptides. The initial hydrolysis rates for the Zn^{II} complexes of the **CA-I** peptides are summarized in Table 4-3. Unfortunately, no significant rate enhancement was observed for any of the peptide-Zn^{II} complexes compared to Zn^{II} or background buffer hydrolysis. A maximum acceleration of only 1.3 times the background buffer rate was observed. It appears that the pH influences the rate of hydrolysis more than the peptide-Zn^{II} complexes. Since these maximum values were observed at pH 8.0 and 8.4, subsequent investigations were performed at these pH values.

Table 4-3 Initial Ac-Gly-ONp Hydrolysis Rates for Zn^{II} Complexes of the **CA-I** Peptides (10^{-3} $AU_{corrected\ 400\ nm}\cdot sec^{-1}$)[a]

pH	Buffer[b]	Zn^{II}	**CA01**-Zn^{II}	**CA02**-Zn^{II}	**CA03**-Zn^{II}
7.2	0.20	0.22	0.26	0.27	0.29
7.5	0.38	0.42	0.47	0.50	0.51
8.0	1.07	1.13	1.18	1.30	1.45
8.4	2.64	2.67	3.01	2.99	3.23
9.3	11.16	12.17	13.04	12.11	13.37

[a] The experiments were carried out at 25°C in the presence of 0.1 M $NaClO_4$, 0.05 M buffer at the appropriate pH and 75 μM $ZnCl_2$ or 75 μM peptide when appropriate.

[b] For the various pH, the Good's buffers were used to minimize interaction between buffer and Zn^{II} (see experimental section for details).

The Cu^{II} and Co^{II} complexes of the **CA-I** peptides were then examined for hydrolase activity. The Cu^{II} complexes were studied due to the higher Lewis acidity for Cu^{II} compared to Zn^{II}, and the Co^{II} complexes were chosen since they frequently serve as models for the corresponding Zn^{II} complexes.[3] The Lewis acidity of Cu^{II} may promote the hydrolysis rate by facilitating the deprotonation of the Cu^{II} bound water to form the Cu^{II} bound hydroxide which may nucleophilically attack the hydrolyzed ester. Alternatively, the Cu^{II} may activate the hydrolyzed ester by binding the carbonyl of the ester. The relative initial Ac-Gly-ONp hydrolysis rates obtained for the peptide-M^{II} complexes of the **CA-I** peptides are summarized in Table 4-4. Unfortunately, no rate enhancement was observed for any of the peptide-M^{II} complexes.

Table 4-4 Relative Initial Ac-Gly-ONp Hydrolysis Rates for the M^{II} Complexes of the **CA-I** Peptides[a]

Peptide	Zn^{II}	Co^{II}	Cu^{II}
No Peptide	1.00	0.99	1.02
CA01	1.13	0.96	0.98
CA02	1.12	0.96	0.93
CA03	1.21	0.96	0.94

[a] The experiments were carried out at 25°C in the presence of 0.1 M $NaClO_4$, 0.05 M *N*-tris(hydroxymethyl)methylaminopropanesulfonic acid (TAPS) buffer at pH 8.4, 75 μM $ZnCl_2$, $CoCl_2$, or $CuCl_2$, 75 μM peptide when appropriate, and 150 μM Ac-Gly-ONp.

The environment around the metal-binding site provided by the peptide is a likely reason for the lack of reactivity for the peptide-M^{II} complexes. Since the reactivity of metallopeptides are a result of a subtle balance among the inherent properties of the metal cation, the primary hydrophilic ligand sphere, and the secondary hydrophobic ligand sphere (for details see Chapter 1),[14, 15] different designs may be able to perturb the

surrounding environment of the metal-binding site to enhance the hydrolase activity of the peptide-M^{II} complexes. Therefore, the **CA-II** peptides were designed and studied to explore a different design that provides a different environment for the metal-binding site.

CA-II Peptides

*The Design of the **CA-II** Series*

To provide a different environment for the Zn^{II} center of the peptide-Zn^{II} complexes, the **CA-II** peptides incorporated metal-binding residues at different position of the ββα scaffold. Two residues on the α-helix (positions 17 and 21) and one on the β-hairpin (position 6) were utilized as metal binding amino acids (Figure 4-12). Incorporating amino acids with similar side chain lengths at positions 17 and 21 would facilitate simultaneous ligation by these two residues. Since it has been demonstrated with the **CA-I** peptides that histidine is most effective in binding Zn^{II}, this amino acid was incorporated at these positions 17 and 21. The metal-binding residue at position 6 would need to present the metal binding functionality in close proximity to His^{17} and His^{21} on the α-helix. Furthermore, results from the **CA-I** peptides indicated that metal-binding residues with longer side chains facilitate Zn^{II} binding. Since the macrocyclic azacrowns have been demonstrated to bind Zn^{II} with high affinity,[11-13] a variety of L-α,ω-diamino acids in addition to histidine were evaluated at position 6 by molecular modeling (Figure 4-13).

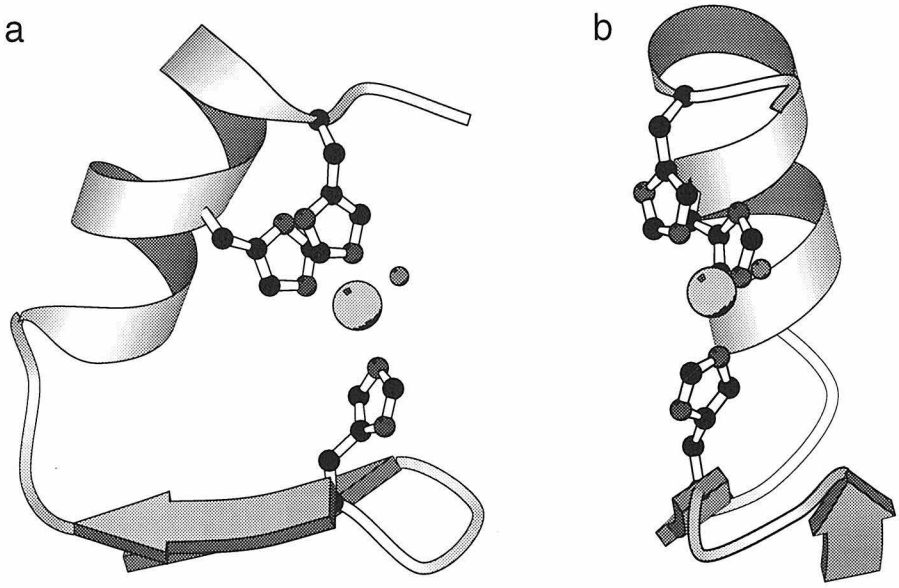

Figure 4-12 (a) Proposed structure of the Zn^{II} complex of a ββα motif with metal-binding histidines at positions 6, 17, and 21. (b) The complex in panel a viewed from a different angle (generated using the program Molscript[1]).

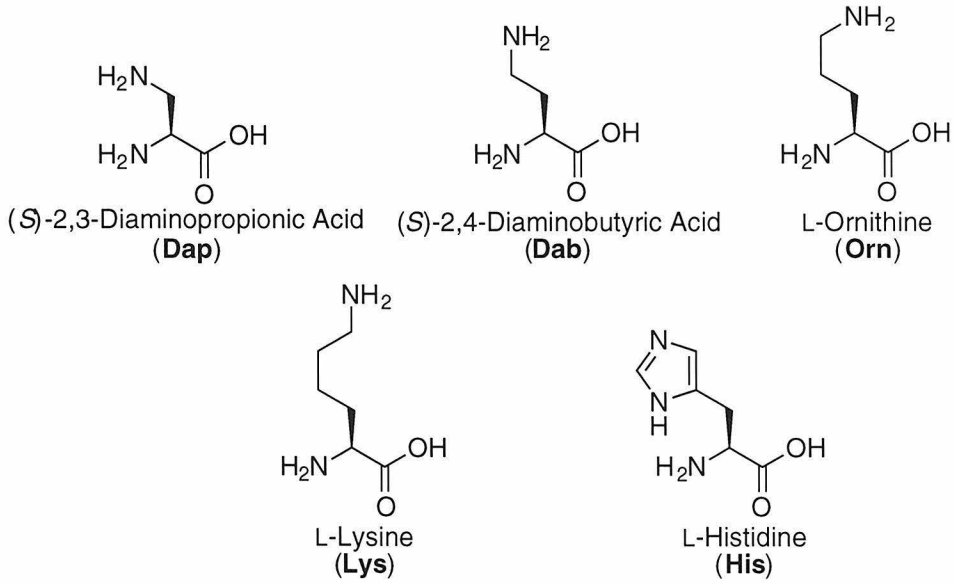

Figure 4-13 Various amino acids with side chains that may serve as ligating residues by ligating through a nitrogen atom.

Results indicated that the putative Zn^{II} complexes of peptides with His, Orn or Lys at position 6 were lower in total energy (Figure 4-12). Therefore, the three **CA-II** peptides incorporated the common sequence Ac-Tyr-Thr-Val-DPro-Ser-**Xaa^6**-Thr-Phe-Ser-Arg-Ser-Asp-Glu-Leu-Ala-Lys-**His^{17}**-Leu-Arg-Leu-**His^{21}**-Ala-Gly-NH_2 with different metal-binding residues at position 6 (Xaa^6 = His, peptide **CA04**; Xaa^6 = Lys, peptide **CA05**; Xaa^6 = Orn, peptide **CA06**) (Figure 4-5). All three **CA-II** peptides were patterned after carbonic anhydrase. Peptide **CA04** could be directly compared to peptide **CA01** to probe the difference in the secondary ligand sphere of the Zn^{II} complexes, since the two peptides have the same primary ligand sphere (His_3).

*Circular Dichroism Studies on the **CA-II** Series*

The Zn^{II} titrations of the **CA-II** peptides were monitored by circular dichroism spectroscopy (CD) to obtain the apparent dissociation constants for the peptide-Zn^{II} complexes and to probe the effect of Zn^{II} on the structure of the peptides. Similar to the **CA-I** peptides, the peptide-Zn^{II} interaction is reversible for the **CA-II** peptides, and the structure of the peptide is independent of ionic strength by CD (data not shown). The apparent dissociation constants for the Zn^{II} complexes of the **CA-II** peptides were obtained as described for the **CA-I** peptides (*vide supra*). The apparent dissociation constants for the peptide-Zn^{II} complexes for the **CA-II** peptides are summarized in Table 4-5.

Table 4-5 Apparent Dissociation Constants for the Zn^{II} Complexes of the **CA-I** and **CA-II** Peptides[a]

Peptide	Putative Ligating Residues	K_D (μM)
CA01	$His^3His^6His^{17}$	8.53
CA02	$Asp^3His^6His^{17}$	29.8
CA03	$Glu^3His^6His^{17}$	13.8
CA04	$His^6His^{17}His^{21}$	11.1
CA05	$Lys^6His^{17}His^{21}$	171
CA06	$Orn^6His^{17}His^{21}$	26.9

[a] The Zn^{II} titrations were performed in 0.01 M TRIS buffer at pH 8.25 and monitored by CD.

Peptide **CA04** exhibited the strongest Zn^{II} affinity among the **CA-II** peptides. This may be the result of the inherent Zn^{II}-binding ability of histidine. The stronger affinity for Zn^{II} observed for peptide **CA06** (Lys^6) compared to peptide **CA05** (Orn^6) could be due to the extra entropic cost for the longer lysine side chain to bind the Zn^{II}. Since similar Zn^{II} binding affinities were observed for peptides **CA01** and **CA04** with the same primary ligand sphere involving metal-binding histidines, cross comparison of Zn^{II} binding affinity between all six peptides would be legitimate. Interestingly, the Zn^{II} binding affinity trend for the metal-binding residues appears to be histidine > carboxylates residues > diamino acids (**CA01**, **CA04** > **CA02**, **CA03** > **CA05**, **CA06**). This may be due to the inherent Zn^{II} binding affinity of the functional groups and their protonation states.

The CD spectra of the **CA-II** peptides and their Zn^{II} complexes resemble those of other ββα motifs (Figures 4-14, 4-15, and 4-16). Compared to the parent structural scaffold peptide **BBA1**, the **CA-II** peptides exhibit CD signals

with similar magnitude. Furthermore, the peptide-Zn^{II} complexes appear to exhibit more secondary structure than the corresponding peptides and peptide **BBA1** as shown by CD.

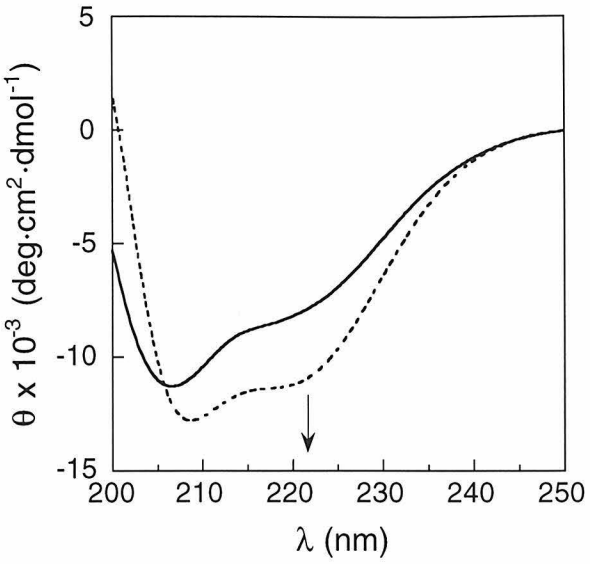

Figure 4-14 CD spectra of peptide **CA04**. The solid line represents the spectrum in the absence of Zn^{II}, and the dashed line is the spectrum upon addition of Zn^{II}. The spectra are reported in mean residue ellipticity.

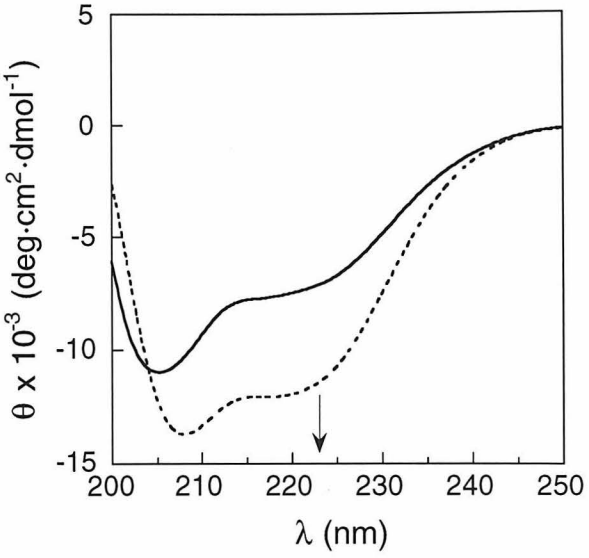

Figure 4-15 CD spectra of peptide **CA05**. The solid line represents the spectrum in the absence of Zn^{II}, and the dashed line is the spectrum upon addition of Zn^{II}. The spectra are reported in mean residue ellipticity.

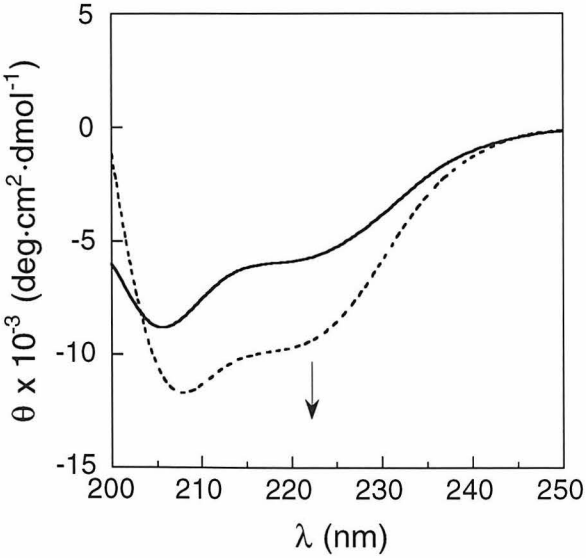

Figure 4-16 CD spectra of peptide **CA06**. The solid line represents the spectrum in the absence of Zn^{II}, and the dashed line is the spectrum upon addition of Zn^{II}. The spectra are reported in mean residue ellipticity.

*Ac-Gly-ONp Hydrolysis with Zn^{II} Complexes of the **CA-II** Peptides*

The uncorrected initial Ac-Gly-ONp hydrolysis rates for the Zn^{II} complexes of the **CA-II** peptides are summarized in Table 4-6. No significant rate enhancement was observed for the peptide-Zn^{II} complexes compared to background hydrolysis by buffer or Zn^{II}. The most likely reason for this lack of rate enhancement may be failure of the ester to interact with the active species, the Zn^{II} bound hydroxide.

Table 4-6 Initial Ac-Gly-ONp Hydrolysis Rates for the Zn^{II} Complexes of the **CA-II** Peptides[a]

Condition	Rate (10^{-3}·$AU_{400\ nm}$·sec^{-1})
Buffer Only	2.15
Zn^{II}	1.98
CA04-Zn^{II}	2.00
CA05-Zn^{II}	2.28
CA06-Zn^{II}	2.20

[a] The experiments were carried out at 25°C in the presence of 0.1 M $NaClO_4$, 0.05 M *N*-2-hydroxyethylpiperazine-*N'*-3-propanesulfonic acid (EPPS) buffer at pH 8.0, 75 μM $ZnCl_2$ or 75 μM peptide when appropriate, and 150 μM Ac-Gly-ONp.

Gly-ONp Hydrolysis with Zn^{II} Complexes of Designed ββα Metallopeptides

To promote the interaction between the metal bound hydroxide and the substrate ester, Gly-ONp was investigated as the substrate (Figure 4-17). This would enable the substrate ester to ligate to the Zn^{II} through its primary amine, and thus be in close proximity to the Zn^{II} bound hydroxide.

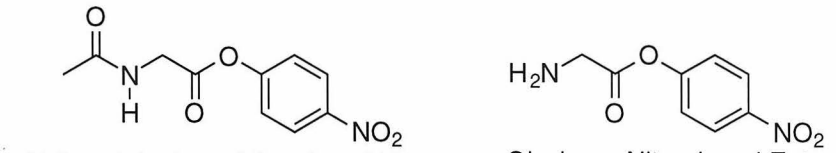

N-Acetylglycine *p*-Nitrophenyl Ester (Ac-Gly-ONp)

Glycine *p*-Nitrophenyl Ester (Gly-ONp)

Figure 4-17 The *p*-nitrophenyl esters of glycine derivatives used as substrates for hydrolysis assays.

Initial Gly-ONp Hydrolysis Rates for Peptide-Zn^{II} Complexes

The initial rates of the Gly-ONp hydrolysis studies on the Zn^{II} complexes of various ββα peptides are summarized in Table 4-7. A clear rate enhancement suggests that the presence of Zn^{II} facilitates the hydrolysis. The Zn^{II} complexes of peptides **ZF05**, **CA01** and **CA05** exhibit some rate enhancement. However, direct comparison among the various metallopeptides requires similar extrapolated initial absorbances. This would indicate that significant hydrolysis had not occurred before the initial data points were collected. Otherwise lower apparent hydrolysis rates that are observed could be due to lower substrate concentrations instead of lower reactivity of the peptide-Zn^{II} complexes. Unfortunately, the extrapolated initial absorbances varied significantly between experiments. Therefore, the pseudo-first order rate constants were measured instead, since these constants are independent of the initial data points.

Table 4-7 Initial Gly-ONp Hydrolysis Rates for Zn^{II} Complexes of Designed ββα Metallopeptides[a]

Condition	$A_{o(extrapolated)}$	Rate (10^3 AU·sec^{-1})
Buffer Only	0.156	16.2
Zn^{II}	0.300	24.0
ZF05-Zn^{II}	0.344	28.8
CA01-Zn^{II}	0.219	25.5
CA02-Zn^{II}	0.170	23.5
CA03-Zn^{II}	0.159	22.6
CA04-Zn^{II}	0.175	21.6
CA05-Zn^{II}	0.242	26.8
CA06-Zn^{II}	0.235	23.5

[a] The experiments were carried out at 25°C in the presence of 0.05 M *N*-2-hydroxyethylpiperazine-*N'*-3-propanesulfonic acid (EPPS) buffer at pH 8.0, 75 μM $ZnCl_2$ or 75 μM peptide when appropriate, and 150 μM Gly-ONp.

Gly-ONp Hydrolysis Under Pseudo-First Order Conditions

The Gly-ONp hydrolysis experiments were performed under pseudo-first order conditions to provide constants independent of the initial time points. The final absorbance A_∞ was approximated and $\ln(A_\infty - A_t)$ was plotted against time (Figure 4-18). The linear portion was considered for calculating the estimated rate constant (Figure 4-19a). Afterwards, a nonlinear fit is employed to consider all data points in the experiment (Figure 4-19b). The pseudo-first order rate constants are obtained from these nonlinear fits. The results are summarized in Table 4-8.

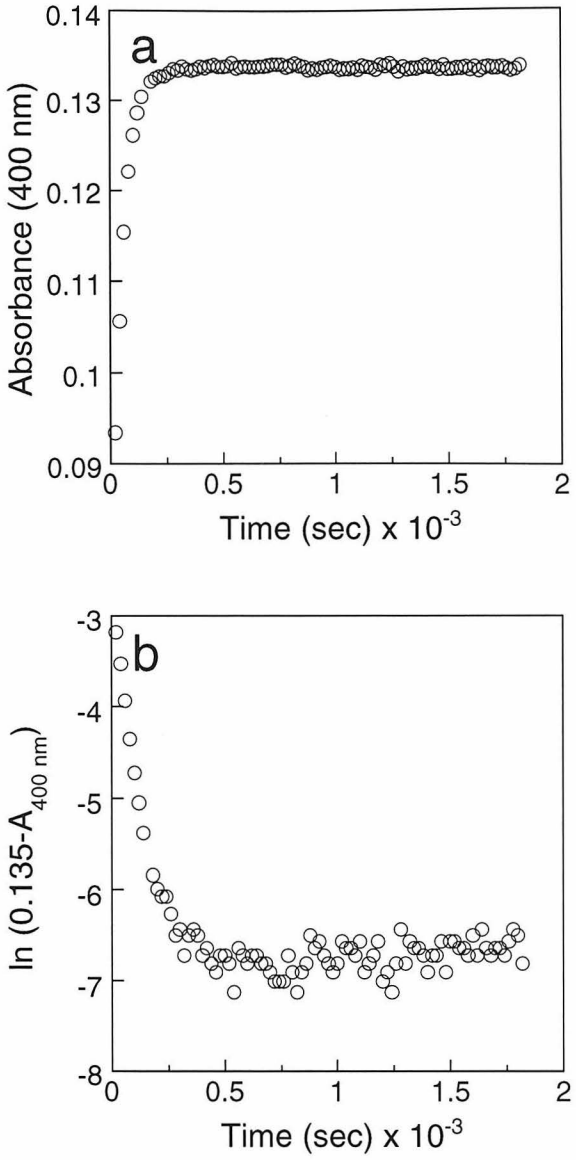

Figure 4-18 A typical Gly-ONp hydrolysis monitored by absorption (UV-vis) spectroscopy with initial analysis. (a) The hydrolysis of 6.7μM Gly-ONp with 75 μM peptide **ZF05** and $ZnCl_2$ in 0.05 M EPPS buffer at pH 8.0 monitored by UV-vis at 400 nm. (b) Plot of $\ln(0.135\text{-}A_{400nm})$ against time for the data in panel a.

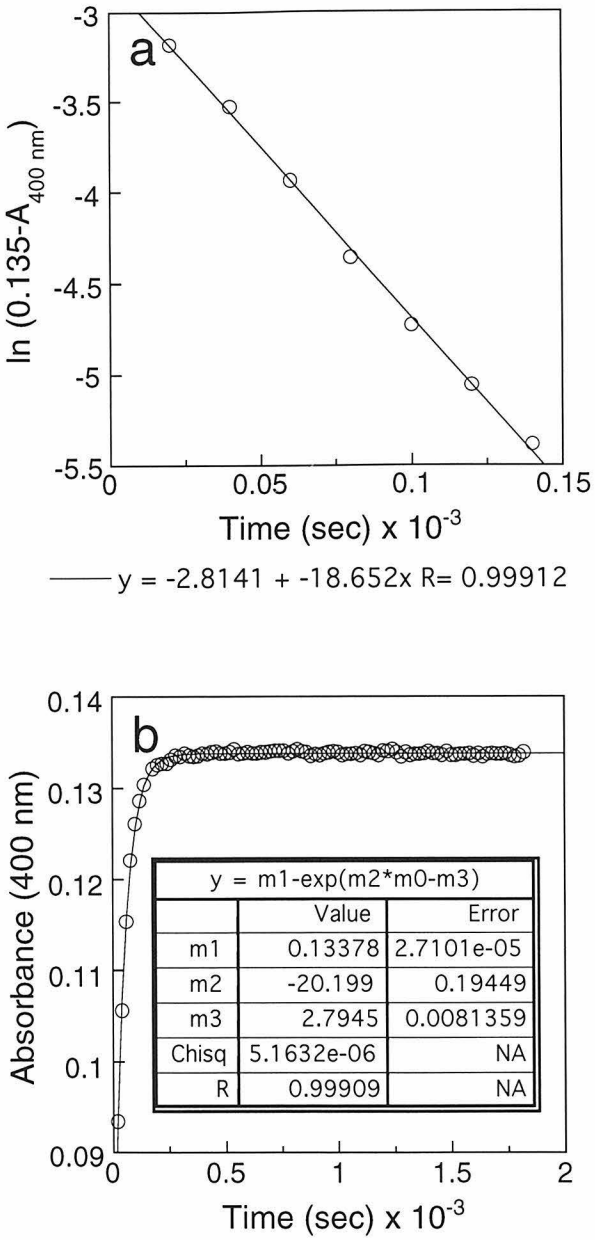

Figure 4-19 The least square fits for the data of a typical Gly-ONp hydrolysis. (a) The linear portion of $\ln(0.135\text{-}A_{400nm})$ against time with the least square fit for the data presented in Figure 4-18. (b) The non-linear least square fit of the raw data presented in Figure 4-18. Results indicate the final absorbance at 400 nm to be 0.1338 and the pseudo-first order rate constant to be 20.20×10^{-3} sec^{-1}.

Table 4-8 Pseudo-First Order Rate Constants for Gly-ONp Hydrolysis for Zn^{II} Complexes of Designed $\beta\beta\alpha$ Metallopeptides[a]

Condition	Putative Ligating Residues	k (10^{-3}·sec^{-1})
Buffer Only	N/A	10.7
Zn^{II}	N/A	18.8
ZF05-Zn^{II}	$Fen^{6}His^{21}$	20.7
CA01-Zn^{II}	$His^{3}His^{6}His^{17}$	14.9
CA02-Zn^{II}	$Asp^{3}His^{6}His^{17}$	13.9
CA03-Zn^{II}	$Glu^{3}His^{6}His^{17}$	12.6
CA04-Zn^{II}	$His^{6}His^{17}His^{21}$	13.5
CA05-Zn^{II}	$Lys^{6}His^{17}His^{21}$	18.9
CA06-Zn^{II}	$Orn^{6}His^{17}His^{21}$	15.2

[a] The experiments were carried out at 25°C in the presence of 0.05 M *N*-2-hydroxyethylpiperazine-*N'*-3-propanesulfonic acid (EPPS) buffer at pH 8.0, 75 μM $ZnCl_2$ or 75 μM peptide when appropriate, and 6.67 μM Gly-ONp.

Slight rate enhancement over buffer was observed for all of the peptide-Zn^{II} complexes. Unfortunately, only peptides **ZF05** and **CA05** exhibited rate constants comparable to that for Zn^{II} in buffer. Since peptide **CA05** does not form a significant amount of peptide-Zn^{II} complex under assay conditions based on the dissociation constant, any rate enhancement over buffer is most likely due to the free Zn^{II} in solution. However, peptide **ZF05** forms the Zn^{II} complex readily under assay conditions, thus the rate enhancement observed is due to the activity of the **ZF05**-Zn^{II} complex. Interestingly, most of the peptides in the presence of Zn^{II} exhibit lower Gly-ONp hydrolysis rates than free Zn^{II} in buffer, indicating formation of the Zn^{II}

complexes results in loss of reactivity. The primary ligand sphere may have neutralized the Lewis acidity of the metal center by forming a negatively charged species upon coordinating Zn^{II}. Therefore, the **CA-III** peptides were designed and studied to investigate this possibility.

CA-III Peptides

The Design of the CA-III Peptides

Among the six **CA-I** and **CA-II** peptides described previously, peptides which bear putative ligand spheres involving all histidines exhibit higher Zn^{II}-binding affinity than peptides involving other residues. However, the imidazole functionality on histidines have a pK_a of 6.5 (Scheme 4-2). Therefore, the Zn^{II}-binding affinity is diminished at pH 7 compared to higher pH values due to the protonation state of the imidazole moiety. Furthermore, the imidazole functionality is susceptible to further deprotonation to give the imidazolate. This species may then reduce the Lewis acidity of the Zn^{II}.

Scheme 4-2 Protonation States for Imidazole and Pyridine

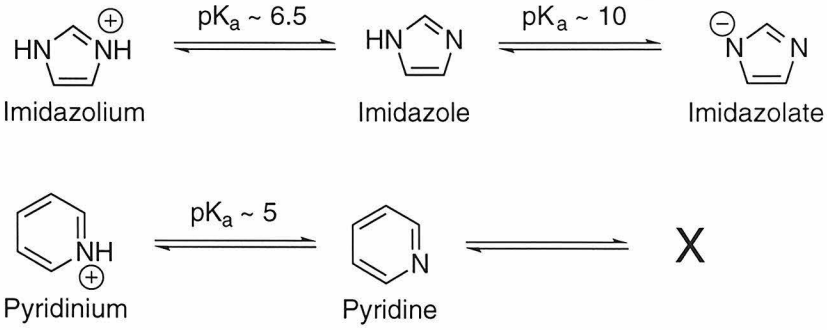

The pyridine functionality, with a pK_a of 5, provides a promising alternative to imidazole (Scheme 4-2). A higher proportion of the metal-

bound species is thus present for pyridine-containing peptides at neutral pH. Furthermore, the pyridine functionality cannot be further deprotonated to form a negatively charged species and neutralize the Lewis acidity of the Zn^{II} center. However, the metal-binding affinity of pyridine is slightly lower than that of imidazole.[16] Conveniently, all three positional isomers for (*S*)-2-amino-3-(pyridyl)propionic acid are commercially available. However, the (*S*)-2-amino-3-(pyrid-2-yl)propionic acid (2Pyr) was not considered since the β-methylene would introduce unfavorable sterics which would hamper metal binding. Therefore, the incorporation of (*S*)-2-amino-3-(pyrid-3-yl)propionic acid (3Pyr) and (*S*)-2-amino-3-(pyrid-4-yl)propionic acid (4Pyr) into the ββα motif was considered.

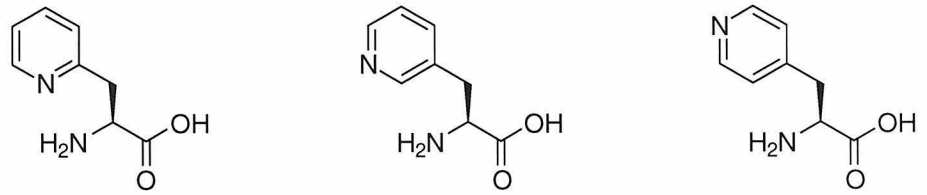

(*S*)-2-Amino-3-(pyrid-2-yl) propionic acid (**2Pyr**) (*S*)-2-Amino-3-(pyrid-3-yl) propionic acid (**3Pyr**) (*S*)-2-Amino-3-(pyrid-4-yl) propionic acid (**4Pyr**)

Figure 4-20 Three positional isomers for (*S*)-2-amino-3-pyridylpropionic acid.

Combinations of positions 3, 6, 17, and 21 have been previously designed to form the ligand sphere. However, since the incorporation of valine at position 3 is crucial for the structure of the ββα motif, therefore this residue was not altered (see Chapter 3 for details). Careful examination of the ββα construct revealed that a ligand sphere formed at positions 6, 18 and 21 would be promising (Figure 4-21). Thus, all combinations of 3Pyr and 4Pyr at these three positions were evaluated by molecular modeling. The four combinations $3Pyr^{6}$-$3Pyr^{18}$-$3Pyr^{21}$, $4Pyr^{6}$-$3Pyr^{18}$-$3Pyr^{21}$, $3Pyr^{6}$-$3Pyr^{18}$-$4Pyr^{21}$, and $4Pyr^{6}$-$3Pyr^{18}$-$4Pyr^{21}$ appeared to be the most promising. Since the structure of 3Pyr resembles histidine more than 4Pyr, the peptides

corresponding to the combination Xaa^{6}3Pyr^{18}3Pyr^{21} were chosen to be investigated. The peptides were synthesized simultaneously in a mother batch up to residue 6. The resin was then split to finish the peptides individually. The two **CA-III** peptides share the sequence Ac-Tyr-Thr-Val-DPro-Ser-**Xaa^6**-Thr-Phe-Ser-Arg-Ser-Asp-Glu-Leu-Ala-Lys-Leu-**3Pyr^{17}**-Arg-Leu-**3Pyr^{21}**-Ala-Gly-NH_2 with different metal-binding residues incorporated at position 6 (Xaa^6 = 3Pyr, peptide **CA07**; Xaa^6 = 4Pyr, peptide **CA08**) (Figure 4-5).

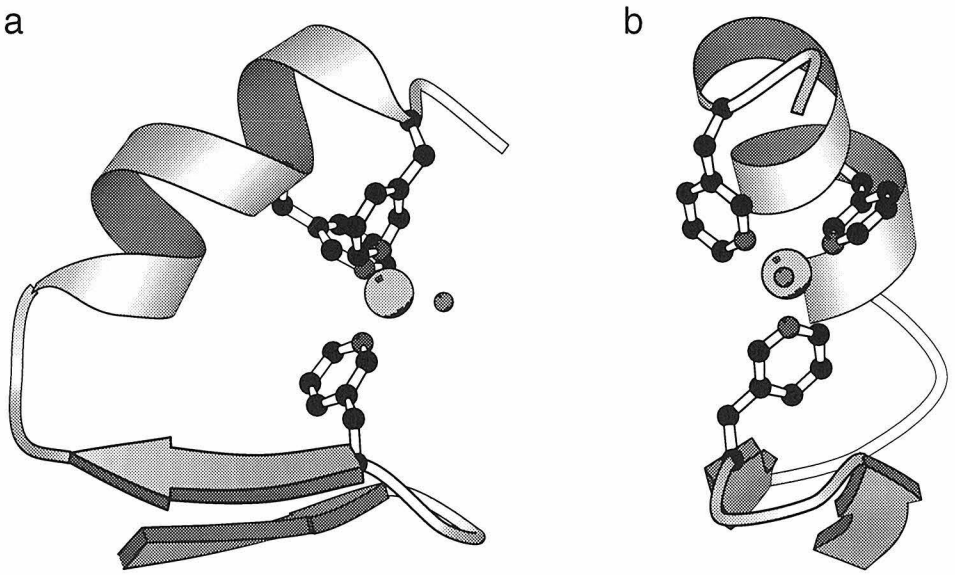

Figure 4-21 (a) Proposed structure of the Zn^{II} complex of a ββα motif with metal-binding 3Pyr at positions 6, 18, and 21. (b) The complex in panel a viewed from a different angle (generated using the program Molscript[1]).

*Circular Dichroism Studies on the **CA-III** Peptides*

The Zn^{II} titrations for peptide **CA07** were monitored by circular dichroism spectroscopy (CD). The CD spectra of the **CA-III** peptides resemble previously designed ββα motifs (Figures 4-22 and 4-23), with similar magnitudes compared to the parent structural scaffold peptide **BBA1**. However, only very small changes in the CD spectra were observed upon addition of Zn^{II} (10% of changes observed in previous titrations for peptide

CA07 and 25% for peptide **CA08**). It is very unlikely that the changes in the CD spectra are due to specific Zn^{II} binding to the putative metal binding site. However, the **CA-III** peptides could be binding Zn^{II} without significant CD spectral changes, which was the case for peptide **BBA1**. Therefore, the titrations were monitored by absorption (UV-vis) spectroscopy. Unfortunately, no changes in the absorption spectra were observed upon addition of Zn^{II} for the **CA-III** peptides. To establish Zn^{II} binding, the Zn^{II} titrations were monitored by nuclear magnetic resonance (NMR) spectroscopy.

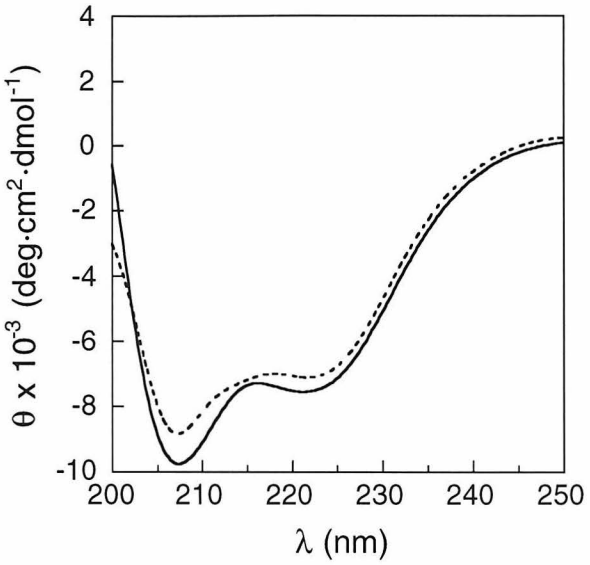

Figure 4-22 CD spectra of peptide **CA07**. The solid line represents the spectrum in the absence of Zn^{II}, and the dashed line is the spectrum upon addition of Zn^{II}. The spectra are reported in mean residue ellipticity.

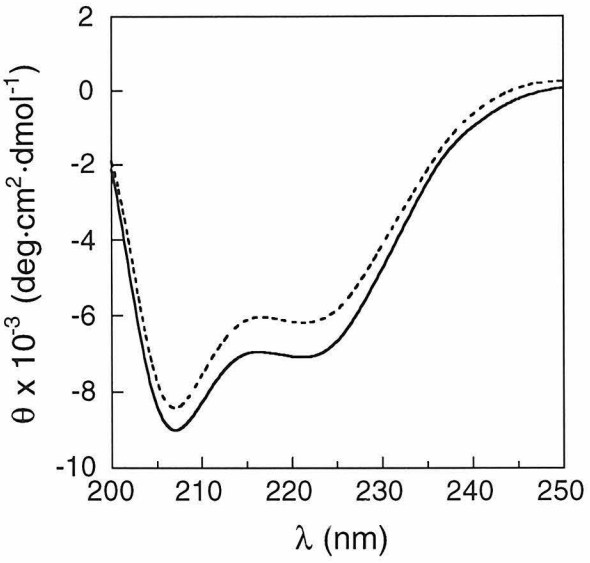

Figure 4-23 CD spectra of peptide **CA08**. The solid line represents the spectrum in the absence of Zn^{II}, and the dashed line is the spectrum upon addition of Zn^{II}. The spectra are reported in mean residue ellipticity.

*Zn^{II} Titration on Peptide **CA08** Monitored by NMR Spectroscopy*

Since neither CD nor UV-vis was able to clearly support Zn^{II} binding, NMR was used to establish metal binding. Studies with peptides **ZF01** and **ZF02** showed that the NMR spectra of a peptides change upon addition of Zn^{II},[17] and both peptides showed definite Zn^{II} binding by CD and UV-vis. By two dimensional NMR (2D-NMR), many cross peaks involving residues near the putative Zn^{II} binding site disappeared or broadened upon addition of Zn^{II}. This phenomenon is probably due to the fast exchange nature of the Zn^{II}. Furthermore, 2D-NMR spectra of individual natural zinc fingers exhibit distinct cross peaks with similar peak shape and magnitude in the absence and presence of Zn^{II}.[18] These observations are consistent with a tightly bound Zn^{II} that is not exchanging. Therefore, if specific Zn^{II} binding were occurring with peptides **CA07** and **CA08**, either magnitude changes or

line broadening would be observed upon binding Zn^{II} for chemical shifts of residues near the putative Zn^{II}-binding site.

Results indicated that there were no significant changes in the NMR spectrum for peptide **CA08** upon addition of Zn^{II}. This suggests that peptide **CA08** does not bind Zn^{II} effectively under the conditions studied. Peptide **CA07** is very similar to peptide **CA08** and it also does not show metal binding by CD or UV-vis, it is most likely that peptide **CA07** also does not bind Zn^{II}. The lack of metal binding resulted in a lack of significant rate enhancement for hydrolase activity of the **CA-III**.[17]

Conclusions

Nine metallopeptides based on the ββα scaffold incorporating combinations of metal-binding residues with phenanthroline (Fen), imidazole (His), carboxylate (Asp and Glu), amine (Orn and Lys), or pyridine (3Pyr and 4Pyr) side chain functionalities were investigated. The metal-binding sites were designed to form in the interior of this motif between the α-helix and β-hairpin by positioning metal-binding residues on both secondary structural elements. The Zn^{II} complexes of these peptides exhibit dissociation constants between 10^{-4} M and 10^{-6} M. Although no significant rate enhancement was observed for the Zn^{II} complexes of these peptides, the Zn^{II}-binding studies of these peptides revealed several key concepts for designing metallopeptides with a ββα super-secondary structure. The Zn^{II} binding affinity for the metal-binding functionalities follows the trend imidazole (His) > carboxylate (Asp and Glu) > amine (Orn and Lys) > pyridine (3Pyr and 4Pyr). Furthermore, it seems that residues with a longer side chain functionality on the β-hairpin facilitates the metal binding.

These initial attempts have demonstrated that it is difficult to generate a metallopeptide with hydrolase activity using simple permutations of the parent structural scaffold peptide **BBA1**. However, many other sequences involving the ββα motif remain to be investigated. Unfortunately, the iterative design process is inherently impeded by studying the peptides individually. Therefore, combining a rational design approach with combinatorial techniques would allow facile screening of multiple peptides to search for a metallopeptide with enhanced hydrolase activity. However, key concepts for designing metallopeptides with the ββα fold derived in this chapter will benefit future design efforts.

Acknowledgments

Quantitative amino acid analysis was performed by Dr. Gary Hathaway at the PPMAL facility at Caltech, Dr. Kristine Swiderick at City of Hope, or Dr. Audree Fowler at UCLA. Mass spectral analysis of peptides were performed by Michael Shogren-Knaak or Duncan Odom.

Experimental Section

Molecular Modeling

Molecular modeling was performed on a Silicon Graphics Personal Indigo 2 using the program Insight II (Biosym Technologies, CA). Minimizations were calculated using the Discover 3 module. Each design was evaluated using one of the lower energy structures for peptide **BBA1** derived from NOE-restrained simulated annealing as the starting

coordinates.[19, 20] These calculations were performed with a putative Zn^{II} bound water included. The CVFF forcefield was chosen due to its reliable prediction of protein and peptide structures. Because no forcefield parameters were available for Zn^{II}, the **CA-I** peptides were modeled with suitable distance restraints between the ligands and Zn^{II} bound water, and the appropriate angle restraints with no explicit metal included. For the **CA-II** peptides, Ca^{II} was used to represent the Zn^{II}. Distances from the crystal structure of carbonic anhydrase was used for the metal-liganding atom distances in the restraints. Furthermore, restraints between the lone pair electrons of the liganding atoms and the metal were used to form reasonable orientations for metal-binding functionality. Additionally, angles from the crystal structure were used for restraints to form geometries similar to the active site in carbonic anhydrase. The ESFF forcefield was chosen for modeling the **CA-III** peptides, since forcefield parameters existed for Zn^{II}.

Peptide Synthesis

The peptides were synthesized on a 0.051 to 0.154 mmole scale by solid phase methods using N^{α}-9-fluorenylmethyloxycarbonyl (Fmoc) amino acid pentafluorophenyl esters on a Milligen 9050 automated peptide synthesizer. Commercially available starting materials and reagents were purchased from Milligen Biosearch, EM Science, Synthetech, and Aldrich Chemical Company. Fmoc-PAL-PEG-PS resin (0.21mmol/g) was used to afford carboxyl terminus primary amides. Typical protocols for coupling a residue involved 30 to 90 minute coupling cycles with three or four equivalents of amino acid. However, Fen was coupled for 2.5 hours with three equivalents of the Fmoc-protected amino acid using *O*-(7-azabenzotriazol-1-yl)-1,1,3,3-tetramethyluronium hexafluorophosphate (HATU) /1-hydroxy-7-

azabenzotriazole (HOAt)/DIEA mediated chemistry in N-methylpyrrolidinone (NMP). Activated esters were formed *in situ* using 1-hydroxybenzotriazole (HOBt) and or diisopropylcarbodiimide (DIPCDI), HOBt and diisopropylethylamine (DIEA). Deprotection of FMOC-protected amine groups were performed using either a 7 minute 20% piperidine/dimethylformamide (DMF) wash or a 5 minute 2% 1,7-diazabicyclo[5,4,0]-undec-7-ene (DBU)/DMF wash. Peptides were *N*-acylated on the resin using either 7 equivalents of acetic anhydride and 7 equivalents of triethylamine (TEA) or 21 equivalents of acetic anhydride and 5 equivalents of triethylamine in 3 mL of DMF for 2 hours. The resin was then washed with DMF and dichloromethane and lyophilized overnight.

The last 20 residues of the **CA-I** peptides were synthesized in the same batch initially, and the three peptides were then completed separately. After the first twenty residues were coupled, the resin was taken off line and lyophilized overnight after solvent exchange. The individual peptides were then completed separately on a 0.051 mmole scale. For the synthesis of the **CA-II** peptides, the resin was taken off line after coupling the last 17 residues and lyophilized over night. The synthesis of each peptide was then completed individually on a 0.051 mmole scale. The last 17 residues of the **CA-III** peptides were synthesized in the same batch initially, and then the two peptides were completed separately. After the last seventeen residues were coupled, the resin was taken off line and lyophilized overnight after solvent exchange. The rest of each peptide was then completed individually on a 0.051 scale.

All peptides were deprotected and cleaved from the resin by treatment with Reagent K [trifluoroacetic acid (TFA)/phenol/H_2O/thioanisole /ethanedithiol] (82.5:5:5:5:2.5).[21] The resin was filtered, washed with TFA and

the combined filtrates were concentrated to 2 mL and precipitated with ether/hexane 1:1 or 2:1 (20 mL). The supernatant was decanted and the peptides were triturated with ether/hexane 1:1 (5 x 20 mL) or ether/hexane 2:1 (3 x 20 mL). The peptides were lyophilized overnight and purified by reverse-phase C_{18} HPLC. Reverse-phase HPLC was performed on a Beckman Series Gold HPLC, equipped with a dual wavelength UV detector. The molecular weight of all peptides was confirmed by mass spectrometry (Table 4-9).

Table 4-9 Mass Spectrometry and HPLC Data on the **CA** Peptides

Peptide	Retention Time[a]	Formula	Observed by ES-MS	Calculated	Observed
CA01	23.2	$C_{117}H_{181}O_{35}N_{37}$	M^+	2665.96	2665.55
CA02	24.6	$C_{115}H_{179}O_{37}N_{35}$	M^+	2643.91	2643.60
CA03	24.6	$C_{116}H_{181}O_{37}N_{35}$	M^+	2657.94	2657.76
CA04	26.4	$C_{118}H_{183}O_{34}N_{37}$	MH_4^{4+}	667.01	667.05
CA05	24.6	$C_{118}H_{188}O_{34}N_{36}$	MH_4^{4+}	664.77	664.65
CA06	25.3	$C_{117}H_{186}O_{34}N_{36}$	MH_4^{4+}	661.26	661.05
CA07	25.4	$C_{124}H_{186}O_{34}N_{34}$	M^+	2697.06	2697.19
CA08	25.5	$C_{124}H_{186}O_{34}N_{34}$	M^+	2697.06	2696.60

[a] All peptides were analyzed on a linear gradient described as follows: 100% H_2O (0.1% v/v TFA) 5 min., linear gradient 0-70% CH_3CN (0.1% v/v TFA)/H_2O (0.1% v/v TFA) 25 min., 70% CH_3CN (0.1% v/v TFA) 5 min., 70-0% CH_3CN (0.1% v/v TFA)/H_2O (0.1% v/v TFA) 2 min.

Determination of the Concentration for the Peptide Stock Solutions

The UV-vis spectra were recorded on a Beckman UV-vis 7500DU. Stock solutions of 10 mM were based on weight obtained from a microanalytical balance. The concentrations of these stock solutions were then determined by the absorption spectra of the peptides in 6 M

guanidinium hydrochloride. All the peptides contain one tyrosine which exhibits an absorbance around 280 nm. The extinction coefficient of a tyrosine containing peptide was been reported to be 1285 $AU \cdot cm^{-1} \cdot M^{-1}$ in 6 M guanidinium hydrochloride.[22] However, the UV-Vis spectra of peptides **CA07** and **CA08** were dominated by the absorption of the pyridine moieties instead. Therefore, the concentration of these stock solutions were determined by quantitative amino acid analysis instead.

Circular Dichroism Spectroscopy

Circular dichroism spectra were recorded on a Jasco J600 Circular Dichroism Spectrometer. The spectra were baseline corrected and noise reduced using the Jasco J600 System Software, and were then transferred to a Macintosh IIci or Power Macintosh computer for further analysis using KaleidaGraph version 3.0 (Abelbeck Software, CA). Metal cation titrations were performed with peptide concentrations ranging from 18 to 95 μM in 0.01 M TRIS buffer (pH 8.25) in either a 0.1 cm or 1 cm pathlength cell. The $NaClO_4$ concentration dependence was performed similarly. The dissociation constants were calculated as described for the UV-Vis experiments in Chapter 2 using an iterative process.

Absorption (UV-vis) Spectroscopy

All hydrolysis assays were monitored on a Beckman UV-vis 7500DU. Hydrolysis rates and pseudo-first order rate constants were calculated on a Power Macintosh personal computer using KaleidaGraph version 3.0 (Abelbeck Software).

Ac-Gly-ONp Hydrolyses

The hydrolyses were performed by mixing 400 μL of 0.075 M buffer at the appropriate pH, 30 μL of 2 M $NaClO_4$, and Zn^{II}, Co^{II}, Cu^{II} or peptide to make a 75 μM solution when appropriate. Suitable amounts of water were added to make up 591 μL of total solution. After equilibrating the temperature at 25°C for 5 minutes, the reaction was initiated by adding 9 μL of 10 mM Ac-Gly-ONp in dioxane. The reactions were monitored at 400 nm at 20 second intervals for 30 minutes. Initial rates were obtained from linear regions of the experiments. For the various pH values, the Good's buffers were used to minimize interaction between buffer and the divalent metal cations. (pH 7.2, 3-*N*-morpholino-propanesulfonic acid, MOPS; pH 7.5, *N*-1-hydroxyethylpiperazine-*N'*-2-ethanesulfonic acid, HEPES; pH 8.0, *N*-2-hydroxyethylpiperazine-*N'*-3-propanesulfonic acid, EPPS; pH 8.4, *N*-tris(hydroxymethyl)methylaminopropanesulfonic acid, TAPS; pH 9.3, 2-(cyclohexylamino)-ethanesulfonic acid, CHES).

Gly-ONp Hydrolyses

The hydrolyses were performed by mixing 200 μL of 0.075 M EPPS buffer at pH 8.0, and Zn^{II} or peptide to make a 75 μM solution when appropriate. Suitable amounts of water were added to make up 298 to 299 μL of total solution. After equilibrating the temperature at 25°C for 5 minutes, the reactions were initiated by adding 4.5 μL of 10 mM Gly-ONp in dimethylsulfoxide. The reactions were monitored at 400 nm in 30 second intervals for 30 minutes. Hydrolysis rates were obtained from linear regions of the experiments by calculations carried out on a Power Macintosh personal computer using KaleidaGraph version 3.0 (Abelbeck Software).

Gly-ONp Hydrolyses to Obtain the Pseudo-First Order Rate Constants

The hydrolyses were performed by mixing 200 μL of 0.075 M EPPS buffer at pH 8.0, with Zn^{II} or peptide to make 75 μM solutions when appropriate. Suitable amounts of water were added to make up 298 to 299 μL of total solution. After equilibrating the temperature at 25°C for 5 minutes, the reactions were initiated by adding 1 μL of 2 mM Gly-ONp. The reactions were monitored at 400 nm in 30 second intervals for 30 minutes. The final absorbance A_∞ was approximated and $\ln(A_t - A_\infty)$ was plotted against time. The estimated rate constants were obtained using linear fits involving earlier time points. A non-linear fit is then employed to the plot of absorbance against time, considering all data points in the experiment using the estimated rate constant as the initial point for fitting. The pseudo-first order rate constants were obtained from these non-linear fits. The pseudo-first order rate constants were determined by calculations carried out on a Power Macintosh personal computer using KaleidaGraph version 3.0 (Abelbeck Software).

Monitoring the Zn^{II} Titration by Nuclear Magnetic Resonance Spectroscopy

The NMR spectra were obtained on a Bruker AMX 500 MHz instrument. The peptide **CA08** was lyophilized from D_2O several times and then dissolved in 495 μL of D_2O. The uncorrected pH of the sample was adjusted to 7.25 using 0.1 N NaOD and 0.1 N DCl. The $ZnCl_2$ was dried down from D_2O several times and then dissolved in 495 μL D_2O. The uncorrected pH of the solution was then adjusted to 6.64 to give a concentration of 0.106 M. The spectra were obtained at 300 K using water suppression. The data were processed with Felix 95 software (Biosym Technologies, CA) on a Silicon Graphics Personal Iris or Indigo work station.

References

1. Kraulis, P. J. *J. Appl. Crystallogr.* **1991**, *24*, 946-950.
2. Eriksson, A. E.; Jones, T. A.; Liljas, A. *Proteins* **1988**, *4*, 274-282.
3. Bertini, I.; Luchinat, C. *Acc. Chem. Res.* **1983**, *16*, 272-279.
4. Xue, Y.; Liljas, A.; Jonsson, B.-H.; Lindskog, S. *Proteins* **1993**, *17*, 93-106.
5. Lindskog, S.; Liljas, A. *Curr. Opin. Struct. Biol.* **1993**, *3*, 915-920.
6. Argos, P.; Garavito, R. M.; Evenstoff, W.; Branden, C. I. *J. Mol. Biol.* **1978**, *126*, 141-158.
7. Christianson, D. W.; Lipscomb, W. N. *Acc. Chem. Res.* **1989**, *22*, 62-69.
8. Brown, R. S.; Zamkanei, M.; Cocho, J. L. *J. Am. Chem. Soc.* **1984**, *106*, 5222-5228.
9. Tagaki, W.; Ogino, K. *Topics Cur. Chem.* **1985**, *128*, 143-174.
10. Ogino, K.; Shindo, K.; Minami, T.; Tagaki, W.; Eiki, T. *Bull. Chem Soc. Jpn.* **1983**, *56*, 1101-1106.
11. Kimura, E.; Shiota, T.; Koike, T.; Shiro, M.; Kodama, M. *J. Am. Chem. Soc.* **1990**, *112*, 5805-5811.
12. Kimura, E.; Nakaruma, I.; Koike, T.; Shionoya, M.; Komada, Y.; Ikeda, T.; Shiro, M. *J. Am. Chem. Soc.* **1994**, *116*, 4764-4771.
13. Koike, T.; Kajitani, S.; Nakamura, I.; Kimura, E.; Chiro, M. *J. Am. Chem. Soc.* **1995**, *117*, 1210-1219.
14. Hellinga, H. W. *Curr. Opin. Biotech.* **1996**, *7*, 437-441.
15. Yamashita, M. M.; Wesson, L.; Eisenman, G.; Eisenberg, D. *Proc. Natl. Acad. Sci. U.S.A.* **1990**, *87*, 5648-5652.
16. Smith, R. M.; Martell, A. E. *Critical Stability Constants, Volume 2, Amines*; Plenum Press: New York, 1975 .
17. Cheng, R. P.; Imperiali, B. unpublished results.

18. Lee, M. S.; Gippert, G. P.; Soman, K. V.; Case, D. A.; Wright, P. E. *Science* **1989**, *245*, 635-637.

19. Struthers, M. D.; Cheng, R. P.; Imperiali, B. *Science* **1996**, *271*, 342-345.

20. Struthers, M. D.; Cheng, R. P.; Imperiali, B. *J. Am. Chem. Soc.* **1996**, *118*, 3073-3081.

21. King, D. S.; Fields, C. G.; Fields, G. B. *Int. J. Pept. Protein Res.* **1990**, *36*, 255-266.

22. Page, C. N.; Vajdos, F.; Fee, L.; Grimsley, G.; Gray, T. *Protein Science* **1995**, *4*, 2411-2423.

Chapter 5

Solid Phase Native Ligation for the Assembly of ββα Peptides

Introduction

Toward the design of metallopeptides that exhibit hydrolase activity, an iterative design approach has been adopted involving two stages: the construction of a structural scaffold and the incorporation of the catalytic function. Following this approach, a 23-residue ββα motif which folds into a well defined structure in the absence of crosslinks has been generated to serve as a structural scaffold (for details see Chapter 3) (Figure 5-1). Furthermore, nine sequences that involved permutations of the scaffold were designed iteratively for implementing the hydrolase activity by incorporating metal-binding residues to mimic the Zn^{II}-binding site of carbonic anhydrase or carboxypeptidase (for details see Chapter 4). Although no significant rate enhancement was observed for the Zn^{II} complexes of these peptides, the Zn^{II}-binding studies revealed several key concepts for designing metallopeptides with a ββα super-secondary structure (for details see Chapter 4). Furthermore, there are many other designs involving the ββα scaffold that remain to be investigated.

While the iterative design process employed allows a range of peptides to be investigated sequentially, a rational approach involving combinatorial techniques would provide the ability to evaluate multiple peptides simultaneously. Most solution phase combinatorial investigations involve the synthesis of a random mixture of peptides in solution, the screening of the mixture for covalent or non-covalent binding to a target molecule, the visualization of the active peptide by fluorescence or immuno-coprecipitation, and the identification and characterization of the desired peptide.[1] Unfortunately, these solution phase combinatorial techniques are

not directly compatible with the screening of metallopeptides that exhibit hydrolase activity.

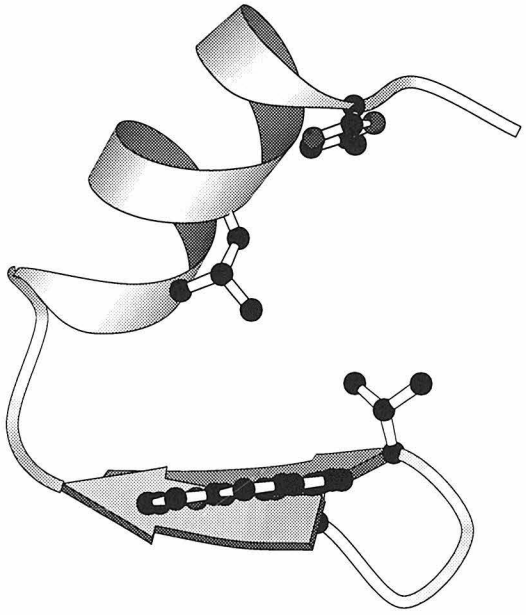

Figure 5-1 The structure of peptide **BBA1** which folds into a well defined structure in the absence of crosslinks (generated using the program Molscript[2]).

The assay cannot be performed with a random library using solution phase combinatorial techniques because the potentially catalytic molecules are present in a mixture of inactive molecules, and a positive signal would prevail so long as a functional molecule is present in the solution mixture. Furthermore, the identification and characterization of the catalytic molecule from this mixture in solution would be a formidable task. For screening these systems, the assay needs be performed on each peptide in the library individually yet maintain the advantage of parallel screening. A library of resin-bound peptides based on the one-bead-one-compound concept presents each individual peptide on different beads to enable physical separation.[3, 4] Furthermore, the actual separation of each bead for screening may be achieved by the one-bead-one-droplet technique developed by Schreiber and coworkers.[5] Additionally, an advantage for screening functional molecules

bound to solid support is that the library may be re-evaluated multiple times, since only simple washing steps are necessary for the recovery of the library after an assay.

One of the biggest concerns in using solid phase bound peptides is generating the peptides in high purity, because purification cannot be performed on molecules bound to the solid support. Standard solid phase peptide synthesis using Fmoc-based chemistry (Fmoc, 9-Fluorenylmethyloxycarbonyl) is fairly efficient in synthesizing peptides linearly,[6] however the synthesis of the 23-residue peptides that adopt a ββα super-secondary structure have been proven difficult using such protocols (for details see Chapter 3). The coupling efficiency is especially low for residues 12 to 8, which correspond to the loop connecting the α-helix and β-hairpin. Therefore, a different synthetic strategy is required for generating the resin bound peptides.

There are several alternatives to the linear synthesis of such peptides including segment coupling,[7, 8] chemical ligation,[9, 10] native ligation,[11-14] and enzymatic ligation (Scheme 5-1).[15-23] All four strategies involve the joining of two peptide segments using different chemistries.

Scheme 5-1 Different Strategies for Joining Two Peptide Segments

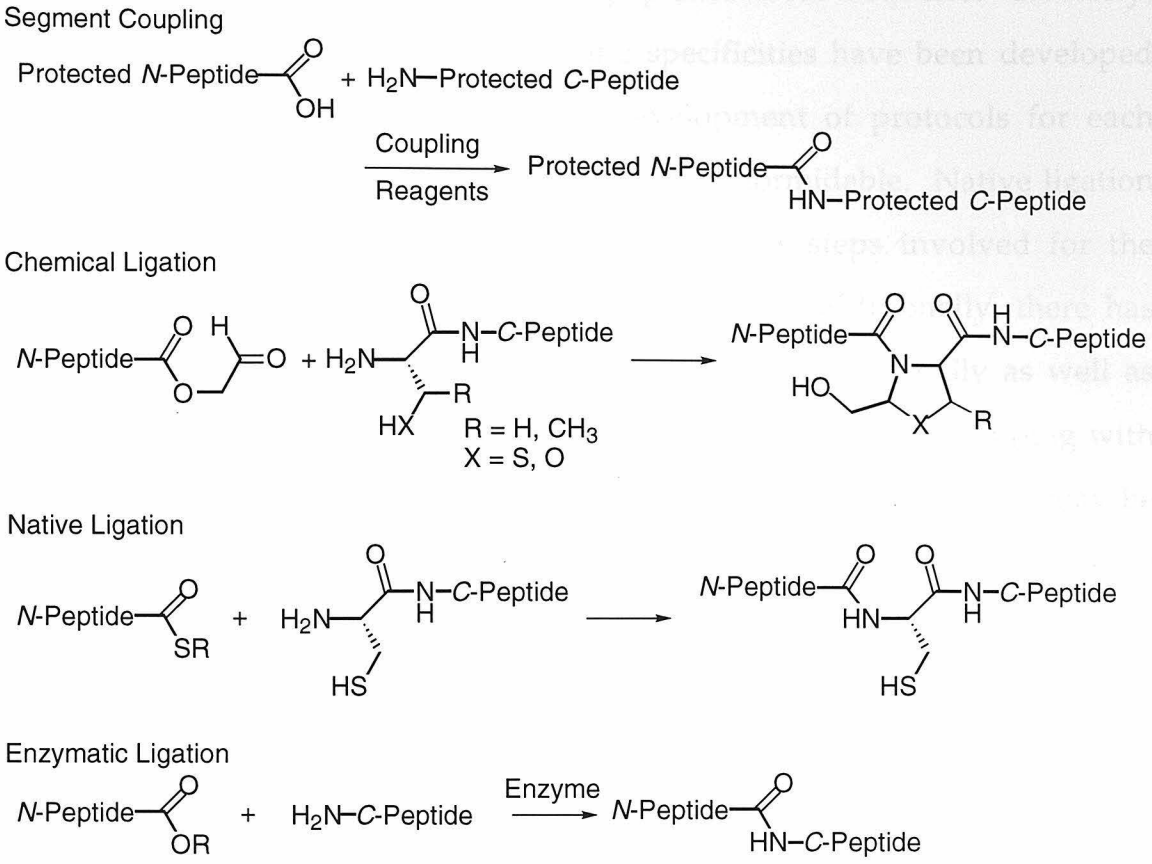

Segment ligation is performed using coupling procedures similar to those for solid phase peptide synthesis (SPPS), thus it is unlikely that the low coupling efficiency for residues 12 through 8 can be improved. Furthermore, this is the only approach that requires protected peptide segments which may suffer from aggregation problems. The three other strategies involve unprotected peptides. For chemical ligation, complicated preparation of the chemical active species for the *N*-peptide is required, and several transformations are necessary after the ligation to obtain the proline analogue. Furthermore, the resulting residue linking the two peptide segments is limited to the proline analogues. For enzymatic ligations, the sequences for the two segments are limited to ones that are recognized by the

enzyme, however the purpose for implementing this approach is to enable the synthesis of a large number of peptides with sequence diversity. Although different enzymes with varying specificities have been developed for joining peptide segments,[15-23] the development of protocols for each enzyme to perform solid phase ligation would be formidable. Native ligation is somewhat similar to chemical ligation with less steps involved for the preparation of the active species for the *N*-peptide. Additionally, there has been development to expand the linking residues to include Gly as well as Cys.[13] Furthermore, selective derivatization of cysteine such as capping with iodoacetamide has been well known,[24] therefore extra functionalities may be attached to the cysteine to provide side chains similar to other natural amino acids.

Native ligation involves the transthioesterfication between the *C*-terminal thioester on the *N*-peptide and the *N*-terminal cysteine side chain thiol on the *C*-peptide (Scheme 5-2). This cysteine thioester intermediate is then transformed into the resulting peptide through an intramolecular nucleophilic attack of the *N*-terminal amine on the thioester. One important feature of native ligation is that no protecting groups are needed because the reaction is specific. While native ligation presents an attractive method for generating peptides bound to the solid support, the technique does suffer some drawbacks. The synthesis of the *N*-peptide thioester has only been achieved using Boc-based chemistry (Boc, *tert*-butyloxycarbonyl) (Scheme 5-3).[25] Boc-based chemistry requires the usage of an HF chamber for cleavage and deprotection to obtain the corresponding thioacid, which is then transformed to the benzyl thioester by reacting with benzyl bromide. An Fmoc-based synthesis of the *N*-peptide thioester would be preferable for general purposes to avoid handling HF. All the native ligations have been

performed in solution to date, however a ligation involving solid phase would be more appropriate to generate resin bound peptides. Therefore, modifications to the solution phase native ligation are necessary to accommodate Fmoc-based chemistry and solid phase conditions.

Scheme 5-2 Mechanism for Native Ligation

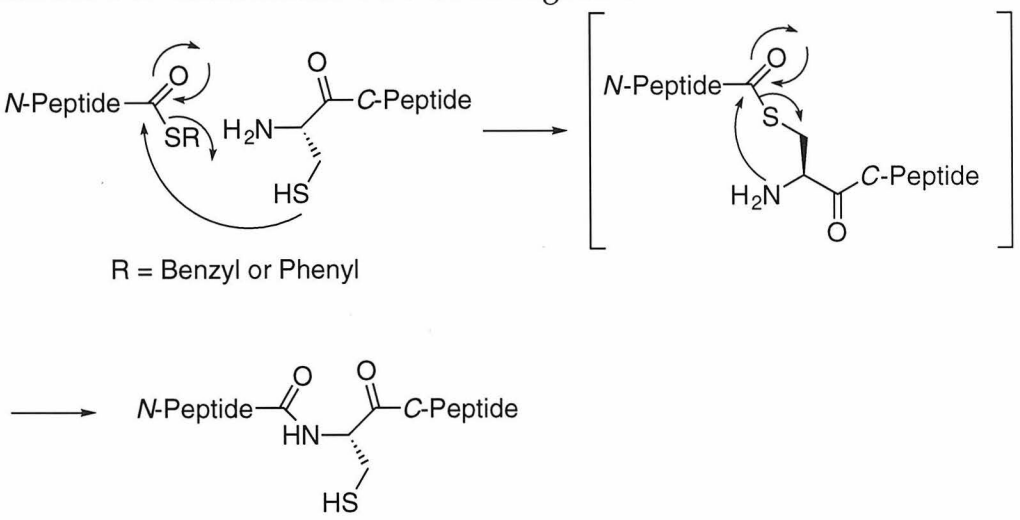

Scheme 5-3 Synthesis of the *N*-Peptide Benzyl Thioester Involving Boc-Based Chemistry

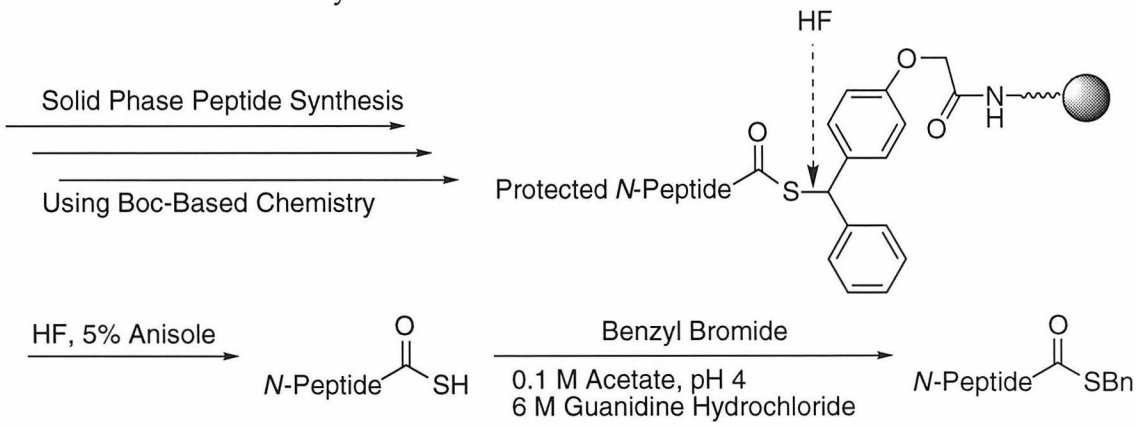

The solid phase native ligation strategy is depicted in Scheme 5-4. The approach involves synthesizing the *N*-peptide benzyl thioester and the resin bound *C*-peptide, followed by ligation of the two segments. Efforts described

in this chapter focus on the development of the synthesis for the *N*-peptide benzyl thioester using Fmoc-based chemistry and solid phase native ligation.

Scheme 5-4 Outline of Solid Phase Native Ligation

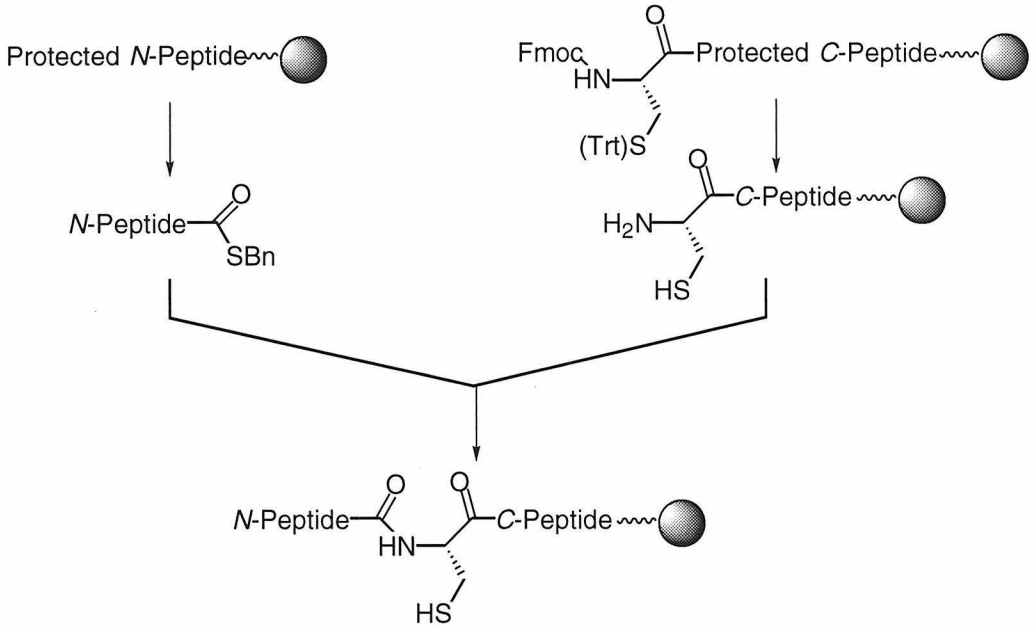

Results and Discussion

Design of the Sequences for the *N*-Peptide and the *C*-Peptide

A peptide designed to exhibit Zn^{II} dependent hydrolase activity based on the ββα construct served as a model system for developing solid phase native ligation. There have been many studies on two families of zinc proteases, thermolysin and metzincins.[26] The two families share a common helix sequence -His-Glu-Xaa-Xaa-His- which provide two histidines involved in the Zn^{II}-binding site and the catalytically crucial proton abstractor glutamate. This sequence was incorporated into the ββα scaffold peptide **BBA1** (Ac-Tyr-Thr-Val-DPro-Ser-Fen-Thr-Phe-Ser-Arg-Ser-Asp-Glu-Leu-Ala-Lys-Leu-Leu-Arg-Leu-His-Ala-Gly-NH_2) at positions 17 through 21, and Fen^6 was

replaced with histidine to mimic the Zn^{II} binding site of carbonic anhydrase based on metal binding results in Chapter 4. Preliminary molecular modeling showed that the Glu^{18} side chain was positioned in close proximity to the Zn^{II} bound water to serve as a potential proton abstractor (Figure 5-2). Therefore, the sequence for the designed peptide was designed to be Ac-Tyr-Thr-Val-DPro-Ser-His-Thr-Phe-Ser-Arg-Ser-Asp-Glu-Leu-Ala-Lys-His-Glu-Arg-Leu-His-Ala-Gly-NH_2. To develop protocols for the synthesis of the peptide benzyl thioester using Fmoc-based chemistry and solid phase native ligations, this peptide was synthesized according to the strategy outlined in Scheme 5-4. However, the site of ligation remained to be determined.

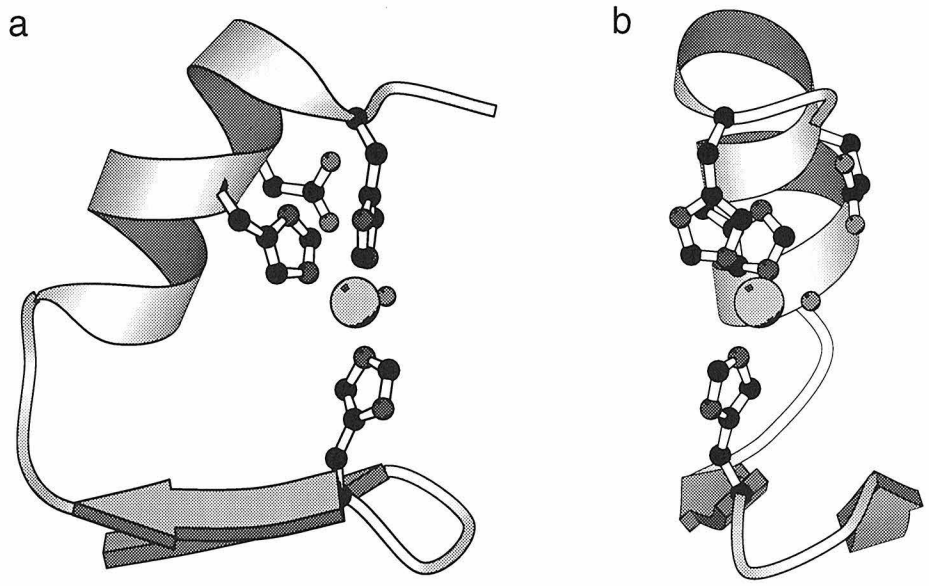

Figure 5-2 (a) Proposed structure of the Zn^{II} complex of a ββα motif with metal-binding histidines at positions 6, 17, and 21, and glutamate at position 18 to serve as a proton abstractor. (b) The complex in panel a viewed from a different angle (generated using the program Molscript[2]).

Dividing the 23-residue peptide into two segments at positions 8 through 11 would avoid couplings that exhibit low efficiencies for linear syntheses of ββα motifs (for details see Chapter 3). Since Asp^{11} is part of the helix cap, which is believed to be crucial for structural formation,[27-32]

ligations involving this position was not considered. Joining two peptide segments between residues 9 and 10 seemed promising, because this could avoid the low efficiency couplings at positions 8 and 9, and preserve the original side chain functionality of Asp[11] for structural reasons. Furthermore, natural zinc fingers often have Gln incorporated at the position corresponding to position 10 in the designed ββα motif.[33] Capping of the cysteine at position 10 with ioidoacetamide after a ligation would give a pseudo-homoglutamine, which exhibits a side chain similar to glutamine (Scheme 5-5). Therefore the *C*-peptide was designed to be Cys-Ser-Asp-Glu-Leu-Ala-Lys-His-Glu-Arg-Leu-His-Ala-Gly-NH_2 (**CPep**) and the *N*-peptide was Ac-Tyr-Thr-Val-DPro-Ser-His-Thr-Phe-Ser-OH (**NPep**). Resin bound *C*-peptide was readily synthesized by Fmoc-based SPPS, however protocols for synthesizing *N*-peptide benzyl thioester needed to be developed.

Scheme 5-5 Iodoacetamide Capping of Cysteine

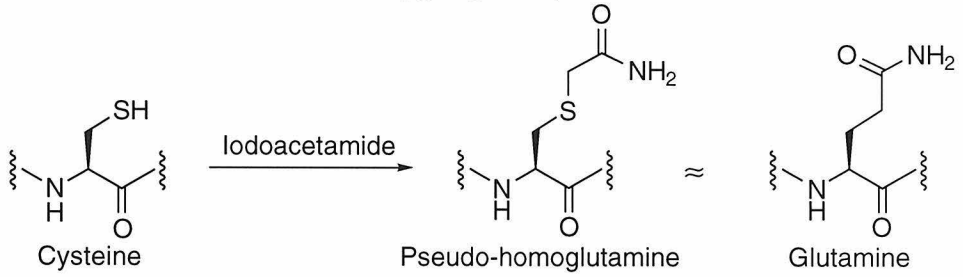

Synthesis of the *N*-Peptide Benzyl Thioester

Synthesis of the N-Peptide Thioester Utilizing the HMBA Linker

One approach for synthesizing the *N*-peptide benzyl thioester using Fmoc-based chemistry involves the synthesis of the corresponding peptide on the hydroxymethylbenzoic acid linker (HMBA), and then reacting the resin bound peptide ester with benzyl mercaptan as the nucleophile (Scheme 5-6).

It has been demonstrated previously that nucleophiles such as hydroxide, ammonia and primary amines can afford the corresponding carboxylate or carboxyamide using the HMBA linker.[34-36] Thus, reacting a peptide-HMBA ester linkage with benzyl mercaptan should afford the corresponding thioester.

Scheme 5-6 Retrosynthetic Scheme for Synthesizing the *N*-Peptide Benzyl Thioester Using the HMBA Linker

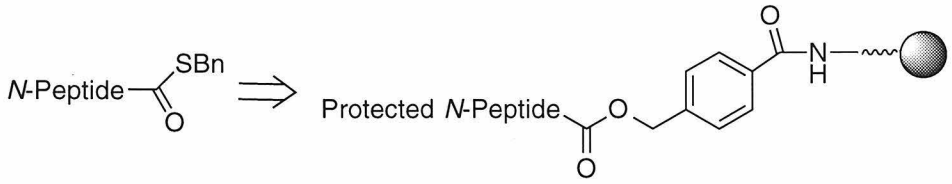

The test peptide Ac-Phe-Ser-OH was synthesized on HMBA-TG resin. The peptide was cleaved off the resin with 0.1 M NaOH(aq) and the desired product was confirmed by electrospray mass spectrometry (ES-MS). Several different conditions were tested for reacting with the benzyl ester, but none gave the desired product (Scheme 5-7).

Scheme 5-7 Attempts to Synthesize Ac-Phe-Ser-SBn Using the HMBA Linker

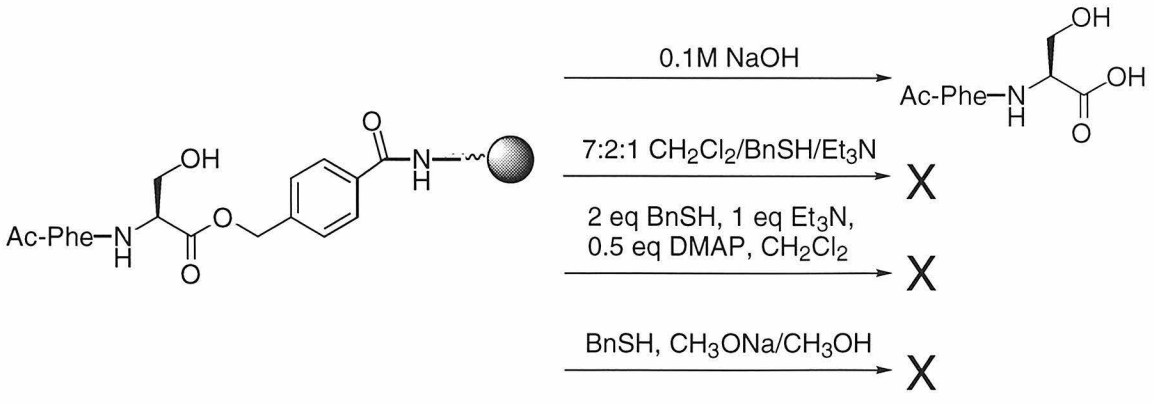

Initial attempts involved reation with benzyl mercaptan and a non-nucleophilic base such as triethylamine, but no reaction was observed even up to 100 equivalents of benzyl mercaptan. The reaction did not proceed even

with small amounts of *N*,*N*-dimethylaminopyridine (DMAP) as an acyl transfer reagent. If the more nucleophilic thiolate species was generated *in situ* prior to the reaction with the resin-bound peptide ester, the benzyl thioester may be formed. However, the generation of the thiolate species with $Na_{(S)}$ was extremely slow and that with $NaH_{(s)}$ was too exothermic. Furthermore, insoluble pale yellow solids were formed in both cases. Since the pK_a of benzyl mercaptan is approximately 10, deprotonation could be efficiently affected by methoxide. The resulting thiolate generated was submitted to the resin-bound ester. Unfortunately, no desired product was observed over several days. Since the HMBA linker strategy was unsuccessful, another approach involving the methoxytrityl thiol resin was investigated.

Synthesis of the N-Peptide Thioester Utilizing the Thiol Methoxytrityl Linker

The strategy to synthesize the fragment using the thiol methoxytrityl linker is depicted in Scheme 5-8. Cleaving the peptide from such a linker affords the thioacid, which can be converted to the benzyl thioester by reacting with benzyl bromide.[11-14] It should be noted that peptide synthesis has never been reported on this particular linker.

Scheme 5-8 Retrosynthetic Scheme for Synthesizing the *N*-Peptide Benzyl Thioester Using the Thiol Methoxytrityl Linker

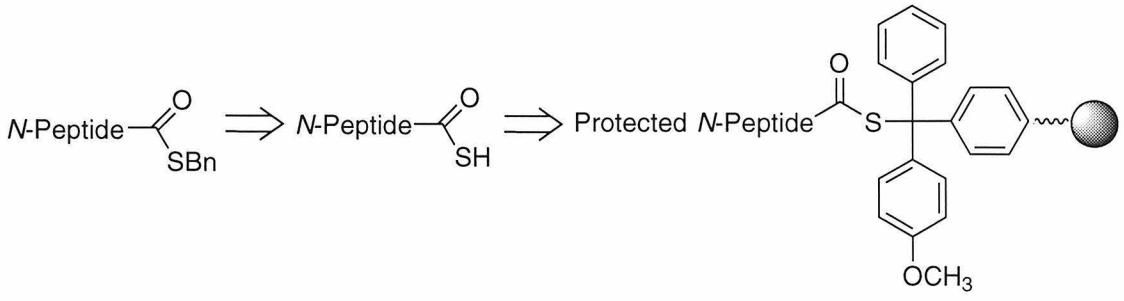

The test peptide Ac-Phe-Ser-SH was synthesized on the methoxytrityl thiol linker. However, the peptide could not be detected after the deblock of the second residue. Since the thioester functionality is known to be quite labile, loss of peptide may be due to intramolecular cyclization by the *N*-terminus amine to form diketopiperazine. Therefore, subsequent coupling onto the resin was performed using a dipeptide cassette. The synthesis of DNS-Thr-Phe-Ser-Arg-SH (DNS, dansylsulfonamide) using the dipeptide cassette Fmoc-Phe-Ser(^{t}Bu)-OH proceeded smoothly, and a DNS group was incorporated at the end of the synthesis to enable product quantification by absorption spectroscopy (UV-vis). Unfortunately, the yield of the synthesis was only 15% as shown by UV-vis, which is impractical for synthesizing the *N*-peptide benzyl thioester for solid phase native ligation.

Synthesis of the N-Peptide Thioester Utilizing the Hydroxytrityl Linker

A third approach for synthesizing the *N*-peptide benzyl thioester is to synthesize the protected peptide carboxylic acid, and transform it into the benzyl thioester (Scheme 5-9). To test this approach, a reaction with a model compound was explored first.

Scheme 5-9 Retrosynthetic Scheme for Synthesizing the *N*-Peptide Benzyl Thioester Using the Hydroxytrityl Linker

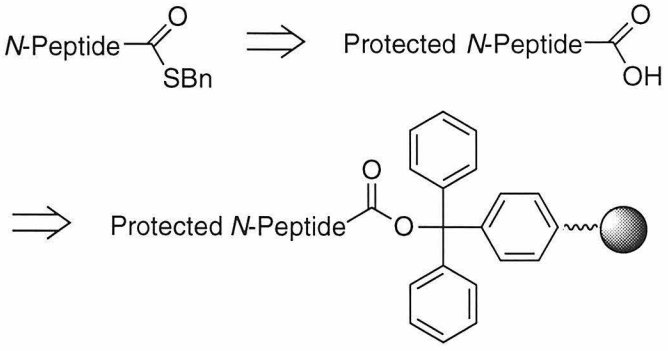

The thioesterfication of a carboxylic acid was investigated with *N*-acetyl-L-phenylalanine (Ac-Phe-OH), and the reaction was carried out using diisopropylcarbodiimide/1-hydroxybenzotriazole (DIPCDI/HOBt) activation chemistry (Scheme 5-10). The product was isolated and purified by flash column chromatography, and confirmed by mass spectrometry. The synthesis of a thioester from the corresponding carboxylic acid was demonstrated to be straightforward. Therefore, the strategy involving the protected peptide acid was further investigated.

Scheme 5-10 Synthesis of *N*-Acetyl-L-Phenylalanine Benzyl Thioester

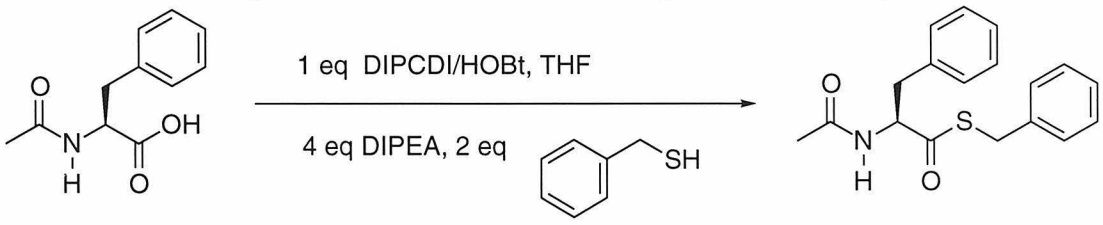

The synthesis of **NPep**-SBn is illustrated in Scheme 5-11. Peptide **NPep** (Ac-Tyr-Thr-Val-DPro-Ser-His-Thr-Phe-Ser-OH) was synthesized on the resin Fmoc-Ser(^{t}Bu)-TGT (TGT, TentaGel resin with hydroxytrityl linker) using Fmoc-based chemistry. The protected peptide Ac-Tyr(Boc)-Thr(^{t}Bu)-Val-DPro-Ser(^{t}Bu)-His-Thr(^{t}Bu)-Phe-Ser(^{t}Bu)-OH was obtained by cleaving with 4:5:1 $CH_2Cl_2/CH_3COOH/CH_3OH$. The synthesis of the benzyl thioester was performed according to the model compound Ac-Phe-SBn with slight modifications. After deprotection using 5% triisopropylsilane /trifluoroacetic acid (TIS/TFA), the product was analyzed by reverse phase high performance liquid chromatography (RP-HPLC) and confirmed to be **NPep**-SBn by electrospray mass spectrometry (ES-MS).

Scheme 5-11 Synthesis of **NPep**-SBn

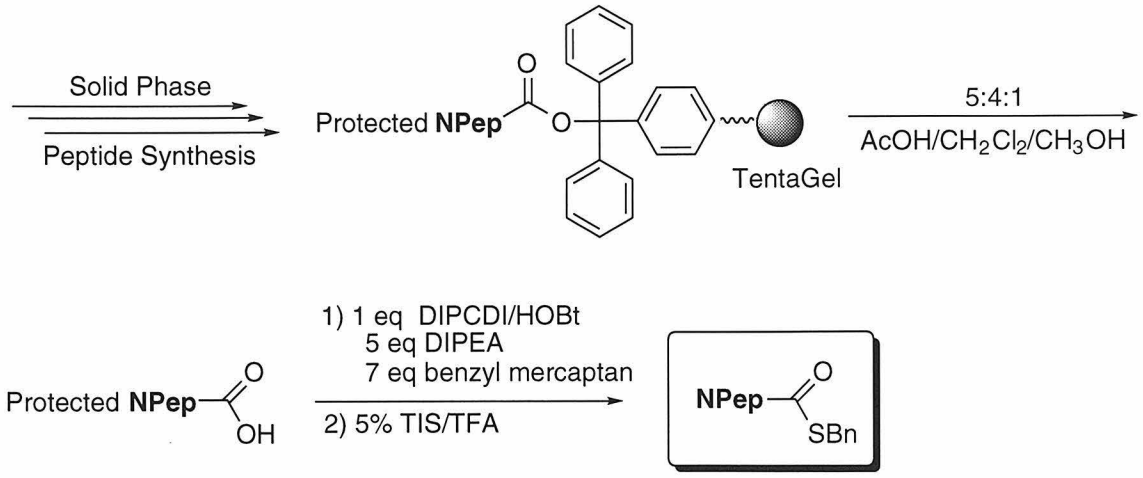

The synthetic route for the synthesis of peptide thioesters using Fmoc-based chemistry has been developed. The chemistry is straightforward yet highly efficient without involving HF, which is required for the Boc-based chemistry previously reported.[11-14, 25] Since the synthesis does not involve HF, it should prove especially useful for laboratories without access to special HF chambers.

Solid Phase Native Ligation

Solid phase ligations were performed with the *C*-peptide on a solid support and both protected and unprotected *N*-peptide thioester in solution according to the strategy outlined in Scheme 5-4. These reactions were monitored by thin layer chromatography (TLC) and RP-HPLC for the consumption of the protected and unprotected *N*-peptide thioester respectively. In both cases, the thioester was fully consumed without hydrolysis to the corresponding acid.

Different solid supports were investigated due to different swelling properties of the resins. Most traditional solid supports for solid phase

peptide synthesis (SPPS) such as polystyrene crosslinked with 2% divinylbenzene, Kieselguhr resin, or polyethyleneglycol-grafted polystyrene do not swell well under aqueous conditions, and thus do not present the resin bound peptide efficiently. Recently, there have been major advancements in generating solid supports that swell considerably well under aqueous conditions which would be optimal for solid phase ligation and future solid phase combinatorial assays (Table 5-1). These resins include TG[TentaGel, polystyrene–poly(ethyleneglycol)–tentacle copolymer],[37-40] PEGA [polyethyleneglycol-poly-(*N*,*N*-dimethylacrylamide) copolymer],[38, 41-43] and CLEAR[cross-linked ethoxylate acrylate resin].[44] The more a resin swells in water, the better the attached peptides are solvated under aqueous conditions. It is important to use resin that swell in both *N*,*N*-dimethylformamide (DMF) and water, since solid phase peptide synthesis is normally performed in DMF, while native ligation and ester hydrolysis assays are performed under aqueous conditions. For TG resin, there are distinct inner sites and outer sites observed under aqueous conditions due to the undesirable swelling properties of the polystyrene matrix in water. Fortunately, both PEGA and CLEAR resins swell considerably well in both DMF and water, however CLEAR is not commercially available yet. Furthermore, none of the three resins were available at the early stages of this project. Therefore, the standard solid support for solid phase peptide synthesis PEG-PS was investigated initially, followed by TG and PEGA resins as they became commercially available.

Table 5-1 Characteristics of Various Solid Supports for Solid Phase Peptide Synthesis

Resin	Swelling DMF	Swelling Water	Commercially Available
PEG-PS	Good	Poor	Yes
TG	Excellent	Good	Recent
PEGA	Excellent	Excellent	Most Recent
CLEAR	Excellent	Excellent	Not Available

Furthermore, the *C*-peptides were attached to the solid supports with various linkers to enable characterization of the resin bound products after ligation (Figure 5-3). The TFA-labile PAL [5-(4'-aminomethyl-3',5'-dimethoxyphenoxy)valeric acid] linker with the mono-methoxytrityl (Mmt) protected cysteine was used for synthesizing peptide **CPep** to enable selective liberation of the thiol side chain under mild acidic conditions that would not affect the PAL linker. The cysteine side chain would thus be available for solid phase ligation, and subsequent cleavage using TFA would afford the resin bound product. With methionine and HMBA (4-hydroxymethyl-benzoic acid), these two linkers are known to be compatible with Fmoc-based SPPS and stable under conditions for removing the side chain protecting groups. After ligation and cleavage of the resulting resin bound peptide under appropriate conditions, the peptides were analyzed by RP-HPLC or amino acid analysis. The results for the ligations are summarized in Table 5-2 and discussed subsequently.

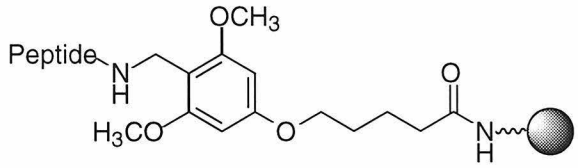

PAL (5-(4'-aminomethyl-3',5'-dimethoxyphenoxy)valeric acid)
Affected by 5% TIS/TFA to give carboxyamides

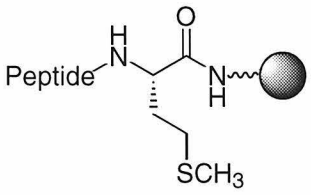

Met (methionine)
Affected by CNBr in 0.1 M HCl
to give homoserine lactones

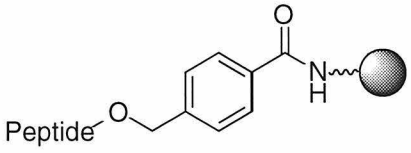

HMBA (4-hydroxymethylbenzoic acid) linker
Affected by NH_3/MeOH to give carboxyamides

Figure 5-3 Various linkers utilized to facilitate characterization of the resin bound product of solid phase ligations.

Table 5-2 Solid Phase Ligations for Synthesizing ββα Peptides[a]

Entry	*N*-Peptide Benzyl Thioester	*C*-Peptide		Solvent[d]	Result[e]
		Linker[b]	Solid Support[c]		
1	Protected	PAL	PEG-PS	DMF	No Ligation
2	Protected	Met	TG	DMF	No Ligation
3	Protected	Met	TG	H_2O	No Ligation
4[f]	Not Protected	HMBA	TG	H_2O	No Ligation
5	Not Protected	N/A	N/A	H_2O	Ligation
6	Not Protected	HMBA	PEGA	H_2O	Ligation[g]

[a] The ligations were performed in the presence of 2.5% benzyl mercaptan and 2.5% thiophenol. **NPep** and **CPep** were used in equimolar ratios as the *N*-peptide and the *C*-peptide respectively. The *C*-peptides were bound to the solid phase except for entry 4 which was in solution. The concentrations of *N*-peptide in solution were approximately 5 mg/mL.

[b] The PAL [5-(4'-aminomethyl-3',5'-dimethoxyphenoxy)valeric acid] linker was cleaved with 5% TIS/TFA. Methionine was cleaved with CNBr in 0.1 N HCl. The HMBA (4-hydroxymethylbenzoic acid) linker was cleaved with NH_3/MeOH.

[c] PEG-PS: polyethyleneglycol grafted onto polystyrene, Perseptive Biosystems. TG: TentaGel, polystyrene–poly(ethyleneglycol)–tentacle copolymer, Novabiochem. PEGA: polyethyleneglycol-poly-(*N*,*N*-dimethylacrylamide) copolymer, Novabiochem.

[d] The ligations were performed in either DMF or aqueous conditions. The aqueous condition involved 0.1 M phosphate and 6 M guanidine hydrochloride at pH 7.5. Entry 4 was also attempted with 33% DMF, however no ligation was observed either.

[e] For entries 1 through 3, the ligations were monitored by TLC. For entries 4 through 6, the ligations were monitored by RP-HPLC. The ligation products were analyzed by RP-HPLC and identified by ES-MS unless specified otherwise.

[f] This ligation was performed in solution phase using **NPep**-SBn and **CPep**-NH_2 under similar conditions as described in footnote a.

[g] The desired product was confirmed by amino acid analysis of the product bound to the solid support. The molecular weight of the cleavage product is consistent with two peptide **NPep-CPep** linked by a disulfide bond. The resin bound product was capped with iodoacetamide and then cleaved to give the desired product by ES-MS.

*Ligation of **CPep**-PAL-PEG-PS and Protected **NPep**-SBn*

Initial attempts at ligation involved the PAL-PEG-PS resin, which is used for standard Fmoc-based SPPS. This linker would enable characterization of the resin bound ligation products without requiring reactions beyond those for Fmoc-based SPPS. Since native ligation only relies on the *N*-terminal cysteine of the *C*-peptide, the reaction can potentially proceed as long as the cysteine is fully deprotected. The Mmt protecting group was chosen, since it can be deprotected and cleaved under mild acidic conditions that does not affect the PAL linker. The ligation products can therefore be cleaved and analyzed by RP-HPLC. Although the PEG-PS resin does not swell under aqueous conditions, solution phase native ligations had previously been performed under both 50% DMF/aqueous and aqueous conditions.[45]

The cysteine on the protected **CPep**-PAL-PEG-PS was selectively deprotected and submitted to ligation conditions with protected **NPep**-SBn in DMF. Although the protected **NPep**-SBn appeared to be consumed by TLC, no ligation product was observed upon cleavage. It seemed crucial that the ligation be performed with fully deprotected peptides under aqueous conditions. Since PEG-PS does not swell well in water and deprotection of the side chains cleaves the peptide from the PAL linker concomitantly, different resins and linkers were therefore investigated.

*Ligation of **CPep**-Met-TG and Protected **NPep**-SBn*

At the time of this study, the only commercially available resin that swells considerably well in water was TG resin. Since methionine is known to be cleaved selectively by treatment with CNBr to give a homoserine lactone, this residue was incorporated at the *C*-terminal of peptide **CPep**. The

ligation of **CPep**-Met-TG and protected **NPep**-SBn was monitored by TLC. Protected **NPep**-SBn appeared to be consumed, however no ligation product was observed upon cleavage with CNBr. This loss of thioester without detection of product may be due to the lack of ligation or the messy cleavage results from the CNBr cleavage. Therefore, a different linker was incorporated to assure cleavage results.

*Ligation of **CPep**-HMBA-TG and **NPep**-SBn*

Since the HMBA linker has been demonstrated to be compatible with Fmoc-based SPPS and is labile only to strong nucleophiles such as ammonia, hydroxide, and primary amines, it was used to attach the *C*-peptide to the TG resin. The ligation of **CPep**-HMBA-TG and **NPep**-SBn was monitored by RP-HPLC. No significant change in the elution profile was observed over 50 hours. Therefore, some DMF was added to facilitate the solvation of the resin bound peptide. However, the HPLC traces were difficult to interpret due to the presence of DMF. The resulting solid support was submitted to cleavage conditions, and no desired product was observed. The lack of solid phase ligation may be due to the specific sequences of the two segments, thus the corresponding solution phase ligation was investigated.

The solution phase ligation was performed and monitored by RP-HPLC. Peaks corresponding to **CPep** and **NPep**-SBn disappeared with concomitant formation a new peak, which was confirmed to be the desired ligation product by ES-MS. Therefore, the lack of solid phase ligation is not due to the sequences, but to non-optimal properties of the TG resin. Since the PEGA resin became commercially available at this time, solid phase ligation was investigated using this solid support.

*Ligation of **CPep**-HMBA-PEGA and **NPep**-SBn*

The PEGA resin swells more than TG resin in water, which would allow full solvation of the resin bound peptide under aqueous conditions. This characteristic of the resin would enable the resin bound peptide to effectively emulate the solvated peptide in solution. Thus, the solid phase ligation performed using PEGA resin should be straightforward. Therefore, peptide **CPep** was synthesized onto HMBA-PEGA resin. The corresponding solid phase ligation was monitored by RP-HPLC, and the peak corresponding to **NPep**-SBn steadily decreased in intensity over 120 hours (Figure 5-4). The desired ligation product bound to the resin was confirmed by amino acid analysis (Table 5-3).

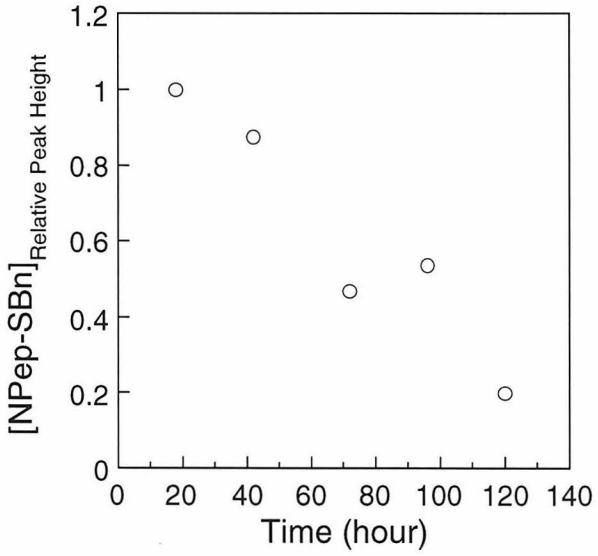

Figure 5-4 The disappearance of **NPep**-SBn monitored by RP-HPLC for the ligation of **CPep**-HMBA-PEGA and **NPep**-SBn.

Table 5-3 Amino Acid Analysis Results of **NPep-CPep**-HMBA-PEGA[a]

Amino Acid	Calculated Amino Acid Ratio			Observed Relative Ratio
	NPep	**CPep**	**NPep-CPep**	
Ala	0	2	2	2.1
Arg	0	1	1	1.0
Asp	0	1	1	1.2
Cys[b]	0	1	1	0[b]
Glu	0	2	2	2.0
Gly	0	1	1	1.3
His	1	2	3	3.2
Leu	0	2	2	1.9
Lys	0	1	1	0.9
Phe	1	0	1	0.9
Pro[c]	1	0	1	1.0
Ser	2	1	3	2.6[d]
Thr	2	0	2	1.8[d]
Val	1	0	1	0.9
Tyr	1	0	1	0.9

[a] The amino acid analysis was performed by Dr. Audree Fowler at UCLA.
[b] Since the analysis is performed under oxidative conditions, the cysteine residue cannot be observed.
[c] Although the residue incorporated is DPro, the two enantiomers cannot be differentiated by this analysis.
[d] Under the conditions of the analysis, the hydroxyl residues Ser and Thr tend to dehydrate slightly, resulting in slightly lower values for these two amino acids.

The amino acid analysis data presented above establishes that the desired ligation product has been synthesized on the PEGA resin by solid phase native ligation. This will enable the generation of combinatorial libraries of resin bound ββα peptides to screen for metallopeptides that exhibit hydrolase activity. Furthermore, the successful development of solid phase native ligation allows the synthesis of much larger peptide constructs

containing several unnatural amino acids, which would involve repetitive ligation of peptide segments to the resin bound peptide.

Conclusion

The synthesis of peptide benzyl thioesters using Fmoc-based chemistry has been demonstrated without involving HF. The synthetic protocols will prove useful for the facile generation of peptide thioesters, which are building blocks for constructing large peptides based on the native ligation approach. Furthermore, solid phase native ligation has been demonstrated for constructing a peptide that adopts a ββα super-secondary structure. This enables the synthesis of combinatorial libraries of resin bound ββα peptides in future studies to screen for metallopeptides that exhibit hydrolase activity. Additionally, much larger peptide constructs containing multiple unnatural amino acids may be synthesized by applying this solid phase ligation approach in a repetitive manner.

Acknowledgments

Discussions with Dr. Philip Dawson were helpful for the development of the chemistry presented in this chapter. The essential electrospray mass spectrometry were almost exclusively performed by Michael Shogren-Knaak. Amino acid analysis was performed by Dr. Audree Fowler at UCLA.

Experimental Section

Solid Phase Peptide Synthesis

The peptides were synthesized essentially according to the protocols reported in Chapter 4. The protected **NPep**-OH was synthesized on TGT resin, and CPep was synthesized on PAL-PEG-PS, TG, HMBA-TG and HMBA-PEGA resins. Initial derivatization of resins with the HMBA linker was performed following published procedures for generating esters on solid supports.[46] In brief, the HMBA-PEGA resin (1.5 g wet, ~0.07 mmole/g) was dried under vacuum. The resin was then suspended in CH_2Cl_2 (3mL) for 30 minutes. A solution of Fmoc-Gly-OH (166.5 mg, 0.58 mmole), diisopropylcarbodiimide (88 μL, 0.56 mmole), and 4-*N*,*N*-dimethylamino-pyridine (3 mg, 0.02 mmole) in 4 mL CH_2Cl_2 was added to the suspension. The mixture was agitated at room temperature overnight. The resin was then filtered and washed with CH_2Cl_2, DMF and methanol. The resulting solid support was dried under vacuum, and the peptide was then synthesized according to procedures reported in Chapter 4.

General Procedures for the Synthesis of CPep-Linker-Resin. The resin bound peptide was deblocked with 20% piperidine/DMF (3 x 20 minutes). The resin was then washed with DMF, CH_2Cl_2, and methanol, and dried under vacuum overnight. The resin bound peptide was then deprotected with 5% TIS/TFA for two hours. The resin is then washed with CH_2Cl_2, methanol, and DMF, and dried under vacuum overnight. For protected **CPep**-PAL-PEG-PS, the Mmt group on the N-terminal cysteine was removed selectively with 95:4:1 CH_2Cl_2/TIS/TFA (3 x 20 minutes). The resin was then washed with CH_2Cl_2, methanol, and DMF, and dried under vacuum overnight.

Protected NPep-OH. The protected **NPep**-TGT (0.4066 g) was cleaved using 10 mL 5:4:1 acetic acid/CH_2Cl_2/methanol for 1.5 hours. The mixture was then filtered into hexanes (300 mL) and washed with 10 mL 5:4:1 acetic acid/CH_2Cl_2/methanol. The filtrate in hexanes was concentrated under reduced pressure to obtain an oil. The oil was resuspended in benzene and lyophilized to give the product as a white fluffy powder (70.0 mg). The product was confirmed to be the protected **NPep** less a *tert*-butyloxycarbonyl protecting group which was believed to be removed from the histidine. ES-MS [$MHNa^{2+}$], calcd. for $C_{70}H_{109}N_{11}O_{16}$ [692]; obsd. [692].

Synthesis

***N*-Acetyl-L-Phenylalanine Benzyl Thioester (Ac-Phe-SBn)**. To a solution of Ac-Phe-OH (0.1042 g, 0.503 mmole) and HOBt (0.0773 g, 0.505 mmole) in THF (1 mL) was added DIPCDI (78 µL, 0.498 mmole). The reaction was stirred at room temperature for 30 minutes to form a white precipitate. The benzyl mercaptan (118 µL, 1.01 mmole) and diisopropylethylamine (350 µL, 2.01 mmole) were added subsequently and stirred for another 3 hours. The reaction mixture was then filtered and washed with THF. The filtrate was combined and resuspended in chlorform (20 mL). The chloroform was washed with 1 N HCl (3 x 20 mL) and brine (20 mL). The organic layer was dried over Na_2SO_4 and concentrated under reduced pressure. The product was purified by silica gel flash column chromatography eluting with chloroform to yield 0.1222 g (0.390 mmole, 78 % yield). FAB-MS [MH^+], calcd. for $C_{18}H_{19}NO_2S$ [314.1215]; obsd. [314.1210]. ^1H NMR ($CDCl_3$) δ: 1.95 (s, 3H), 3.11 (d, 2H, J = 6.1 Hz), 4.10 (s, 2H), 5.01 (dt, 1H, J = 8.6, 6.0 Hz), 5.76 (d, 1H, J = 8.3 Hz), 7.01-7.04 (m, 2H), 7.20-7.30 (m, 8H); ^{13}C NMR ($CDCl_3$) δ: 23.7, 33.9, 38.8, 59.9, 128.0, 129.2, 129.5, 129.9, 135.9.

NPep-SBn. To a solution of protected **NPep**-OH (70 mg, 51 μmole) and HOBt (7.3 mg, 48 μmole) in THF (500 μL) was added DIPCDI (7.5 μL, 48 μmole). The reaction was stirred at room temperature for 30 minutes to form a white suspension. The benzyl mercaptan (39 μL, 332 μmole) and DIPEA (42 μL, 240 μmole) were added subsequently and stirred at room temperature overnight. The reaction mixture was then concentrated under reduced pressure. The resulting oil was resuspended in chloroform (25 mL). The chloroform was washed with 1 N HCl (3 x 20 mL) and brine (20 mL). The aqueous layers were combined and extracted with chloroform (3 x 20 mL). The organic layers were combined, dried over Na_2SO_4, and concentrated under reduced pressure to give a pale yellow oil. The oil was resuspended in benzene and lyophilized to dryness to give a white fluffy powder (90.7 mg). The solid was then deprotected with 200 μL of 5% TIS/TFA for 2 hours at room temperature. The reaction was blown down with nitrogen and triturated with 1.5 mL 1:1 ether/hexanes 3 times. The solid was then resuspended in water and lyophilized to give the desired product as a white fluffy powder (54.2 mg, 46 μmole). ES-MS [MH^+], calcd. for $C_{57}H_{75}N_{11}O_{15}S$ [1185.52]; obsd. [1186].

Solid Phase Ligations

The solid phase ligations were performed in 0.1 M phosphate and 6 M guanidine hydrochloride at pH 7.5 or in DMF. In both cases 2.5 % benzyl mercaptan and thiophenol were present in the reaction. The concentrations of protected and deprotected **NPep**-SBn were approximately 10 and 5 mg/mL respectively, and the **CPep**-linker-resins were present in approximately equimolar quantities. The ligations were performed with the thioester on a 0.5 to 17 mg scale. The reactions were agitated at room temperature and

monitored by TLC and RP-HPLC for consumption of the protected and deprotected **NPep**-SBn respectively. After consumption of the thioester, the resin was washed with water, methanol, DMF, and CH_2Cl_2. The solid support was then dried under vacuum overnight.

Cleavage of the Peptides Bound to the Resin

The resins from the ligations were cleaved according to the following procedures for the different linkers. The result of the peptide syntheses on the varying linkers were cleaved to confirm the formation of the desired peptides. The PAL-PEG-PS and TGT resins were cleaved according to protocols presented in Chapter 3. The results of the ES-MS for the peptides are presented in Table 5-4.

Table 5-4 Mass Analysis on Various Resin Bound Peptides After Cleavage

Peptide	Linker-Resin	MS Detected Species	Calculated	Observed[a]
NPep	TGT	$MHNa^{2+}$	552	552
CPep	PAL-PEG-PS	MH_3^{3+}	522	522
CPep	Met-TG	$MHNa_2^{3+}$	566	566
$(CPep)_2$[b]	HMBA-TG	MH_6^{6+}	522	522
$(CPep)_2$[b]	HMBA-PEGA	MH_6^{6+}	522	522

[a] The values presented correspond to the peak with the highest intensity in the ES-MS spectrum.

[b] The values observed in the ES-MS spectrum are consistent with the formation of the covalently linked dimer by oxidation of the cysteines to form the disulfide bond.

General Procedure for Cleavage Involving Methionine as a Linker. The CNBr (50 mg) was dissolved in 100 μL of acetonitrile, and added to the peptide bound TG resin (2 μL/mg) suspended in 0.1 N HCl (20 μL/mg). The

mixture was agitated for 24 hours at room temperature. The reaction was then filtered and washed with ample amount of water. The filtrate was lyophilized to give the product.

General Procedure for Cleavage Involving the HMBA Linker. The NH_3/MeOH was added to the peptide-HMBA-resin (20 μL/mg). The mixture was agitated for 24 hours at room temperature. The reaction was then filtered and washed with ample amount of MeOH. The filtrate was concentrated under reduced pressure to give a pale yellow oil. The oil was then resuspended in water and lyophilized to give the product.

Solution Phase Ligation

The solution phase ligations were performed according to procedures described for solid phase ligations, except that the concentration of **CPep** was 5 mg/mL. After ligation was complete, the mixture was blown down with nitrogen and desalted by Sep-Pak. Fractions containing the desired peptide were combined and lyophilized to give a white fluffy powder.

References

1. Jung, G. *Combinatorial Peptide and Nonpeptide Libraries*; VCH Publishers, Inc.: New York, 1996 .
2. Kraulis, P. J. *J. Appl. Crystallogr.* **1991**, *24*, 946-950.
3. Lam, K. S.; Lebl, M.; Krchnák, V. *Chem. Rev.* **1997**, *97*, 411-448 and references therein.
4. Lam, K. S.; Lebl, M. "*Combinatorial Library Based on One-Bead-One-Compound Concept*" in *Combinatorial Peptide and Nonpeptide Libraries*, VCH Publishers, Inc., New York, 1996; pp

5. Schreiber, S. L. *et. al.* unpublished results.

6. Fields, G. B.; Noble, R. L. *Int. J. Pept. Protein Res.* **1990**, *35*, 161-214.

7. Bodi, J.; Suli-Vargha, H.; Ludanyi, K.; Vekey, K.; Orosz, G. *Tetrahedron Lett.* **1997**, *38*, 3293-3296.

8. Lloyd-Williams, P.; Albericio, F.; Giralt, E. *Tetrahedron* **1993**, *49*, 11065-11133.

9. Liu, C.-F.; Tam, J. P. *Proc. Natl. Acad. Sci. U.S.A.* **1994**,

10. Liu, C.-F.; Tam, J. P. *J. Am. Chem. Soc.* **1994**, *116*, 4149-4153.

11. Dawson, P. E.; Churchill, M. J.; Ghadiri, M. R.; Kent, S. B. H. *J. Am. Chem. Soc.* **1997**, *119*, 4325-4329.

12. Lu, W.; Qasim, M. A.; Kent, S. B. H. *J. Am. Chem. Soc.* **1996**, *118*, 8518-8523.

13. Canne, L. E.; Bark, S. J.; Kent, S. B. H. *J. Am. Chem. Soc.* **1996**, *118*, 5891-5896.

14. Dawson, P. E.; Muir, T. W.; Clark-Lewis, I.; Kent, S. B. H. *Science* **1994**, *266*, 776-779.

15. Gill, I.; Lopez-Fandino, R.; Vulfson, E. *J. Am. Chem. Soc.* **1995**, *117*, 6175-6181.

16. Jackson, D. Y.; Burnier, J.; Quan, C.; Stanley, M.; Tom, J.; Wells, J. A. *Science* **1994**, *266*, 243-247.

17. Bongers, J.; Offord, R. E.; Felix, A. M.; Campbell, R. M.; Heimer, E. P. *Int. J. Peptide Protein Res.* **1992**, *40*, 268-273.

18. Nishino, N.; Xu, M.; Mihara, H.; Fujimoto, T. *Chem. Lett.* **1992**, 327-330.

19. Abrahsen, L.; Tom, J.; Burnier, J.; Butcher, K. A.; Kossiakoff, A.; Wells, J. A. *Biochemistry* **1991**, *30*, 4151-4159.

20. Schellenberger, V.; Jakubke, H.-D. *Angew. Chem. Int. Ed. Engl.* **1991**, *30*, 1437-1449.

21. Breddam, K.; Widmer, F.; Meldal, M. *Int. J. Peptide Protein Res.* **1991**, *37*, 153-160.

22. Kitaguchi, H.; Klibanov, A. M. *J. Am. Chem. Soc.* **1989**, *111*, 9282-9273.

23. Sakina, K.; Kawazura, K.; Morihara, K. *Int. J. Peptide Protein Res.* **1988**, *31*, 245-252.

24. Lundblad, R. L. *Techniques in Protein Modification*; CRC Press: Boca Raton, 1995 .

25. Canne, L. E.; Walker, S. M.; Kent, S. B. H. *Tetrahedron Lett.* **1995**, *36*, 1217-1220.

26. Lipscomb, W. N.; Strater, N. *Chem. Rev.* **1996**, *96*, 2375-2433.

27. Chakrabartty, A.; Doig, A. J.; Baldwin, R. L. *Proc. Natl. Acad. Sci. U.S.A.* **1993**, *90*, 11332-11336.

28. Dasgupta, S.; Bell, J. A. *Int. J. Peptide Protein Res.* **1993**, *41*, 499-511.

29. Harper, E. T.; Rose, G. D. *Biochemistry* **1993**, *32*, 7605-7609.

30. Lyu, P. C.; Zhou, H. X.; Jelveh, N.; Wemmer, D. E.; Kallenbach, N. R. *J. Am. Chem. Soc.* **1992**, *114*, 6560-6562.

31. Richardson, J. S.; Richardson, D. C. *Science* **1988**, *240*, 1648-1652.

32. Presta, L. G.; Rose, G. D. *Science* **1988**, *240*, 1632-1641.

33. Krizek, B. A.; Amaan, B. T.; Kilfoil, V. J.; Merkle, D. L.; Berg, J. M. *J. Am. Chem. Soc.* **1991**, *113*,

34. Sheppard, R. C.; Williams, B. J. *Int. J. Peptide Protein Res.* **1982**, *20*, 451-454.

35. Atherton, E.; Logan, C. J.; Sheppard, R. C. *J. Chem. Soc., Perkin I Trans.* **1981**, 538-546.

36. Brown, E.; Williams, B. J.; Sheppard, R. C. *J. Chem. Soc., Chem. Commun.* **1980**, 1093-1095.

37. Rapp, W. "*PEG Grafted Polystyrene Tentacle Polymers: Physico-Chemical Properties and Application in Chemical Synthesis*" in *Combinatorial*

Peptide and Nonpeptide Libraries, VCH Publishers, Inc., New York, 1996; pp

38. Winter, M. "*Supports for Solid Phase Organic Synthesis*" in *Combinatorial Peptide and Nonpeptide Libraries*, VCH Publishers, Inc., New York, 1996; pp
39. Erb, E.; Janda, K. D.; Nrenner, S. *Proc. Natl. Acad. Sci. U.S.A.* **1994**, *91*, 11422-11426.
40. Bayer, E. *Angew. Chem. Int. Ed. Engl.* **1991**, *30*, 113-216.
41. Meldal, M.; Auzanneau, F.-I.; Hindsgaul, O.; Palcic, M. M. *J. Chem. Soc., Chem. Commun.* **1994**, 1849-1850.
42. Meldal, M. *Tetrahedron Lett.* **1992**, *21*, 3077-3080.
43. Meldal, M.; Svendsen, I.; Breddam, K.; Auzanneau, F.-I. *Proc. Natl. Acad. Sci. U.S.A.* **1991**, *91*, 3314-3318.
44. Kempe, M.; Barany, G. *J. Am. Chem. Soc.* **1996**, *118*, 7083-7093.
45. personal communication with Dr. Philip E. Dawson.
46. Judice, J. K.; Namenuk, A. K.; Burnier, J. P. *Bioorg. Med. Chem. Lett.* **1996**, *6*, 1961-1966.